



With the support of the
Erasmus+ Programme
of the European Union



University of Évora

ARCHMAT

(ERASMUS MUNDUS MASTER in ARCHaeological MATerial Science)

Mestrado em Arqueologia e Ambiente

**Characterization of Mortars from
Aqueduct of Água da Prata (Évora, Portugal)**

Nur Deniz Kabil Bozkurt
m43468

Paula Cristina Gonçalves Pereira Galacho
(Supervisor - University of Évora)

Patrícia Sofia Martins Moita
(Co-supervisor - University of Évora)

José Rui Ribeiro dos Santos
(Co-supervisor – Regional Directorate of Culture of Alentejo)

Évora, Portugal, December 2020





With the support of the
Erasmus+ Programme
of the European Union



Universidade de Évora

ARCHMAT

(ERASMUS MUNDUS MASTER in ARCHaeological MATerial Science)

Mestrado em Arqueologia e Ambiente

Caracterização de Argamassas do Aqueduto da Água da Prata (Évora, Portugal)

Nur Deniz Kabil Bozkurt

m43468

Paula Cristina Gonçalves Pereira Galacho
(Orientador - Universidade de Évora)

Patrícia Sofia Martins Moita
(Co-orientador - Universidade de Évora)

José Rui Ribeiro dos Santos
(Co-orientador - Direção Regional de Cultura do Alentejo)

Évora, Portugal, Dezembro 2020



PANEL OF JURY

Presidente: Cristina Barrocas Dias, Professora Associada c/ Agregação
Universidade de Évora

Arguente: Carlos da Silva Ribeiro, Professor Auxiliar
Universidade de Évora

Orientador: Paula Cristina Galacho, Professora Auxiliar
Universidade de Évora

Vogal: Laura Parducci, Professora Auxiliar
Università di Roma La Sapienza

ABSTRACT

Characterization of Mortars from Aqueduct of Água da Prata (Évora, Portugal)

The aqueduct of Água da Prata has been amongst the most prestigious constructions of the XVI century in the city of Évora which has been declared as a World Heritage Site by UNESCO in 1986. The aqueduct itself has been classified as a National Monument in 1910 due to its patrimonial value and has been added to the 'Watch List' of the World Monuments Fund (WMF) in 2016 to promote the preservation and the monitoring of the cultural heritage.

The aim of the work is to bring a clear understanding to the mortars of the aqueduct from a textural, mineralogical and chemical point of view to identify the different construction phases including the restorations and decorative interventions (ranging from the Roman period to XIX century), the technology used for their production and the origin of the raw materials. The results provide valuable information about the monument's history by enlightening its Roman pre-existence and contribute to future restoration practices for the preparation of compatible repair mortars.

A total of 20 mortar samples have been collected from the various sections of the aqueduct with different structural uses (filler and render) and examined by a multi-analytical approach by means of Optical Microscopy (Stereo zoom and Petrographic microscope), X-ray Diffraction (XRD), Scanning Electron Microscopy - Energy Dispersive X-ray Spectroscopy (SEM-EDS), Thermogravimetric analysis (TGA-DTG), Acid attack and Granulometric analysis.

The results revealed similar mineralogical compositions of the aggregates which are compatible with the local geology but distinctive binder properties based on their construction periods and different functional needs that are clayish binders with a small amount of calcitic lime, calcitic lime and dolomitic lime binders.

Key Words: Água da Prata, aqueduct, mortars, characterization, materials, aggregates, binder, raw materials, provenance, heritage science, archaeometry.

RESUMO

Caracterização de Argamassas do Aqueduto da Água da Prata (Évora, Portugal)

O aqueduto da Água da Prata é uma das mais prestigiadas construções do século XVI na cidade de Évora tendo sido classificado como Monumento Nacional em 1910 devido ao seu valor patrimonial. Em 1986 foi declarado Património Mundial pela UNESCO e em, 2016, integrou a lista de monumentos de interesse mundial com necessidade de preservação da *World Monuments Fund* (WMF), organização sem fins lucrativos e que promove o programa *World Monuments Watch* cuja finalidade passa por conservar a herança cultural em todo o mundo.

O trabalho apresentado teve como objetivo a caracterização de argamassas do aqueduto do ponto de vista textural, mineralógico e químico, permitindo identificar as diferentes fases construtivas, a tecnologia utilizada para a sua produção e a origem das matérias-primas. Os resultados fornecem informações valiosas sobre a história do monumento, corroborando a sua pré-existência romana, e que contribuem para futuras práticas de reabilitação, nomeadamente, para a preparação de argamassas de reparação compatíveis com as existentes.

Foram recolhidas 20 amostras de argamassas, em diferentes partes do aqueduto, e analisadas por uma abordagem multi-analítica: Microscopia Ótica (estereomicroscopia e petrografia), Difração de raios X (DRX), Microscopia Eletrónica de Varrimento – Espectroscopia de Energia Dispersiva de raios X (MEV-EDS), Análise Termogravimétrica (ATG-DTG), Ataque Ácido e Análise Granulometria.

Os resultados revelaram que as argamassas estudadas são similares no que respeita aos agregados, compatíveis com a geologia local, mas com propriedades ligantes distintas, com base nas diferentes necessidades funcionais e temporais, nomeadamente ligantes argilosos com uma pequena quantidade de cal calcítica, ligantes de cal calcítica e ligantes de cal dolomítica.

Palavras-chave: Água da Prata, aqueduto, argamassas, caracterização, materiais, agregados, ligante, matérias-primas, proveniência, ciência do património, arqueometria.

ACKNOWLEDGMENTS

The thesis would not have been realized without the assistance and encouragement of various people that deserve special thanks for their contribution to this academic work.

I would like to express my deepest gratitude to my supervisor Prof. Cristina Galacho, my co-supervisors Prof. Patrícia Moita and Archae. José Rui Santos, for giving me the opportunity to take part in this exciting project. I appreciate their inspiration, valuable guidance and feedback which allowed me to gain a better understanding in the field of archaeometric research. Without their trust and precious support, this project would not have been possible.

I would like to thank Arch. Eduardo Miranda from the Municipality of Évora (CME, Divisão de Cultura e Património) and Engr. Pedro Ribeiro from A2P Consult, Estudos e Projectos Lda and Dr. Mestre Patrícia M. Carvalho for providing me the samples with the essential data and the relevant bibliography needed. I would also like to thank the Rector Padre José Gomes de Sousa and Mr. Joaquim Ferreira from the Seminário Redemptoris Mater (Quinta de Santo António da Piedade) for their cooperation and support. Besides, I would like to express my gratitude to Mestre Francisco Bilou from the Regional Directorate of Culture of Alentejo (Direção Regional de Cultura do Alentejo) for the generosity of joining the site visits, answering my questions and providing all the information I need about the archaeological context.

I would also like to thank Prof. Nick Schiavon and the ARCHMAT EMMC Committee, for giving me the opportunity for participation in this program including all professors that provided valuable knowledge to develop the necessary skills in the field of heritage science. I am grateful to all the academic staff, researches and students of the HERCULES Laboratory for their technical support and recommendations during my research. I would like to express my special thanks to Ms. Sandra Velez and Ms. Aida Graça for their assistance and expertise during the laboratory works.

I am deeply grateful to all my friends, colleagues and my family for the constant encouragement and motivation they provided me at all circumstances. Finally, I owe a great depth of gratitude to my greatest support Yuliyán Hadzhiev for the devotion and trust before and during all the phases of this work.

TABLE OF CONTENTS

ABSTRACT	I
RESUMO	II
ACKNOWLEDGMENTS	III
LIST OF FIGURES	VI
LIST OF TABLES	X
LIST OF APPENDICES	XI
1 INTRODUCTION	1
1.1 AIM OF THE STUDY	2
1.2 MORTARS.....	3
2 ARCHAEOLOGICAL CONTEXT.....	7
2.1 HISTORICAL BACKGROUND.....	7
2.2 THE AQUEDUCT OF ÁGUA DA PRATA.....	9
3 METHODOLOGY	15
3.1 SAMPLING.....	16
3.2 SAMPLE PREPARATION.....	22
3.2.1 Unbundled Samples - Preparation for XRD and TGA Analysis	23
3.2.2 Sectioned Samples – Preparation for Optical/Stereo Microscopy and SEM-EDS	24
3.2.3 Fragmented Samples – Preparation for Acid Attack and Granulometric Analysis	26
3.3 EXPERIMENTAL CONDITIONS.....	26
3.3.1 Experimental Conditions for Stereo Microscopy.....	26
3.3.2 Experimental Conditions for Optical Microscopy	26
3.3.3 Experimental Conditions for X-Ray Diffraction (XRD)	27

3.3.4	Experimental Conditions for Thermogravimetric Analysis (TGA-DTG)	27
3.3.5	Experimental Conditions for Scanning Electron Microscopy – Energy Dispersive X-ray Spectrometry (SEM-EDS)	28
3.3.6	Experimental Conditions for Acid Attack and Granulometric Analysis	28
4	RESULTS	30
4.3	OPTICAL MICROSCOPY	37
4.4	X-RAY DIFFRACTION (XRD)	39
4.5	THERMOGRAVIMETRIC ANALYSIS (TGA-DTG)	44
4.6	SCANNING ELECTRON MICROSCOPY – ENERGY DISPERSIVE X-RAY SPECTROMETRY (SEM-EDS)	49
4.7	ACID ATTACK AND GRANULOMETRIC ANALYSIS	56
5	DISCUSSION	62
5.1	RAW MATERIALS	63
5.1.1	Binder	63
5.1.2	Aggregates	65
5.2	PROVENANCE	66
5.3	PRODUCTION TECHNOLOGY	69
6	CONCLUSION	72
7	BIBLIOGRAPHY	75
8	APPENDICES	80

LIST OF FIGURES

Figure 1-1. Lime Cycle.....	4
Figure 2-1. Diagram showing the elements of Roman aqueducts in various topographies (Mays, 2010).....	8
Figure 2-2. Drawing of the aqueduct and the pumping stations by Daniel Sanches, 1951 (Claro, 2019).....	10
Figure 2-3. a) Aqueduct in Torralva section, drone image by Slyvie Claro, 2016; b) Aqueduct in Cartuxa section, drone image by Francisco Brito, 2016 (Claro, 2019).	11
Figure 2-4. a) Aqueduct in Fortress of Santo António section; b) Aqueduct in Intramural section, both drone images by Francisco Brito, 2016 (Claro, 2019).	12
Figure 2-5. a) The monumental archway of the aqueduct, 1940-1950, AFCME (APS 351); b) Aqueduct after it exits the Fortress of Santo António, supported with buttresses, 1960s, AFCME (APS 193); (Claro, 2019).....	13
Figure 3-1. Methodology used and the information gathered for the characterization of the mortars.....	15
Figure 3-2. a) Photogrammetric image of the sampling pits from Cartuxa b) General view of survey pits, c) Pit C.1, d) Pits C.-2 and C.-3 (All images obtained from CME-DCP, 2018).	17
Figure 3-3. a-b) Photogrammetric images of Torralva survey pit, c-d) Photos of XVI century pillar and Roman base. (Photogrammetric images obtained from CME-DCP, 2018, photos taken by author in September 2020).	17
Figure 3-4. a-b) Orthophoto and digital photo of sampling spots AP-01 and AP-02, c) Orthophoto of sampling spots AP-03, AP-04 and AP-05, d-e-f) Photos of the sampling spots AP-03, AP-04 and AP-05 respectively.....	18
Figure 3-5. a) Orthophoto of sampling spots AP-06 – AP-10, b-c-d) Photos of the monumental fountain’s decoration, e-f-g-h-l) Sampling spots of AP-06, AP-07, AP-08, AP-09 and AP-10 respectively.	19
Figure 3-6. a-b) Orthophoto and digital photo of sampling spot AP-11, c-d-e) Orthophoto and digital photos of sampling spot AP-12.....	20
Figure 3-7. Sample preparation diagram.....	22

Figure 3-8. Tools used for the preparation of the powdered samples: a) Disaggregation by mortar and pestle, b) Powdering equipment PM 100 Planetary Ball Mill (Retsch), c) Agate grinding jar and grinding balls.....23

Figure 3-9. Thin section preparation: a) Samples in epoxy resin for cross sections, b) Cutting using Discoplan-TS, c) Grinding by Logitech PM5, d-e) Gluing the glass slides on cross sections, application of epoxy resin (e), f) System Abele press, g-h) Cutting out the thin sections under vacuum using a Logitech CS10 Thin Section Cut Off Saw (h), i) Mitutoyo digital micrometer, j-k) Results of AP-03, cross section (j) and thin section (k) under microscope.25

Figure 3-10. Experimentation of the analysis: a) Preparation of HCl aqueous solution, b) Heating up the sample + HCl aqueous solution on hot plate up to boiling temperature, c) Filtration under vacuum using a Büchner funnel + filter paper, d) Sieving using ASTM E11 test sieves. ..29

Figure 4-1. Photographic documentation of the samples before disaggregation.31

Figure 4-2. Photographic documentation of the samples before disaggregation (continuation).
.....32

Figure 4-3. Representative petrographic images of AP-12, PPL(a) and XPL(b); AP-12U (referring the whiter layer); presence of carbonated grains within the binder forming a more homogenous appearance, AP-12D (referring the darker layer); has more aggregates and less binder.39

Figure 4-4. Representative XRD pattern of the XVI century filling mortar; diffractogram of EVR-01 GF (black), FF (red), (Q: quartz, C: calcite, F: feldspar, Mi: mica, Amp: amphibole, V: vermiculite).....40

Figure 4-5. Representative XRD pattern of the Roman filling mortar; diffractogram of EVR-04 GF (black), FF (red), (Q: quartz, C: calcite, F: feldspar, Mi: mica, Amp: amphibole, V: vermiculite)
.....40

Figure 4-6. XRD Patterns of the stratigraphic layers of decorative mortar AP-12; Light coloured layer AP-12U (red), darker coloured layer AP-12D (black), (Q: quartz, C: calcite, F: feldspar, Mi: mica, Amp: amphibole, Mg: magnesite).....42

Figure 4-7. Patterns of the stratigraphic layers of the render mortar AP-10; Light coloured layer AP-10U (red), darker coloured layer AP-10D (black), (Q: quartz, C: calcite, F: feldspar, Mi: mica, Amp: amphibole, Cl: chlorite).....42

Figure 4-8. XRD Patterns of the samples with decorative use and AP-05 (Q: quartz, C: calcite, F: feldspar, Mi: mica, Amp: amphibole, Hm: hydromagnesite) (marked with red box), Mg: magnesite (marked with black box). 43

Figure 4-9. TG/DTG curves of samples AP-03 (blue), AP-05 (magenta), AP-06 (green) and AP-09U (cyan), continuous curves representing TG and dashed curve representing DTG data 45

Figure 4-10. TG/DTG curves of samples AP-12U (purple), AP-12D (orange), continuous curves representing TG and dashed curve representing DTG data..... 45

Figure 4-11. TG/DTG curves of XVI c. filling mortars; EVR-01 (blue), EVR-06 (black), EVR-08 (red); continuous curves representing TG and dashed curve representing DTG data..... 47

Figure 4-12. TG/DTG curves of the Roman filling mortars; EVR-02 (green), EVR-03 (magenta), EVR-04 (blue), EVR-05 (black), EVR-07 (red); continuous curves representing TG and dashed curve representing DTG data. 47

Figure 4-13. Elemental maps of AP-02; a) BSE image of the general composition, b) Siliceous aggregates within the composition c) Mg, Ca, Al elemental map, Al related to feldspars d) Ca, Fe, Si elemental map, Fe related to biotite. Yellow: Si, blue: Ca, green: Mg, orange: Al, red: Fe. 49

Figure 4-14. a-b) BSE image of AP-03, c) EDS spectra of the point analysis marked in (b). . 50

Figure 4-15. a-b) BSE image of AP-03, c) EDS spectra of the point analysis marked in (b). . 50

Figure 4-16. a) BSE image of AP-06, b) EDS spectra of the point analysis marked in (a). 50

Figure 4-17. Representative image of binder microstructure; a-b) Sample AP-09U, c-d) Sample AP-01; BSE images on the left and elemental distribution maps of calcium (blue) and magnesium (green) on the right, respectively. 51

Figure 4-18. a) General aspect of lime lump and binder of AP-01; b) Elemental map of (a), c-h) Point analysis and corresponding EDS spectrum of lump (P1) in AP-01, Ca rich (P2) in AP-01 and Ca rich (P3) in AP-12, respectively..... 52

Figure 4-19. BSE image of the point analysis and corresponding EDS spectrums of the magnesite crystals within the binder matrix; a-b) AP-01, c-d) AP-03 and e-f) AP-05..... 53

Figure 4-20. a) Representative image of binder microstructure of AP-11, b) Elemental map of (a) Ca and Mg, c-f) BSE image of the multipoint analysis in the binder of AP-04 and corresponding EDS spectrums of the (A1) Mg bearing area and (A2) Ca bearing area. 54

Figure 4-21. a) BSE image of the general composition of EVR-04 (Roman sample), b) Elemental map of (a) with Mg, Ca and Al, c) BSE image of a more focused on the binder area with

calclitic lime on the right, d) Elemental map of (c) with Ca and Al, e-f) Point analysis P7 on the binder (e) and P8 on the calclitic lime binder (f).....	55
Figure 4-22. a) BSE image of the general composition of EVR-06 (XVI century sample), b) Elemental map of (a) with Mg, Ca and Si, c) BSE image of a more focused on the binder area, d) Point analysis P9 on the binder (c).	56
Figure 4-23. Grain size distributions of filler mortars from Roman period (upper) and XVI century (lower).	58
Figure 4-24. Grain size distribution curves of render mortars; decorative mortars (upper) and render mortars (lower).	59
Figure 4-25. Gravel:mud:sand diagram from GRADISTAT.....	61
Figure 5-1. EDS analysis of Ca rich (upper) and Mg rich (lower) points within the binder of the samples (%).	64
Figure 5-2. Geological map of Évora and its surroundings (Moita <i>et al.</i> , 2009).....	66
Figure 5-3. Geological scheme from Évora (40-A) and Viana do Alentejo (40-C) geological maps in 35 km of radius between Évora and Viana do Alentejo , scale of 1/50000 (taken and adapted from Laboratório Nacional de Energia e Geologia (LNEG), http://geoportal.lneg.pt/geoportal/mapas/index.html).	68
Figure 5-4. Carbon Dioxide / Structurally Bound Water <i>versus</i> Carbon Dioxide (%).	71

LIST OF TABLES

Table 3-1. General description of the samples.....	21
Table 4-1. General aspect of the samples under stereo microscope.....	33
Table 4-2. Preliminary assessment and microscopic observations.....	34
Table 4-3. Petrographic images, representing render (a, b, c) and decorative (d, e, f) mortars.	37
Table 4-4. Images of the isolated minerals observed under XPL (cross polarized light) and PPL (plane polarized light).	38
Table 4-5. Mineralogical compositions of the GF and FF powders of EVR samples by XRD analysis.....	41
Table 4-6. Mineralogical compositions of the AP samples by XRD analysis.....	43
Table 4-7. TG/DTG temperature ranges (°C) and weight losses (%).	48
Table 4-8. Mean values obtained from the soluble and insoluble fractions after the acid attack.	57
Table 4-9. Description of the insoluble residue.....	60
Table 5-1. Division of groups used for the discussion of the results	62
Table 5-2. Simplified compositions of the mortars (%) using Jedrzejewska method (Jedrzejewska, 1960).	70

LIST OF APPENDICES

Appendix 1. Sections of the aqueduct of Água da Prata as described in the study.	80
Appendix 2. Photos of the aqueduct from Torralva section (Taken by the author in Sept. 2020).	81
Appendix 3. Photos of the aqueduct from Cartuxa section, the monumental archway. (Top, taken by author in Sept. 2020; bottom, taken by Whotips, 2020).	82
Appendix 4. Photos of the aqueduct from Cartuxa section. (Top, taken by Whotips, 2020; bottom, taken by the author in Sept. 2020).	83
Appendix 5. Photos of the aqueduct from Fortress of Santo António section (Taken by author in Sept. 2020).	84
Appendix 6. Photos of the aqueduct from Intramural section, (Taken by Whotips, 2020).	85
Appendix 7. X-ray diffractograms of the powdered samples from the aqueduct of Água da Prata (Global Fractions).....	86
Appendix 8. X-ray diffractograms of the powdered samples from the aqueduct of Água da Prata (Fine Fractions)	89
Appendix 9. Thermograms of the global fraction powders of the samples from the aqueduct of Água da Prata.	92
Appendix 10. Results of the acid attack analysis of the samples from the aqueduct of Água da Prata.	95
Appendix 11. Results of the granulometric analysis, grain size distribution of the insoluble residue.	96
Appendix 12. Insoluble residues obtained after acid attack, observations under Stereozoom microscope.....	97

1 INTRODUCTION

Mortars are manufactured building materials that are composed of a mixture of aggregates, binder and water together with some organic or inorganic additives for special constructional needs. As an important part of masonry building material, they are used to fill the gaps, waterproof walls, regularize surfaces and surface finishes. They hold the bricks and rocks together, develop strength and provide stability to the structures after hardening (Stefanidou *et al.*, 2014). Their various characteristics are determined by their desired functions and technological knowledge developed by the ancient populations (Ergenç and Fort, 2019). Characterization of historical building materials is crucial to reveal the ancient construction technologies, raw materials and their manufacturing receipts (Miriello *et al.*, 2010). The information deriving from such studies provides significant data about how such complex architectural structures were built and survived through long periods of time and the traces about the technological background of certain historical periods. Additionally, mortar studies provide essential knowledge for future restoration activities and studies of materials provenances.

The subject of the study is the analytical characterization of the historical mortars of the Aqueduct of Água da Prata, located in Évora, in the Alentejo region of Portugal which has been classified as a World Heritage Site by UNESCO in 1986. The structure has been considered one of the most significant constructions of the XVI century's Portugal and has been classified as a National Monument in 1910. It has been under protection by law to maintain its authenticity and integrity as state property of a civil architecture under the category of 'military aqueduct' (CME-DCP, 2019).

In 2008, The Silver Water Route (Percurso Ambiental da Água da Prata) was created by the Municipality of Évora (CME) to promote the heritage and bring awareness to its social and historical value. The aqueduct itself has been added in the 'Watch List' of the World Monuments Fund (WMF) in 2016 to promote the preservation and the monitoring of the cultural heritage. It is one of the prestigious constructions of the city of Évora together with several other structures such as the Roman Temple of Évora, the medieval city walls, the religious convent complexes around the city, the university building of Espírito Santo and Santa Maria Church in Évora which is also known also as Cathedral Sé. The aqueduct is a part of the urban structures of the city which has survived throughout centuries as a reference to the city's historical evolution.

1.1 AIM OF THE STUDY

This work is aimed to achieve a complete characterization of the mortars used in the aqueduct of Água da Prata from a textural, mineralogical and chemical point of view by the means of analytical techniques. The results obtained by the study will bring a clear understanding of the technology used for their production and the origin of the raw materials used by the integration of geological and archaeological data. The outcome will lead to the identification of different construction phases of the aqueduct and provide valuable information about the monument's history. The relations between the selection of the materials with the expected performances will be evaluated. The work will also contribute to the restoration practices that will be carried out in the future for the preparation of compatible repair mortars.

The aqueduct has previously been studied by several scholars (Conde and Magalhaes, 2008; Bilou, 2010; Monteiro, 2012; Claro, 2019) from the archaeological and historical point of views aiming to identify the historical background and the valorisation of the monument. It has also been studied under the 'Conservation and Consolidation Program of Aqueduct Água da Prata' carried out by the Municipality of Évora (CME) in collaboration with the Regional Directorate for Culture of the Alentejo (DRCAentejo) and the Directorate General for Cultural Heritage (DGPC). In 2016, archaeological surveys have been carried out within the scope of the conservation and rehabilitation project of the aqueduct under the supervision of archaeologist José Rui Santos by CME-DGPC together with HERCULES Laboratory of the University of Évora as the scientific partner (CME-DCP, 2018). The aim of the survey was the examination of the Roman pre-existence of the aqueduct as proposed by the previous research by Bilou, 2010 and the material characterization of the XVI century construction. The sampling was performed accordingly to bring a clear understanding to both of the research questions and the samples were analysed as a part of this study.

20 samples, from the archaeological surveys of CME-DGPC were collected from different parts of Água da Prata and examined under the chosen analytical methods during the study. The analysis was conducted in HERCULES Laboratory in the University of Évora, Portugal as a part of Joint Master's Degree of Erasmus Mundus Programme in Archaeological Materials Science (ARCHMAT). The analytical techniques for the determination of the characteristics of the samples were performed by the use of Stereo and Optical Microscopy (OM), powder X-ray Diffraction (XRD), Thermogravimetric analysis (TGA-DTG), Scanning Electron Microscopy coupled with Energy Dispersive X-ray Spectroscopy (SEM-EDS), Acid Attack and Granulometric Analysis.

1.2 MORTARS

Mortars are artificial materials made of a mixture of aggregates, binder and water together with some organic or inorganic additives for special constructional needs (Stefanidou *et al.*, 2014). As an artificial building material, mortars show different characteristics depending on where they serve and how they were manufactured. The construction need of mortars may vary from structural supporting, joining, flooring, finishing internally or externally as rendering or plastering, decorating or waterproofing (Elsen, 2006). Their compositional characteristics depend on the raw materials used for their production and the technological knowledge of the time of production (Riccardi *et al.*, 2007). Due to the advances in technology, characterization of the ancient mortars made it possible for the researchers to understand their production receipts and their secrets of their functionality and long-lasting performance (Ergenç and Fort, 2019).

Aggregates are proportionally the main components in mortars and may vary depending on where they were acquired. Typically, natural sand is the most abundant form of an aggregate although crushed stones or shells are used through a series of manufacturing processes (Schnabel, 2008). The primary function of the aggregates is to restrict the shrinkage of the mortar paste during drying. Aggregate grains, mainly deriving from quartz sand as sediment from a river or a sand quarry. Through a series of examinations on the composition, size and shape of the aggregates the origin and the source of the raw materials may be tracked since they do not significantly alter or interact with other materials in the mortar during the production steps of the mortar making (Schnabel, 2008).

Binders are materials added to the mixture to keep the aggregate grains together. The two main types of binders are aerial (non-hydraulic) binders which set in contact with air and hydraulic binders which set in contact with water. The expected function of a mortar thus is important for the selection of the appropriate binders. Most typically, there are three types of binders that have been used throughout history until recent times which are mud/clay, gypsum and lime (Elsen, 2006). The oldest examples of mud binders can be found at the Walls of Jericho (Israel) dating from 8300 BC and structures in Çatalhöyük (Turkey) dating from 6000-7500 BC. Since no heat treatment is needed for their production, mud binders are not as durable and show less strength against the degradation caused by weathering (Rodríguez-Navarro, 2012). The other two binders gypsum and lime are products of heating processes in which gypsum needed less temperature whereas lime needed higher, suggesting that the use of gypsum was dating back earlier than the use of lime as a binder material (Elsen, Van Balen and Mertens, 2013).

Among the Roman mortars, lime has been considered the most common mortar binder in the historical context (Schnabel, 2008). It is produced through a series of processes that occur in three stages starting with calcination, followed by hydration and finalized by carbonation which is called a Lime Cycle (Fig. 1-1).

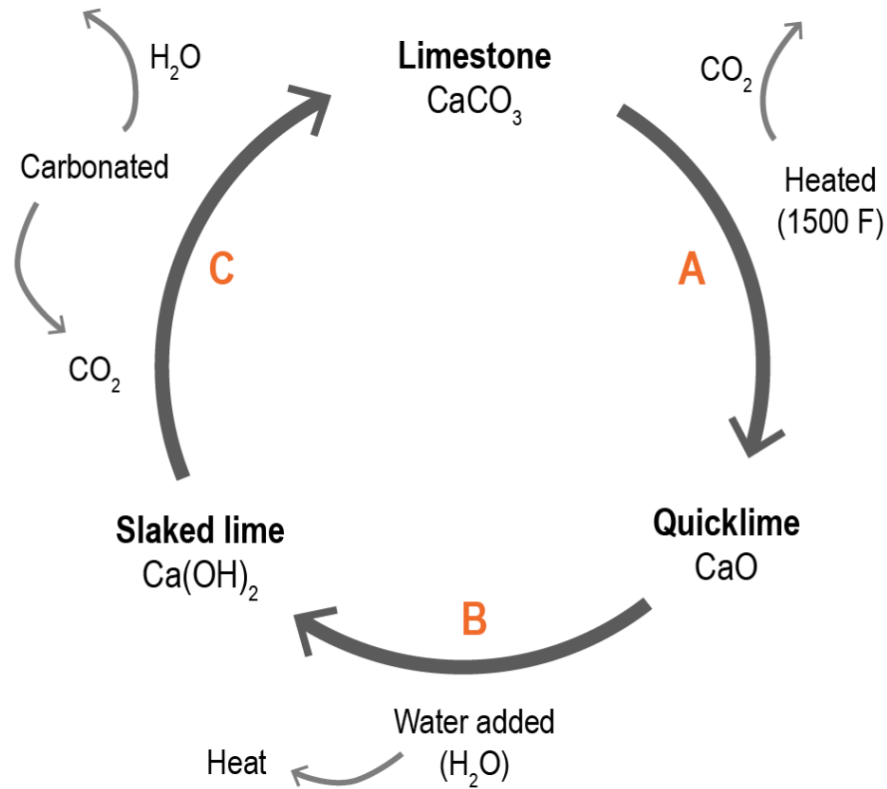
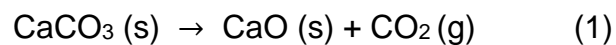


Figure 1-1. Lime Cycle.

The three-step procedure of the Lime Cycle is explained as:

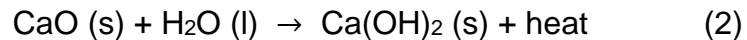
1. Calcination (A);

During the stage of calcination, the calcite (CaCO_3) in the limestone decomposes at high temperature (900 - 1000°C) forming calcium oxide (CaO) also named as quicklime and releasing carbon dioxide (CO_2) as shown in the equation (1). This burning process occurs in a kiln in which the limestone from a quarry was put and the final product is also known as burnt lime or lump lime.



2. Hydration (B);

The production of quicklime is followed by the second step which is called hydration. During this process water (H₂O) is added for the hydration of the quicklime, forming calcium hydroxide, (Ca(OH)₂), and generating heat as shown in equation (2). There are two possible outcomes of the hydration process where either a dry powder or a lime paste is formed. The dry powder which is also called hydrated lime is formed when just enough water was involved in the slaking process. Whereas lime paste or lime putty which is also known as slaked lime is formed by the addition of excess water (Rodríguez-Navarro, 2012).



3. Carbonation (C);

The final step of the lime cycle is carbonation in which the slaked lime produced by the hydration turns back into calcium carbonate (CaCO₃) by absorbing carbon dioxide from the atmosphere and forming water as shown in the equation (3).



The limestone used for the burning may not only contain calcium carbonate but also magnesium carbonate in its composition. Such situation may affect the temperature of the calcination since they behave slightly differently due to their magnesium content. In the case of dolomitic limes, the slaking would happen slowly in comparison to the calcitic lime (Schnabel, 2008). A solid mixture is created after the hardening of the calcium carbonate. The external conditions during the carbonation process could affect the size of the calcite crystals and their textural properties (Elsen, 2006).

Within the final binder composition, the presence of binder-related particles such as lime-lumps could be observed. These particles can be identified as rounded porous inclusions within the matrix. The reason for their presence may be either due to the lack of water or time during slaking (Elsen, 2006). Lime-lumps can be used to obtain information about the provenance of the raw materials and the technology used for lime production as they are representative of the initial raw material.

Several types of additives can be found in the mortar compositions to improve the performance of the mortars for the specific needs. Such additives may have organic origin such as straw, hair and egg or an inorganic origin like pozzolanic minerals or powdered ceramic materials commonly pottery and tiles (Elsen, Van Balen and Mertens, 2013). The additives may alter the properties of the final material aesthetically to give a certain colour or sparkle to modify the appearance of the mortar. In historical records, such properties could be gained with the addition of pigments, mica flakes or crushed coal (Schnabel, 2008). Another practical use of additives is to improve the physical properties of the mortars with the addition of iron fillings, fly ash and powdered ceramics. Such inclusions improve the hardness of the final materials by the reactions through time (Schnabel, 2008).

For the need of waterproofing one of the very well-known additive that was used by ancient Roman builders for the production of hydraulic mortars was 'pozzolana' which was a natural deposit found around Mount Vesuvius and very similar to the siliceous volcanic earth found on Santorini Island formerly used in the construction of the draining canals by the Greeks (Elsen *et al.*, 2013). Another additive that is widely used for adding hydraulic properties to the mortars was crushed ceramics used especially when natural pozzolans were not acquirable (Matias *et al.*, 2014). The crushed ceramics also known as *cociopesto* has been identified in many structures in Portugal related to water and moisture such as in the bath building in Ammaia (Cardoso *et al.*, 2014), the river tower in Mértola (A. Santos Silva *et al.*, 2006), wells and other water-related structures in Troia (A. S. Silva *et al.*, 2006) and thermal baths in Pisões (Borsoi *et al.*, 2019).

These additives have also been mentioned in historical written sources such as *The Ten Books on Architecture* by Vitruvius in Book II, Chapter V. describing that additives for hydraulic properties could be originating from volcanic pyroclastic rocks or from powdered ceramic materials such as pottery and tiles (Elsen, 2006).

2 ARCHAEOLOGICAL CONTEXT

2.1 HISTORICAL BACKGROUND

Aqueducts are structures that were built to deliver the water from a source to a place where it was needed by the use of gravity. The necessity of water has always been the major concern for all civilizations to support life and production. In the early stages, settlements were located alongside rivers, streams and springs to obtain water directly from natural sources (Sürmeli Hindi, 2010). As the populations grew larger, supplying clean water and disposing of the wastewater required additional systems such as conduits, cisterns, fountains and aqueducts. Throughout time such infrastructures evolved from smaller scale projects to fulfil the demand for water to mega-structures as a matter of prestige and luxury (Mays, 2010).

The early examples of water management systems were developed for irrigation needs for the agricultural practices and later advanced to provide fresh water for the early urban centres (Mays, 2010). Starting from the Minoan periods through classical and Hellenistic times urban aqueduct constructions evolved by various technological achievements (De Feo, 2013). Before the Roman era which is mainly dominated by the Greek world, the political situation was not as stable since there were battles going on between the city states of Asia Minor and Greece, wars between Alexander the Great, his successors and Persia (Fahlbusch, 2010). Such conditions led the states to build their water supply systems that are not easily visible by the enemy due to security reasons and underground aqueducts and subterranean pipe systems were preferred. Besides, groundwater was more favourable for them rather than open air water sources perhaps due to the hygienic motives (Mays, 2010). In the early examples of Greek aqueducts closed pipe systems are found in which the enemy could not reach and pollute the water (Fahlbusch, 2000). Some examples of such systems can be seen in the Peisistratean aqueduct in Athens and the aqueduct of Samos the Tunnel of Eupalinos (Mays, 2010).

During the Roman era there was a dramatic change in the political situation in which Rome became the major Mediterranean power. The internal wars among the city states were almost ended and the larger scale building projects emerged showing the great power of the Empire (Berking, 2018). Besides the growing populations, constructions of the infrastructures for public use were also expanded with the increasing number of public baths, ornamental pools and fountains. The escalating demand for water led to the manufacturing of more advanced water

structures that have larger cross-sections allowing the flow of more water. The monumental bridges and arcades were built to carry the water along the large valleys and it became one of the symbolic features of the Roman aqueducts representing the prestige and wealth of the cities (Hodge, 2013).

The aqueducts were formed of several elements to carry the water in the desired direction like shafts, tanks, tunnels, bridges, siphons, arcades and distribution basins that are designed accordingly with the landscape features. The ancient Roman treatises of Vitruvius and Frontinus provide insight into finding a healthy water source, constructing and maintenance of the aqueducts and distribution of water (Mays, 2010).

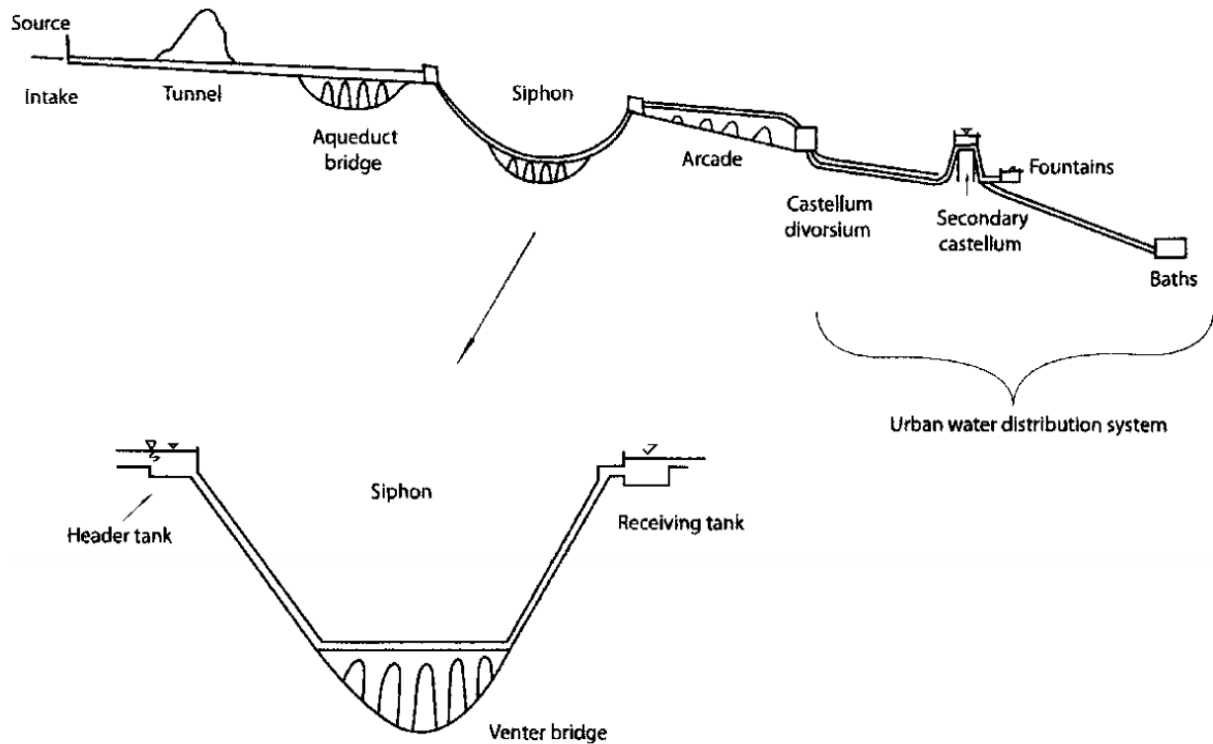


Figure 2-1. Diagram showing the elements of Roman aqueducts in various topographies (Mays, 2010).

2.2 THE AQUEDUCT OF ÁGUA DA PRATA

The aqueduct of Água da Prata which can be literally translated as 'The Silver Water' is located in the district of Évora between the coordinates 38°64'84.30" N, 7°98'49.65" W and 38°57'16.86" N, 7°90'94.56" W, in Alentejo Province of Portugal. The aqueduct itself has been classified as a National Monument in 1910 due to its patrimonial value and it is also one of the most significant constructions of the city of Évora which has been declared as a World Heritage Site by UNESCO in 1986.

The city of Évora which is the capital of Alentejo Province is located in a slightly wavy terrain in which the altitudes are ranging between 200 to 240 meters and often interrupted by valleys. It is surrounded by three river basins that are Tejo, Guadiana and Sado. The terrain's natural vegetation is mainly cork oak and has a Mediterranean temperature regime (Pereira, 2012). The area was occupied since prehistoric times as known by the historical findings in the region like megalithic structures, dolmens and menhirs from the Neolithic period.

During antiquity due to its favourable geographical position, the city itself gained importance as a connection point of the trade routes from the coasts both of the south and the west. In Roman times, the city was given the name Eborá Liberalitas Julia as an honourable recognition of its status as a Roman municipality (CME-DCP, 2019). The remains of the Roman city are still found today with two major structures that are the Roman baths in Travessa do Sertório and the Roman Temple of Évora also referred as the Temple of Diana at the highest point in the city. After the Visigoth and Muslim dominations, the city reached its highest growth in the middle ages with the construction of the royal palace, monuments, religious buildings and the aqueduct. The buildings of the XVI century are mainly characterized by the Manueline style (UNESCO, 1986).

The aqueduct of Água da Prata is an 18 km long construction connecting the urban centre of Évora with the springs by passing through both rural and urban landscapes (Fig. 2-2). The aqueduct originates from the springs of Graça do Divor located in the northwest of the city and reaches to the Giraldo Square in the urban centre of the city. From the furthest point of the spring the water flows through a water channel for around 16 km until it reaches São Bento de Cástris convent and continues for around 2 km before bringing the water within the city walls (Monteiro, 2012). During the photogrammetric survey carried out by CME, the last part from São Bento de Cástris to its final destination within the city, the structure has been divided into four sections for a better description which are; Torralva, Cartuxa, Fortress of Santo António and Intramural (CME-DCP, 2019) (Appx. 1).



Figure 2-2. Drawing of the aqueduct and the pumping stations by Daniel Sanches, 1951 (Claro, 2019).

The first section of Torralva covers the area of approximately 660 metres long in which the water moves from a water box to another throughout the way from São Bento de Cástris Convent to Torralva water box (Fig. 2.3a). The architectural elements of the aqueduct change adapting the geographical features of the area from subterranean water channels to arched surface structures (Monteiro, 2012) (Appx. 2). This section includes the pillars from 1 to 90 which are numbered according to the study of CME (CME-DCP, 2019). This area is partially covered with plaster on which some inscriptions and initials could be seen indicating dates and possible calculations about the length of the work (Bilou, 2010). In this section, the re-used granite blocks were also identified possibly deriving from the remains of the former Roman aqueduct (Bilou, 2010).

The second section Cartuxa begins from the Torralva water box and continues its way for around 670 m until it reaches a rotation point before entering the Fortress of Santo António. It covers the length of the construction starting from pillar 91 to 197 (CME-DCP, 2019). The aqueduct passes through the Arraiolos-Évora road (R114-4) with a monumental section composing of a decorated archway (Appx. 3). On the central pillar where the water box is located, two niches are integrated on both sides for the saints São Bruno and São Bento, the saints of the two neighbouring monasteries. Underneath is a cornice where the upper part of the pillar continues in a classic form of plasters and niches whereas the dome is decorated as a fine example of the XVI century Manueline expression (CME-DCP, 2019). Starting from the ground level until the decorative cornices, on both sides of the road, the pillars have fake stone masonry applied on the surface using dark and light coloured plasters which is called *sgraffito* decoration. Such technique is practiced by the application of white plaster to pronounce the joints of masonry as a mural decoration technique which requires an advanced level of knowledge on plasters (Salema, 2008).

After the monumental arc, the aqueduct continues its way through the Cartuxa convent until it reaches the Cartuxa water tank (Appx. 4). From this point on, the structure changes its direction towards the city (Fig. 2.3b). Parallel to the aqueduct, the remains of a former construction are visible on the surface. This area has been examined through the archaeological surveys under 'Conservation and Consolidation Program of Aqueduct Água da Prata' carried out by Évora City Hall, Division of Culture and Heritage (CME-DCP, 2018).

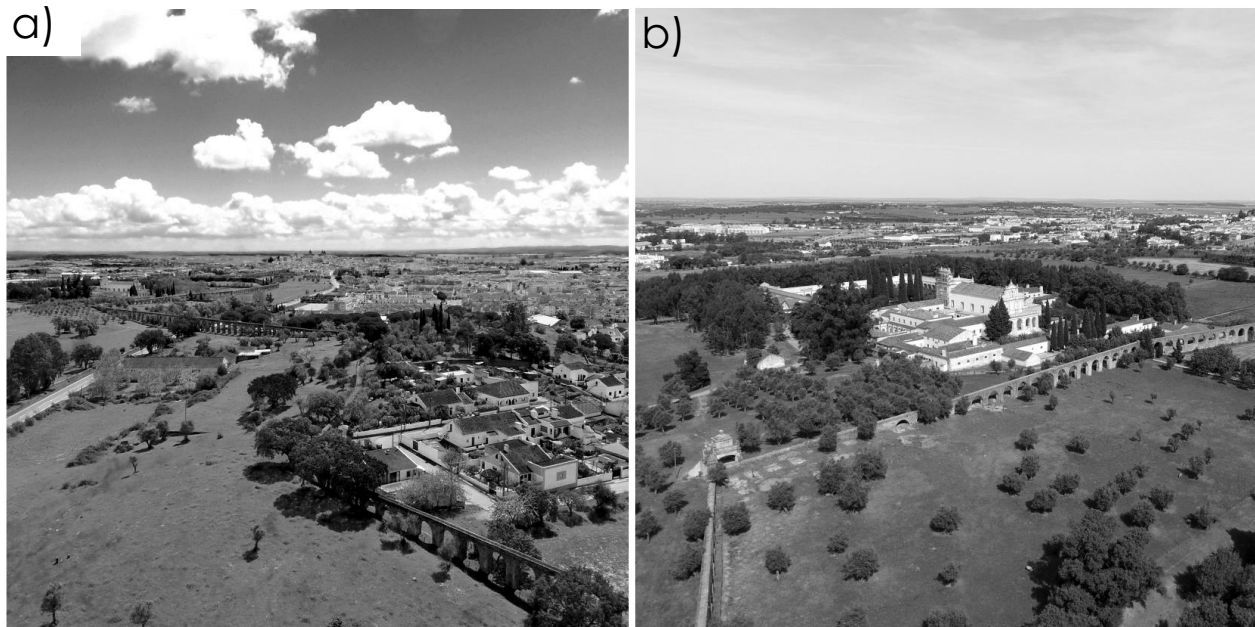


Figure 2-3. a) Aqueduct in Torralva section, drone image by Slyvie Claro, 2016; b) Aqueduct in Cartuxa section, drone image by Francisco Brito, 2016 (Claro, 2019).

The third section is the Fortress of Santo António where the aqueduct passes through the fortress and reaches the city walls. It is defined with the pillars starting from 198 to 289 according to the study of CME (CME-DCP, 2019). Within the central area of the fortress where the aqueduct is slightly redirected, is located the monumental fountain (Fig. 2.4a). The fountain itself is placed on the main axis facing towards the convent building of Santo António da Piedade. It is a well decorated structure with a large pool on the ground level. In the middle part of the pool is a water tank decorated with rocks and plaster resembling a cave where the spring flows. On both sides of the tank, the arches are closed with plastered masonry and decorated on the surfaces. The composition of the fountain is formed using elements with various colours embedded in the plaster. It is a production of a specific work campaign which is closely related to the historical context of the Convent of Santo António da Piedade (CME-DCP, 2019). The aqueduct exits the fortress on the southeast side and reaches its maximum height. It is supported occasionally by buttresses until it reaches the city walls (Appx. 5). It is partly covered by plaster on which some inscriptions and ornamental figures could be seen. On the arcade between the pillars 248 and 249 the

inscription '1670' is engraved on the plaster probably representing the period of the renovations carried out by Francisco Ferreira after the Spanish siege in 1663 (CME-DCP, 2019).

In the final section Intramural, the aqueduct gets in the city walls and continues its destination in the urban context (Fig. 2.4b). It enters the city from Rua da Muro and continues through Rua do Cano, Rua Pedro Simões, Rua do Salvador, Travessa do Sertório and finalizes at Rua Nova where the final water box is located in a form of a small classic temple with three façades. Within the walls, private housings were constructed under the span of the arches creating a characteristic appearance in Rua do Cano and Rua Pedro Simões (Appx. 6). Such formation is a result of the demolition of the pre-existing structures and the opening of new streets caused during the construction of the aqueduct inside the city walls (Bilou, 2010; Monteiro, 2012).

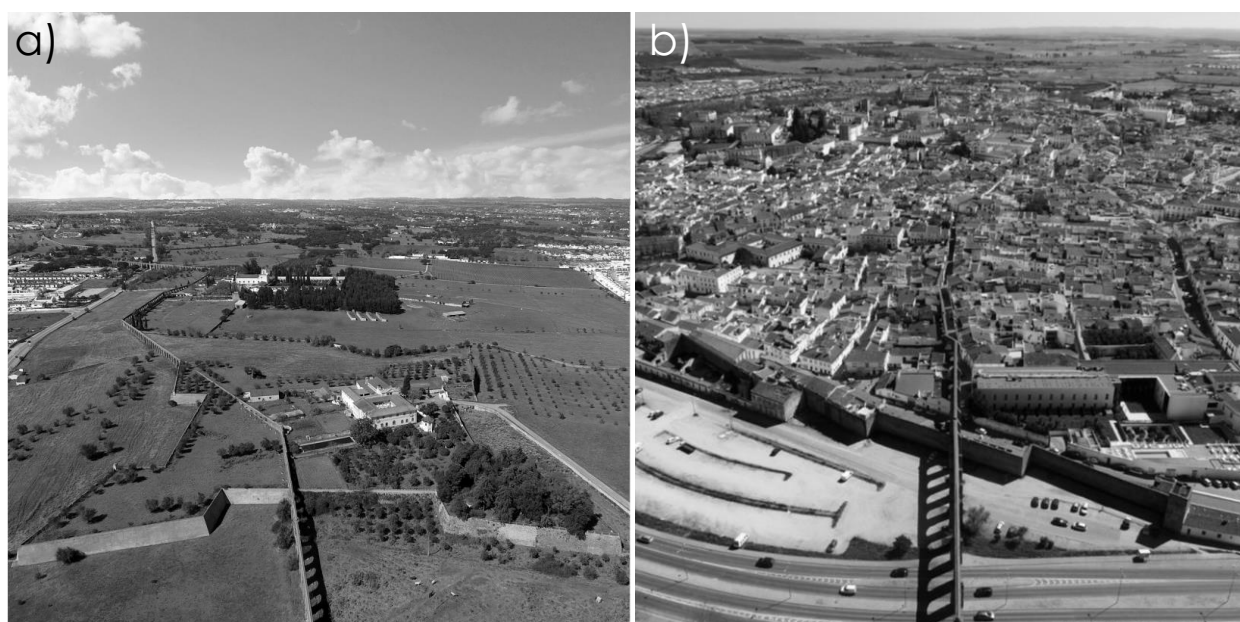


Figure 2-4. a) Aqueduct in Fortress of Santo António section; b) Aqueduct in Intramural section, both drone images by Francisco Brito, 2016 (Claro, 2019).

The aqueduct is composed of a masonry construction made of stone and bricks. Plastering appears in some areas of the surface of the pillars and arches. The water conduit is built on semicircular arches that are made of mainly bricks but in some sections with stone fragments. A rectangular masonry box is supported by the arches, in which runs a water channel of prefabricated pieces of curved ceramics. In this space, the water flows freely due to gravity (Martinez, 2016). The upper part of the water channel is covered by rectangular ceramic plates and plastered with mortar but in some areas, they are covered with stone slabs (CME-DCP, 2019).

The construction of the aqueduct was conducted in XVI century through the order of King D. João III to bring water into the city (Monteiro, 2012). Besides the city itself, it was also designed to

carry water to the surrounding religious communities in São Bento de Cástris, Cartuxa and Convent of Santo António da Piedade before entering the city. The construction work was directed by the architect Francisco Arruda. The route has also been developed according to the topography of the terrain passing from one hill to another to reduce the amount of major constructive work as much as possible to fit in a narrow time frame since the water was needed urgently for public health reasons (Bilou, 2010; Monteiro, 2012). The construction started in 1533 with the order of King D. João III, and finalized in 1537 with the arrival of the water in Giraldo Square. Other additions were implemented until 1539 for the arrival of the water to the royal palace together with the Church of S. Francisco according to the projects by Miguel Arruda. Besides the monumental structure, the aqueduct was carried through the underground to feed the city's fountains. With the completion of the remarkable work, the city of Évora strengthened its status to be the most powerful city in the kingdom after Lisbon (Fig. 2.5a-b) (CME-DCP, 2018).

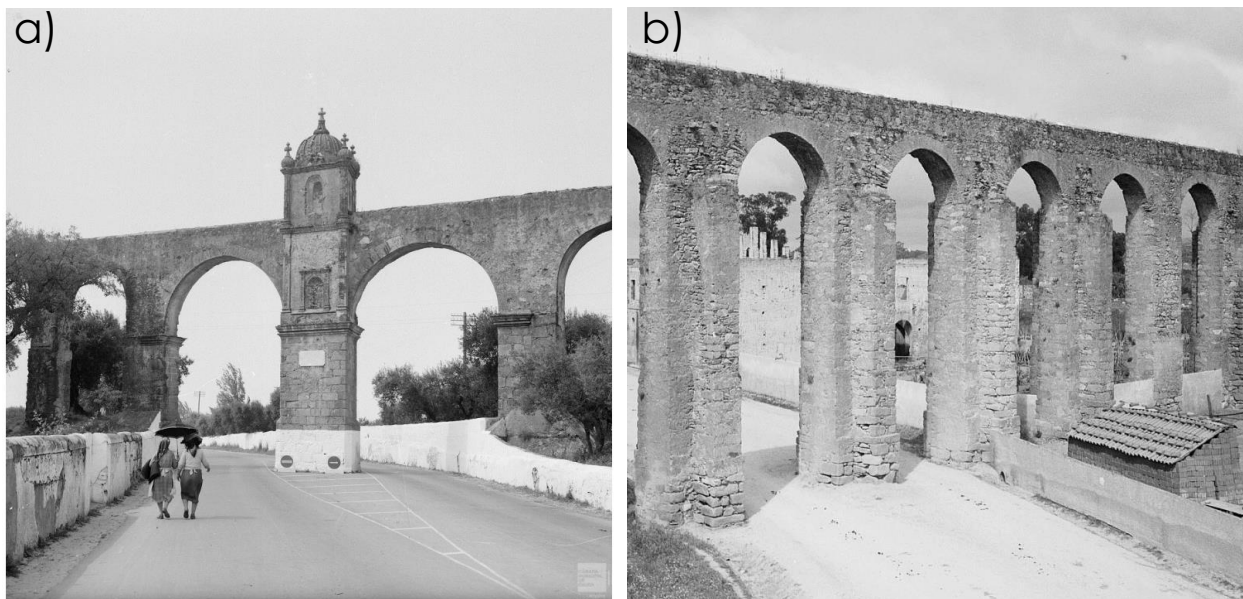


Figure 2-5. a) The monumental archway of the aqueduct, 1940-1950, AFCME (APS 351); b) Aqueduct after it exits the Fortress of Santo António, supported with buttresses, 1960s, AFCME (APS 193); (Claro, 2019).

Although the construction known today is dating back to the XVI century, with the discovery of the Roman baths in the basement of the City Hall and the water tanks next to the Roman Temple revealed the need for a hydraulic structure in the ancient Roman city (CME-DCP, 2018). Based on the previous academic studies and fieldworks by the archaeologist and historian Francisco Bilou (Bilou, 2010) and the findings in the archaeological surveys carried out by archaeologist José Rui Santos in 2016 (CME-DCP, 2019) the Roman pre-existences has been revealed at the level of its foundations. Further determinations through their mortars were conducted as a part of this research in the following chapters.

As a key element for the growth of the city during its life, the aqueduct had gone through several interventions for maintenance and improvement purposes. The pipe was covered with tiles to preserve the water quality and there has been the addition of elements like water boxes and fountains in several locations (Claro, 2019). Major restoration work was needed after the Spanish siege in 1663 due to the demolishment that occurred in different parts of the structure. The work was carried out by Francisco Ferreira in the following years in the XVII century.

In 1910, the aqueduct of Água da Prata together with the fountain in Giraldo Square are classified as National Monuments. In the following years, other fountains were also involved in the classification. Some restoration works have been carried out in the 20th century for better preservation of the monument. In 2008, 'The Silver Water Route' was created by the municipality (CME) to promote the heritage and bring awareness to its social and historical value among the community. In 2015, the aqueduct of Água da Prata entered the list of the World Monument Fund (WMF). The excavations in Cartuxa and Torralva areas were also carried out in 2016 for the re-discovery of its Roman existences by the Municipality of Évora together with the Regional Directorate of Culture and Heritage in collaboration with HERCULES Laboratory of the University of Évora (CME-DCP, 2018). The architectural survey was prepared the same year by Alberto Martinez.

3 METHODOLOGY

The methodology used for the characterization of the mortars comprises a diverse set of analytical techniques that complement each other. The work contains several steps starting with the collection of samples from the most representative places of the architectural structure, sample preparation, analysis and data treatment. Sampling and sample preparation procedures will be explained consecutively in sections 3.1 and 3.2. The type of analysis includes microscopic techniques which are Stereo and Optical Microscopy, Scanning Electron Microscopy with Energy Dispersive X-ray Spectrometry (SEM-EDS), X-ray Diffraction (XRD), Thermogravimetric analysis (TGA-DTG), Acid Attack and Granulometric Analysis. The techniques used and the information obtained from them have been described in Fig. 3-1. The experimental conditions of each technique will be explained in Section 3.3.

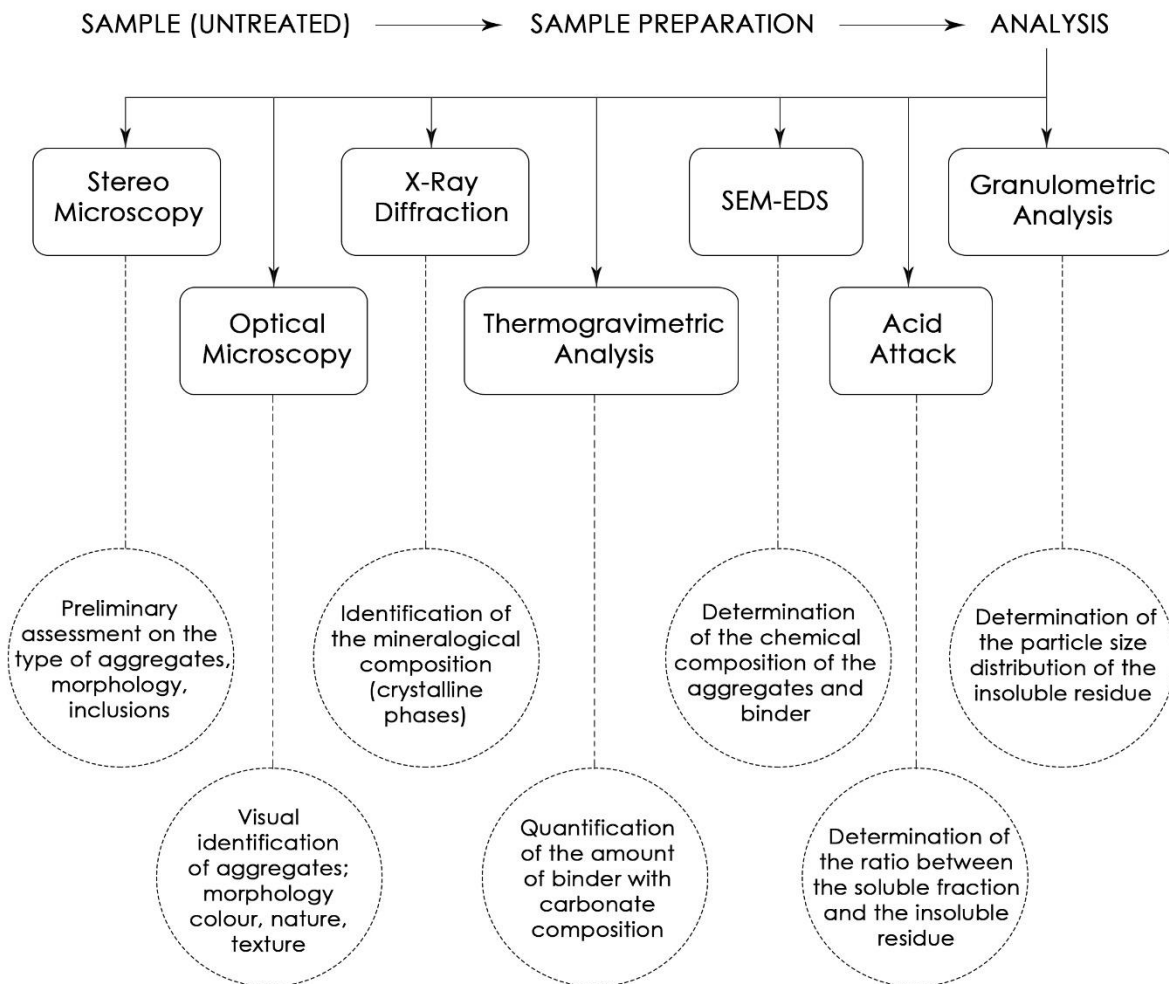


Figure 3-1. Methodology used and the information gathered for the characterization of the mortars.

3.1 SAMPLING

A total of 20 samples were obtained and studied as a part of the thesis work. All samples were collected under the 'Conservation and Consolidation Program of Aqueduct Água da Prata' carried out by Évora City Hall, Division of Culture and Heritage. The samples were acquired in two campaigns; first in 2017 and second in 2019. To be able to capture a larger set of information as much as possible, samples were selected after a detailed inspection on site so that they will be representative for different construction phases of the Roman and XVI century, restorations of the XVII century and later interventions of XVIII and XIX centuries. The extraction of samples was executed using hammer and chisel by a technical team under the coordination of the archaeologist José Rui Santos. To reduce the risk of damage, the pieces which were already loose were preferred. Sampling spots were marked and photographed, samples were deposited in plastic bags, labeled and photographed.

The first group obtained in 2017 consists of 8 samples which are all filler mortars representing Roman and XVI century construction periods. They were all acquired from archaeological survey pits from Cartuxa and Torralva sections of the aqueduct. The labels of this group were given as Aqueduct (AQD)- Evora (EVR) and followed by numbers, *i.e.* AQD-EVR-01.

From Cartuxa section, samples EVR-1, EVR-2, EVR-3, EVR-4 and EVR-6 were collected. This section is particularly selected as the remains of the foundation of the Roman aqueduct is discovered right next to the still standing XVI century aqueduct. As the foundations of the Roman and the XVI century constructions are visibly separate, it allowed the sampling of the filler mortars of both periods. Sampling was carried out from the survey pits C.1, C.-2 and C.-3 as described in Figure 3-2.

From the Torralva section, samples EVR-05, EVR-07 and EVR-08 were collected. Torralva survey pit which is located at the area of pillar 42 was chosen as a sampling spot since it contains characteristics of both Roman and XVI century constructions. As described in the technical report of the archaeological surveys, the pillars of the Torralva section indicate characteristics of XVI century construction which are supported by several inscriptions of dates 1534 and 1535 carved on the wet mortar still visible on site. Whereas the base of the pillars, demonstrate Roman characteristics of building manufacture regarding the type of blocks used for construction (*opus quadratum*) typically showing the rustic surface on the face of the ashlar stones as seen in Figure 3-3 (CME-DCP, 2018). The samples extracted from the Torralva survey pit represent filler mortars from both periods.

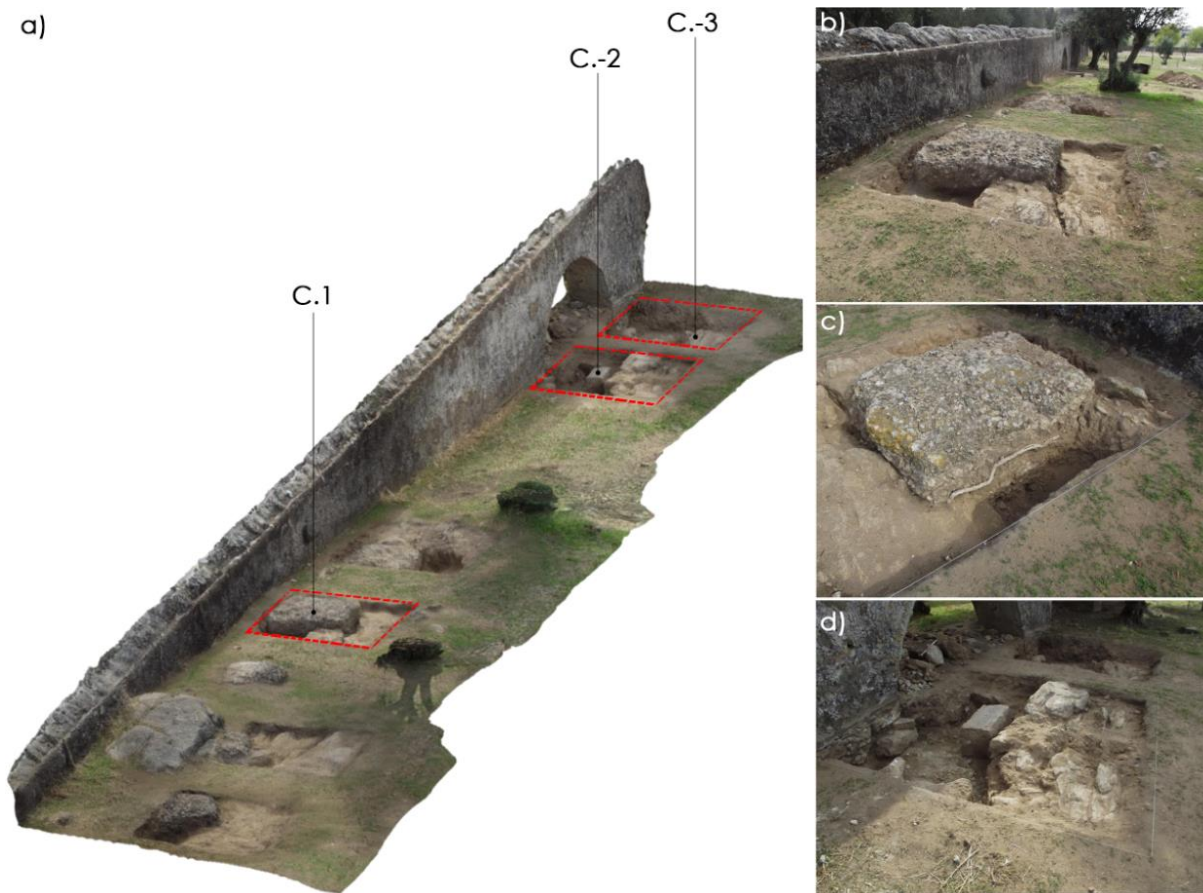


Figure 3-2. a) Photogrammetric image of the sampling pits from Cartuxa b) General view of survey pits, c) Pit C.1, d) Pits C.-2 and C.-3 (All images obtained from CME-DCP, 2018).



Figure 3-3. a-b) Photogrammetric images of Torralva survey pit, c-d) Photos of XVI century pillar and Roman base. (Photogrammetric images obtained from CME-DCP, 2018, photos taken by author in September 2020).

A total of 12 mortar samples were collected from various parts of the aqueduct from the second campaign in 2019. Samples were acquired from the 3 sections of the aqueduct which are Fortress of Santo António, Cartuxa and Torralva. They are all rendering mortars representing different construction phases, restorations and later interventions. They display a diverse set of structural or decorative needs deriving from load-bearing pillars, monumental arches, water related functions like fountains and ornamental surfaces. The labels of this group are given as Aqueduct (AQD) - Aqua da Prata (AP) and followed by numbers, *i.e.* AQD-AP-01.

From the section of Fortress of Santo António, 5 samples were collected (AP-01, AP-02, AP-03, AP-04 and AP-05). Samples AP-01 and AP-02 were obtained from the same spot in which sample AP-02 represents the inner part of AP-01 (Fig. 3-4a-b). The sampling spot was located on the southern façade of pillar 248 that is situated next to the inscription '1670' and representing most probably the period of the renovations carried out by Francisco Ferreira after the Spanish siege in 1663 (CME-DCP, 2019). Samples AP-03 and AP-04 were also obtained from the same spot in which sample AP-04 represents the inner part of AP-03. The sampling spot was located on the northern façade of pillar 248 (Fig. 3-4c-d-e). Sample AP-05 was located on pillar 246, having a pinkish chromatic layer probably belonging to later interventions of the XIX century (Fig. 3-4c-f).



Figure 3-4. a-b) Orthophoto and digital photo of sampling spots AP-01 and AP-02, c) Orthophoto of sampling spots AP-03, AP-04 and AP-05, d-e-f) Photos of the sampling spots AP-03, AP-04 and AP-05 respectively.

Another group of 5 samples (AP-06, AP-07, AP-08, AP-09, AP-10) were collected from the monumental fountain which is also located inside the fortress of Santo António. The fountain is positioned between the pillars 238-240. The water tank is found in the central part of pillar 239 that resembles a cave in which the spring flows. Both sides are decorated with mortars given colors by immersing fragments of stones, ceramics and coal. The assemblage of the mortar decoration simulates white pilasters connected together with black balusters over a white surface and below is a reddish surface framed with a black colored decoration mortar. The whole composition is enclosed with two vases on both sides together with a cornice around the top edge and a large pool on the ground (Fig. 3-5a-b-c-d). It is considered that the entire configuration of the fountain is a later intervention dating back to the XIX century. The mortar samples collected were selected to be representative of the use of different colors which are black (AP-06) acquired from the balusters, red (AP-07) a ceramic fragment from the lower panel and white (AP-08) from the background. Also, two other samples were obtained from the base of the vases on sides (AP-09) and from the exterior surface of the pool (AP-10) as shown in Fig. 3-5.

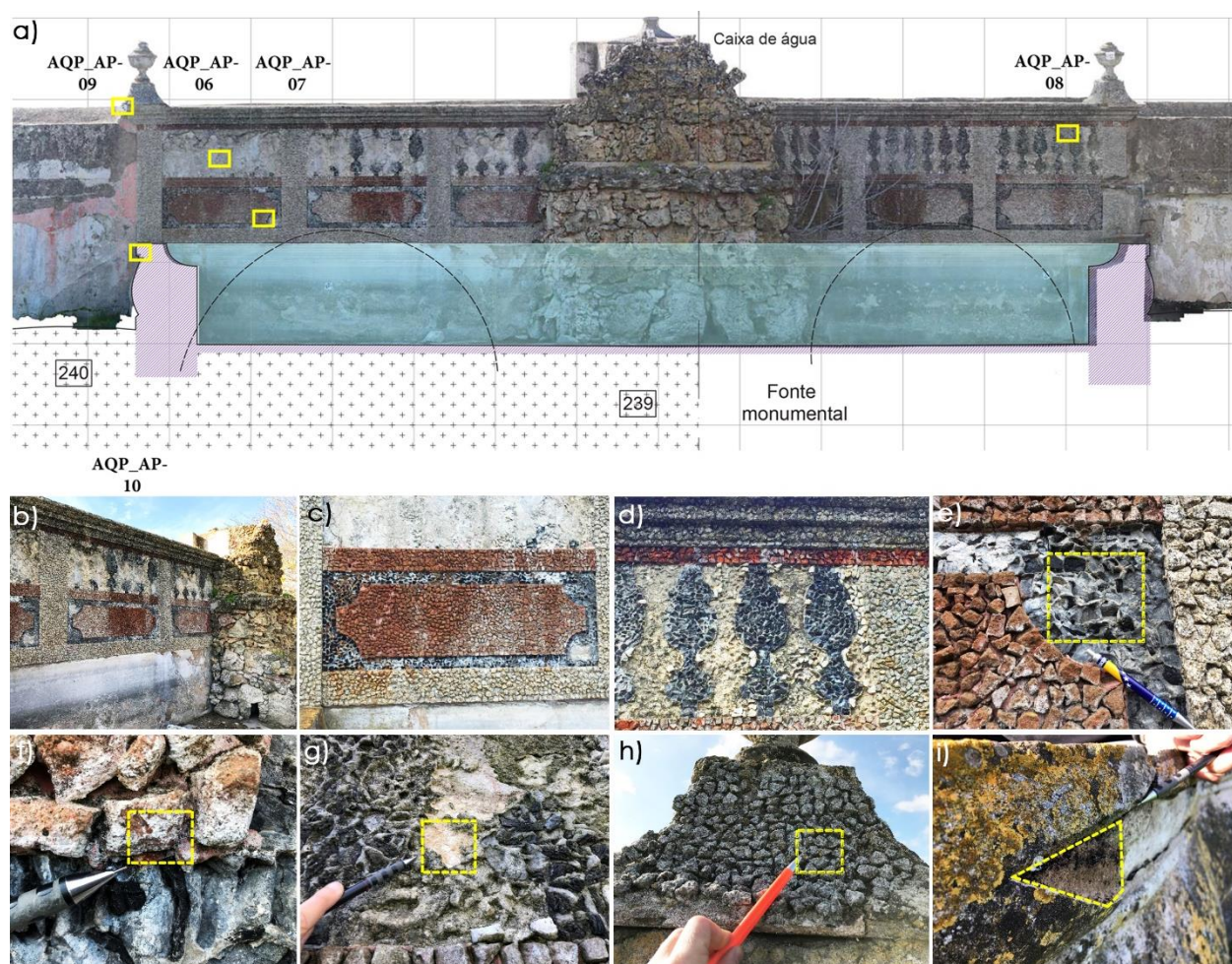


Figure 3-5. a) Orthophoto of sampling spots AP-06 – AP-10, b-c-d) Photos of the monumental fountain's decoration, e-f-g-h-i) Sampling spots of AP-06, AP-07, AP-08, AP-09 and AP-10 respectively.

From the Torralva section, sample AP-11 was collected. The render mortar was obtained from the lower part of pillar 62 (Fig. 3-6a-b). Due to the inscriptions of dates and figures found in this section of the aqueduct, it is considered that AP-11 could be a render mortar originating from the XVI century construction.

The last sample of the study (AP-12) was acquired from the monumental arch located in the Cartuxa section of the aqueduct. The sampling spot was the elevated archway that is situated on the Arraiolos- Évora road (Fig. 3-6c-d-e). As known by the inscriptions, the monumental arch was erected in the XVI century and it has been considered as a fine example of its time with its decorative style of Manueline expression (CME-DCP, 2019). The water tank is located on pillar 117 and it is connected by arches to pillars 116 and 118 on both sides of the road. Starting from the ground level until the decorative cornices, all 3 pillars have fake stone masonry with pronounced joints in white plaster which is a mural decoration technique known as *sgraffito* (Salema, 2008). The sampling was carried out on the *sgraffito* decoration on pillar 116.

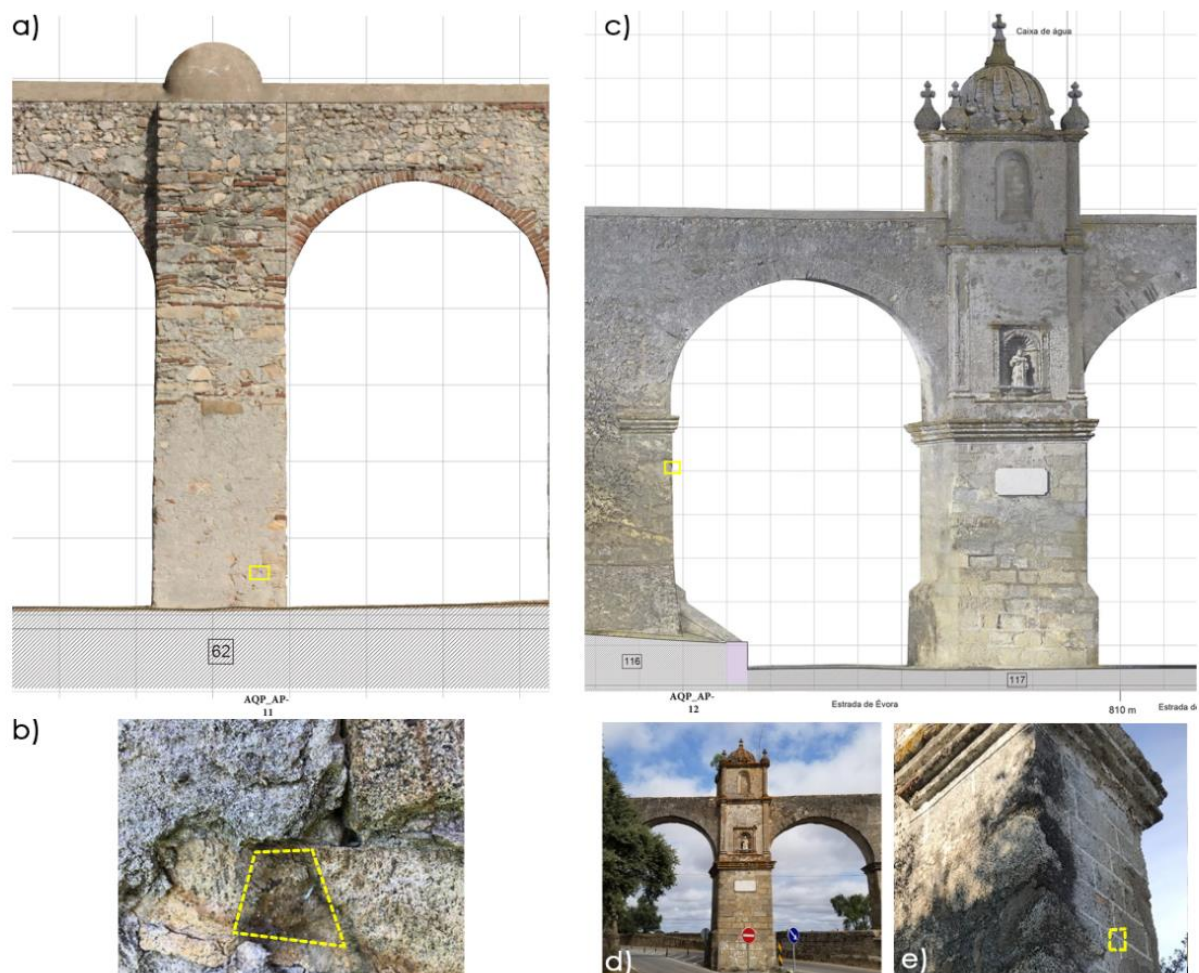


Figure 3-6. a-b) Orthophoto and digital photo of sampling spot AP-11, c-d-e) Orthophoto and digital photos of sampling spot AP-12.

Table 3-1, reports all samples consisting of; 8 filler mortars, from the Roman period (EVR-02, EVR-03, EVR-04, EVR-05, EVR-07) and XVI century (EVR-01, EVR-06, EVR-08) constructions, 11 render mortars; from XVI century (AP-03, AP-04, AP-11, AP-12), XVII century (AP-01, AP-02) and XIX century (AP-05, AP-06, AP-08, AP-09, AP-10) interventions and 1 ceramic fragment (AP-07) used for ornamental needs. Among the 11 render mortars, 5 of the samples are the productions of decorative purposes collected from the monumental fountain (AP-06, AP-08, AP-09) and mural decorations called *sgraffito* (AP-03, AP-12). Only one sample (AP-05) has a chromatic layer over its surface. The general description of all samples is presented in Tab. 3-1.

Table 3-1. General description of the samples.

Sample	Function	Period / Century	Section	Location
EVR-01	Filler mortar	XVI	Cartuxa	C.-3 survey pit (XVI c. foundation)
EVR-02	Filler mortar	Roman	Cartuxa	C.-3 survey pit (Roman foundation)
EVR-03	Filler mortar	Roman	Cartuxa	C.-2 survey pit (Roman foundation)
EVR-04	Filler mortar	Roman	Cartuxa	C.1 survey pit (<i>Opus caementicium</i>)
EVR-05	Filler mortar	Roman	Torralva	Torralva survey pit (<i>Opus quadratum</i>)
EVR-06	Filler mortar	XVI	Cartuxa	C.-2 survey pit (XVI c. foundation)
EVR-07	Filler mortar	Roman	Torralva	Torralva survey pit
EVR-08	Filler mortar	XVI	Torralva	Torralva survey pit
AP-01	Render - outer layer	XVII	Fort. of S. Antonio	Pillar 248 (southern façade)
AP-02	Render - inner layer of AP-01	XVII	Fort. of S. Antonio	Pillar 248 (southern façade)
AP-03	Render – decoration (<i>sgraffito</i>)	XVI?	Fort. of S. Antonio	Pillar 248 (northern façade)
AP-04	Render - inner layer of AP-03	XVI?	Fort. of S. Antonio	Pillar 248 (northern façade)
AP-05	Render – (has chromatic layer)	XIX	Fort. of S. Antonio	Pillar 246
AP-06	Render - decoration	XIX	Fort. of S. Antonio	Fountain (black decoration)
AP-07	Ceramic fragment	XIX	Fort. of S. Antonio	Fountain (reddish decoration)
AP-08	Render - decoration	XIX	Fort. of S. Antonio	Fountain (white decoration)
AP-09	Render - decoration	XIX	Fort. of S. Antonio	Fountain (below the vase)
AP-10	Render mortar	XIX	Fort. of S. Antonio	Fountain (exterior of the pool)
AP-11	Render mortar	XVI	Torralva	Pillar 62
AP-12	Render – decoration (<i>sgraffito</i>)	XVI?	Cartuxa	Pillar 116 (monumental arch)

3.2 SAMPLE PREPARATION

Samples have been treated by the following preparation procedures in correlation with the desired analytical technique. The relation between sample preparation and the type of analysis has been described in the following diagram Figure 3-7. Preparation procedures are divided into 3 main groups and each group is described in detail in the following sections, 3.2.1, 3.2.2, 3.2.3.

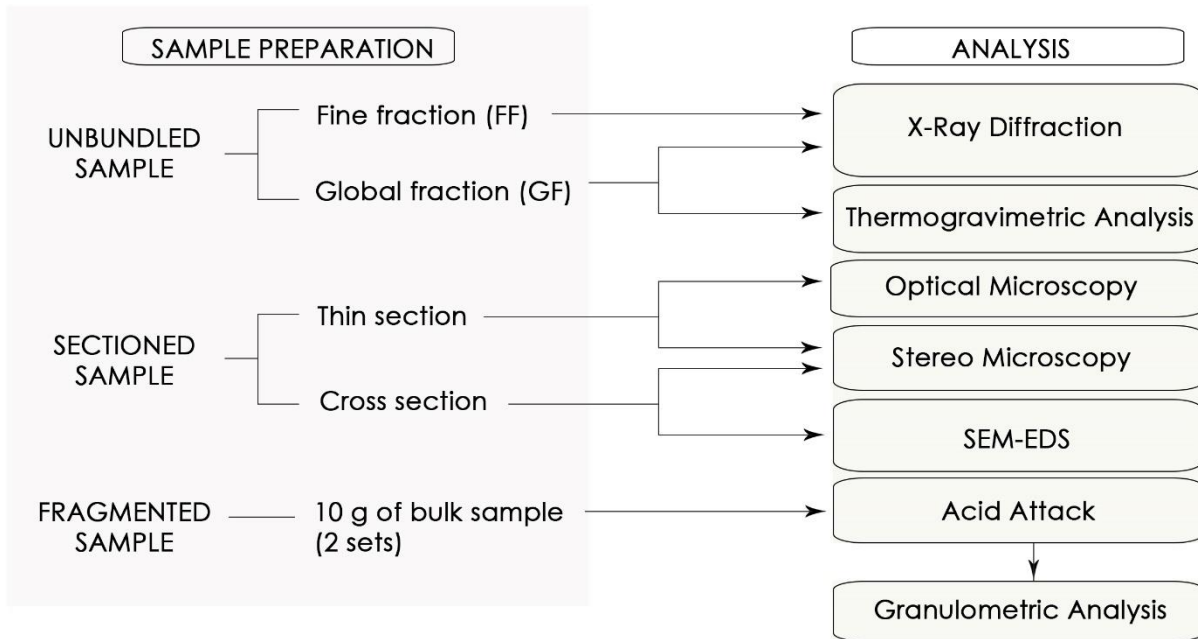


Figure 3-7. Sample preparation diagram.

Before initiating any preparation procedures, all samples were left to dry in a ventilated oven overnight at 40 °C. Later, they were cleaned with a brush, chisel and scalpel to remove the dirt, dust and any kind of biological colonization like lichens, molds and insects. Cleaned samples were once again dried in the oven overnight to guarantee a well-cleaned surface without any moisture. After the cleaning process is completed, all samples were photographed and observed for the record of their macroscopic characteristics such as color, texture, stratigraphy, type of aggregates and additives (fragments of ceramics, coal, etc.).

Among all the specimen acquired, three of the samples (AP-9, AP-10 and AP-12) had a clear stratigraphy. The stratigraphic layers were divided carefully using a hammer and chisel and labeled as 'U' for the upper layer and 'D' for the inner layer respectively at the end of the sample name, *i.e.* AQD-AP-09U.

3.2.1 Unbundled Samples - Preparation for XRD and TGA Analysis

Powdered samples were prepared for the analysis to be performed in powder XRD and TGA analysis. Two types of powders were produced which are global fractions (GF), representing the bulk sample and fine fractions (FF), containing particles smaller than 0.063 mm in size, thus representing a larger percentage of the binder.

The preparations started firstly by obtaining approximately 10 g of the samples using a hammer and chisel. The separated fragments were then disaggregated by hand into smaller fractions using a mortar and a pestle (Fig. 3-8a). Each sample was later grounded into a fine powder using a PM 100 Planetary Ball Mill (Retsch) (Fig. 3-8b). For this procedure, an agate grinding jar with 3 grinding balls (<1cm Ø) were used (Fig. 3-8c). The dry grinding was done at 500 rpm for a run of 10 minutes. The process was repeated in cases where larger grains of quartz were still present. The final product of the process was a homogeneous fine powder representing the bulk of the sample (GF). For the fine fractions (FF), the powder obtained from the segregated sample during the disaggregation by hand using a mortar and a pestle was sieved with a stainless steel test sieve (ASTM E11, 100 mm x 40 mm, Retsch) with a mesh size of 63 µm.

Both GF and FF powders were used for the mineralogical characterization by powder XRD. The two diffractograms obtained by the analysis were compared to identify the differences between the binder enriched and the global fractions. For TGA analysis 25-30 mg of GF powder was used to quantify the carbonate compositions within the bulk sample. Since the analysis of the GF powders was already performed both in XRD and TGA for the EVR sample group, sample preparations were only carried out for their FF powders.



Figure 3-8. Tools used for the preparation of the powdered samples: a) Disaggregation by mortar and pestle, b) Powdering equipment PM 100 Planetary Ball Mill (Retsch), c) Agate grinding jar and grinding balls

3.2.2 Sectioned Samples – Preparation for Optical/Stereo Microscopy and SEM-EDS

Sectioned samples were prepared as cross sections for Stereo microscopy and SEM-EDS analysis and as thin sections for petrographic analysis using Optical microscopy. Thin sections were prepared out of cross sections using TS-Method developed by Struers (Struers, 2014).

For the preparation of cross sections, a representative piece of the cleaned samples was removed using a rubber mallet and a chisel. The pieces were positioned separately facing downwards in circular mounting plastic cups, 2 cm in diameter. The larger pieces were positioned together in a larger plastic container. All pieces were later embedded in epoxy resin with a mixture of 25 parts of Struers EpoFix Resin and 3 parts of Struers EpoFix Hardener by weight. A total amount of 200 grams of resin was used for the consolidation of all AQD-AP sample group. The cross sections were later left to dry 12-16 hours at room temperature and pressure (Fig. 3-9a). After hardened, they were dismantled from the plastic containers and cut in the Discoplan-TS (Fig. 3-9b). They were later sanded and polished by hand using P #800 and P #1000 silicon carbide paper respectively to achieve a flat and smooth surface.

For the thin section preparation, glass slides were unpolished for a better penetration using Logitech PM5 on a cast iron disc with a solution of 1.5 L of water with 675 g of P #600 silicon carbide powder (Fig. 3-9c). The grinding of the slides was done at 60 rpm for a run of 65 minutes until the polished surfaces are completely removed. The glass slides were later cleaned with acetone and put on a hot plate for drying to be ready for the gluing. Cross sections were also cleaned using an air compressor before the application of the glue. For gluing, a mixture of 2 g of Buehler Epoxy Resin and 0,9 g Buehler Epoxy Hardener was prepared and applied on cross sections before they were mounted on the unpolished surfaces of the glass slides (Fig. 3-9d-e). After the application, they were left under pressure in System Abele press overnight for hardening (Fig. 3-9f). As the hardening process is over, all glasses were cleaned using a scalpel and acetone to get rid of the excessive resin. Later they were cut under vacuum using a Logitech CS10 Thin Section Cut Off Saw (Fig. 3-9g-h). The grinding of the thin sections was done in several steps that began with using Logitech PM5 on a cast iron disc with a solution of 1.5 L of water with 675 g of P #600 silicon carbide powder. The grinding was done carefully in 3 runs at 60 rpm for a duration of 15 minutes for each run. The thickness was controlled precisely after every run using Mitutoyo digital micrometer (Fig.3-9i). Final grinding and polishing were done by hand using P #1000 and P #2500 silicon carbide sand sheet respectively until the samples showed the first order Birefringence color in the Michel-Levy chart under Optical Microscope. None of the samples were coated for SEM-EDS analysis. They were photographed under stereo microscope (Fig 3-9j-k).

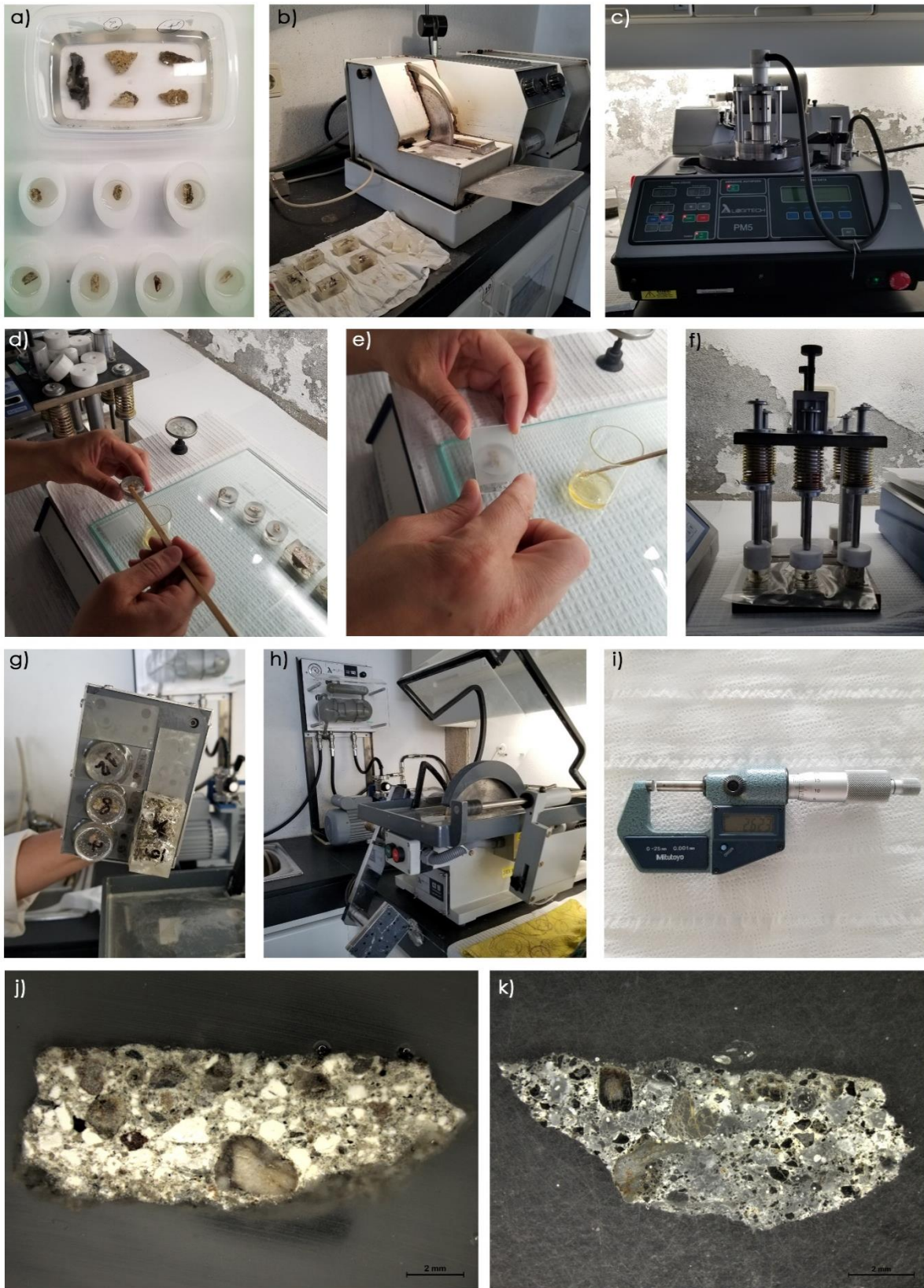


Figure 3-9. Thin section preparation: a) Samples in epoxy resin for cross sections, b) Cutting using Discolplan-TS, c) Grinding by Logitech PM5, d-e) Gluing the glass slides on cross sections, application of epoxy resin (e), f) System Abele press, g-h) Cutting out the thin sections under vacuum using a Logitech CS10 Thin Section Cut Off Saw (h), i) Mitutoyo digital micrometer, j-k) Results of AP-03, cross section (j) and thin section (k) under microscope.

3.2.3 Fragmented Samples – Preparation for Acid Attack and Granulometric Analysis

For acid attack and granulometric analysis, around 20 g of material was acquired from the samples. The samples which do not have such quantity (AP-02, AP-07, AP-09 and AP-12) were not analyzed. Sample AP-10 which showed a stratigraphy could only be analyzed on the inner layer (AP-10D) due to the lack of material of the outer layer (AP-10U). Sample AP-03 was analyzed from a total amount of 10 g since there was not enough material to obtain 20 g. Additionally, samples deriving from the 2017 campaign (EVR-01, EVR-02, EVR-03, EVR-04, EVR-06, EVR-07, EVR-08) were also subjected to preparation procedures as they were not previously analyzed. The only formerly studied sample EVR-05 was not subjected to any preparation or analysis but its results were acquired and treated together with all the others.

The sample preparation consisted of the disintegration of the samples into smaller fractions using a rubber hammer and acquiring 2 sets of 10 g of material. The selection of the material is done carefully containing a mixture of all fractions homogeneously to be able to be representative of the whole sample. The initial weights of each set were recorded before the analysis so that they could be compared with the final weights. Both sets of fragments were firstly subjected to acid attack and later to granulometric analysis. The study was performed in duplicate and the average values were recorded.

3.3 EXPERIMENTAL CONDITIONS

3.3.1 Experimental Conditions for Stereo Microscopy

Stereo microscopy was used for the preliminary assessment of the samples regarding the type of aggregates, morphology, inclusions (ceramics, coal, etc.) and identification of the stratigraphic layers. The observations were made by means of Leica M205 C Stereoscopic Microscope and the images were obtained by a Leica DFC 295 digital camera.

3.3.2 Experimental Conditions for Optical Microscopy

Optical microscopy was used for capturing information about the mineralogical structures of the samples and their morphological characteristics together with the identification of aggregates in terms of their color, texture and light reflection (Raith *et al.*, 2011). Another functional use of such technique is that it provides information about the provenance of the raw materials by correlating the mineralogical patterns of the sample with the geological data (Elsen, 2006). It was used as a complementary technique together with XRD and SEM-EDS analysis.

The analysis was carried out with a Leica DM2500 P, Modular Polarization Microscope under plane polarized light (PPL) and cross polarized light (XPL). The images were obtained by a Leica MC170 HD digital camera.

3.3.3 Experimental Conditions for X-Ray Diffraction (XRD)

X-ray Diffraction (XRD) was used for the determination of the mineralogical composition of the samples and their crystalline phases both in the global fractions representing the bulk sample and fine fractions representing more of the binder. Such analysis allows the identification of the type of binder (calclitic lime, dolomitic lime) and aggregates (siliceous, calcareous) within the mortar samples (Middendorf *et al.*, 2005).

Diffractionograms were obtained by using a Bruker D8 Discover X-ray Diffractometer with a Cu-K α X-ray generator working at 40 kV voltage and current at 40 mA. The diffractionograms were obtained at a 2θ , scanning between an angular range from 3° to 75° with a velocity of 0,05° per second measuring time by a LYNXEYE linear detector. The standard polymer sample holders filled with approximately 1 g of powdered samples were used for the analysis. The interpretation of the diffractionograms was performed using DIFFRAC. SUITE EVA software together with the Powder Diffraction Files of the International Centre for Diffraction Data (ICDD PDF)-2 database. The results obtained by XRD analysis were used as complementary with the results obtained by OM and SEM-EDS analysis.

3.3.4 Experimental Conditions for Thermogravimetric Analysis (TGA-DTG)

Thermogravimetric analysis (TGA-DTG) was used for the identification and quantification of the amount of binder with carbonate composition within the samples. For such identification, the unique patterns of the weight losses are used as a result of their physical and chemical changes throughout a heating program (Stuart, 2007). For the analysis, 25-30 mg of GF powder was put inside a platinum crucible and placed into a furnace in which the mass of the crucible is measured by a sensitive balance. The furnace is then heated under a controlled temperature program in an inert atmosphere and the changes in the sample mass are recorded in a thermogram. As a result of the analysis, a TGA curve is plotted as the sample mass (in percentage) as a function of temperature. By the use of the derivative technique, a DTG curve is also obtained from the initial thermal curve which allows us to capture the specific temperatures in high accuracy in which the characteristic changes occur (Földvári, 2011). The results of the thermogravimetric analysis were used as complementary with the results obtained by acid attack and granulometric analysis.

The samples were analyzed in a Simultaneous Thermal Analyzer STA 449 F3 Jupiter by NETZSCH, under an inert atmosphere of Nitrogen (Air Liquide Alphagaz compressed N₂) with a flow rate of 70 mL/min. The heating program was set at a linear velocity with an increase of 10°C/min starting from 40°C and until reaching to 1000°C. The quantitative analysis in the selected temperature ranges was performed by using Proteus software.

3.3.5 Experimental Conditions for Scanning Electron Microscopy – Energy Dispersive X-ray Spectrometry (SEM-EDS)

Scanning Electron Microscopy coupled with Energy Dispersive X-ray Spectroscopy (SEM-EDS) was used for image acquisition, elemental analysis and elemental mapping. The technique allows the observation of the mortar samples under high magnification and the characterization of the aggregates together with the binder by determining their chemical compositions through elemental analysis (Varella, 2013). Experimentation was carried out on the cross sections prepared according to the procedure as explained in section 3.2.2. No coating applied on the samples before the analysis.

The equipment used for the observation of the samples is a variable pressure Scanning Electron Microscope HITACHI S-3700N coupled with a Bruker XFlash 5010 with a Silicon Drift Detector (SDD) Energy Dispersive X-ray Spectrometer. The analysis was carried out under variable pressure, operated with an accelerating voltage of 20 kV and a chamber pressure of 40 Pa. The spectra for the chemical analysis were plotted on an energy scale of 0-20 keV with a spectral resolution of 129 eV at Mn K α . Data were obtained in the form of elemental distribution maps, point and multipoint analysis processed with Esprit 1.9 software. The SEM images were acquired in backscattering (BSE) mode, for capturing the information about the textural features of the samples.

3.3.6 Experimental Conditions for Acid Attack and Granulometric Analysis

By acid attack analysis, the ratio between the soluble fraction and the insoluble residue was determined. To perform the experiment, an aqueous solution of hydrochloric acid (HCl), with a concentration of 1:3 (v/v) was prepared (Fig. 3-10a). The analysis was carried out in duplicate for each set of samples prepared according to the procedure as explained in section 3.2.3. All sets were weighted and recorded for the comparison of the initial and the final weights.

The experimentation was carried out by slowly adding 120 mL of the solution into a 250mL beaker containing 10 g of fragmented sample. After the release of CO₂, the beaker was put on a

hot plate and the mixture was heated up to boiling temperature and left for 10 more minutes while stirring (Fig. 3-10b). The mixture was then cooled down by adding distilled water. After it reached room temperature, it was filtered under vacuum using a Büchner funnel and VWR grade 413 qualitative filter paper (Fig. 3-10c). During this process, the insoluble residues were washed at least twice with distilled water. After the filtration, they were left in the oven for at least 48 h at around 60°C to ensure the moisture is completely removed. The dry insoluble residues were once again weighed and recorded. The initial and the final values were plotted (Appx. 10) for the determination of the soluble fraction:insoluble residue ratio for each set of samples.

The granulometric analysis was performed for the determination of the particle size distribution of the insoluble residue that is representing the silicious aggregates within the samples. It was carried out on the resultants of the acid attack by sieving them through stainless steel test sieves ASTM E11 with a diameter of 100 mm x 40 mm by RETSCH (Fig. 3-10d). The sieves used for the analysis had mesh sizes of 4, 2, 1, 0.500, 0.250, 0.125 and 0.063 mm. To capture the granulometric distributions of the samples, the insoluble residue obtained by each sieve was weighed and recorded. Each fraction was observed under a Leica M205 C Stereoscopic Microscope and photographed by a Leica DFC 295 digital camera. The results were presented in plots and diagrams. The data was used as a complementary to the results achieved by the thermogravimetric analysis. Together they were used to determine the production of the historical mortars of the Água da Prata according to the method introduced by Hanna Jedrzejewska (Jedrzejewska, 1960).

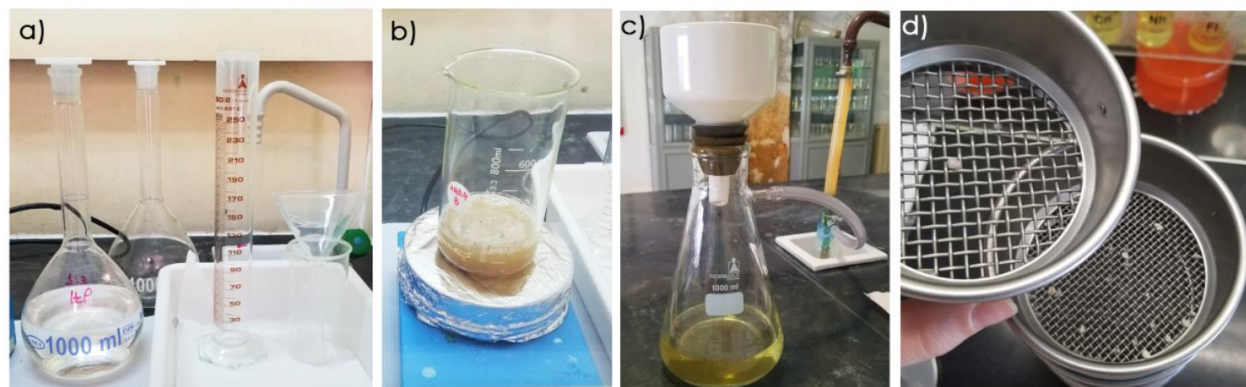


Figure 3-10. Experimentation of the analysis: a) Preparation of HCl aqueous solution, b) Heating up the sample + HCl aqueous solution on hot plate up to boiling temperature, c) Filtration under vacuum using a Büchner funnel + filter paper, d) Sieving using ASTM E11 test sieves.

4 RESULTS

Results provide the data deriving from the analytical techniques used for the study of the historical mortars of the aqueduct in terms of their production technologies, raw materials and manufacturing receipts. It gathers all information starting from preliminary assessments by Stereo Microscopy, mineralogical characterizations by Optical Microscopy and X-ray Diffraction (XRD) compositional and elemental characterizations by Thermogravimetric Analysis (TGA-DTG), Scanning Electron Microscopy coupled with Energy Dispersive X-ray Spectrometry (SEM-EDS), Acid Attack and Granulometric Analysis.

4.1 VISUAL INSPECTION AND PRELIMINARY OBSERVATIONS

Visual inspection of the samples was made to examine their macro characteristics visible to the naked eye. Such examination allowed to investigate the samples in terms of their colour, strength, identification of the stratigraphic layers and major inclusions (lime nodules, lithic fragments, *i.e.*). All samples were photographed and documented (Fig. 4-1, 4-2). Their similarities and distinctive properties were noted among the groups that represent the same construction periods or functional needs. EVR samples were not subjected to visual inspection since they were already treated with certain preparation procedures. Sample AP-07 was excluded from the comparisons with the other samples and examined separately since it was not representing a mortar but a ceramic fragment immersed inside the mortar to give a reddish colour on the surface.

According to the observations, the colours of the samples vary from greyish to brownish tones apart from sample AP-06 which has a distinctive black colour. Samples that suffered more from weathering (AP-02, AP-03, AP-08, AP-10 and AP-11) have colour changes on their surface. Samples AP-9, AP-10 and AP-12 showed a clear separation composing of lighter and darker coloured layers therefore divided into two, according to their stratigraphy.

The resistance of samples was also observed during the disaggregation. The samples showing less mechanical strength were the lighter coloured samples having decorative functions (AP-03, AP-08 and both layers of AP-12). Whereas the hardest mortar samples were AP-06 and AP-09D which are the darkest coloured (black and dark grey) samples. All the rest showed a medium mechanical strength. The inclusions visible to the naked eye were the lime nodules that appeared in all samples however, no ceramic additives were observed. In sample AP-06, fragments of coal were present embedded on its surface (Fig. 4-1). After the documentation, the coal fragments were removed from the sample before analysis.

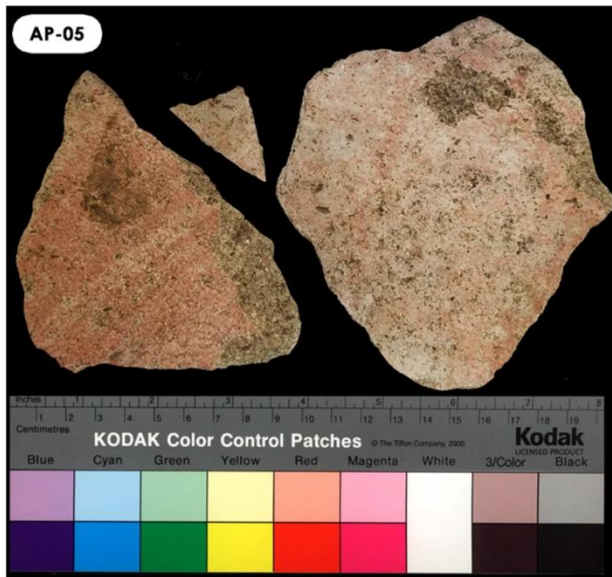
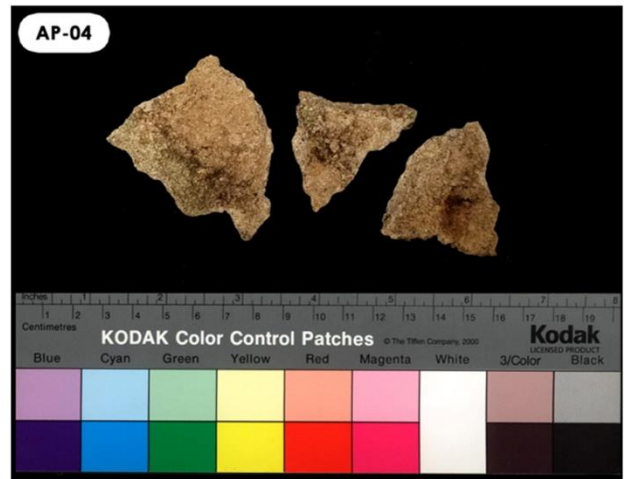
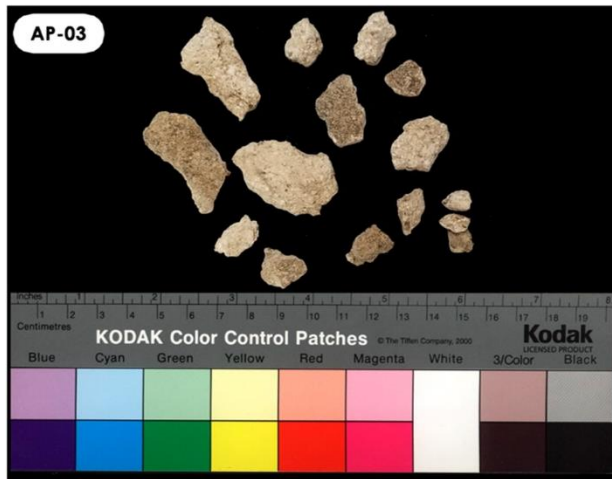
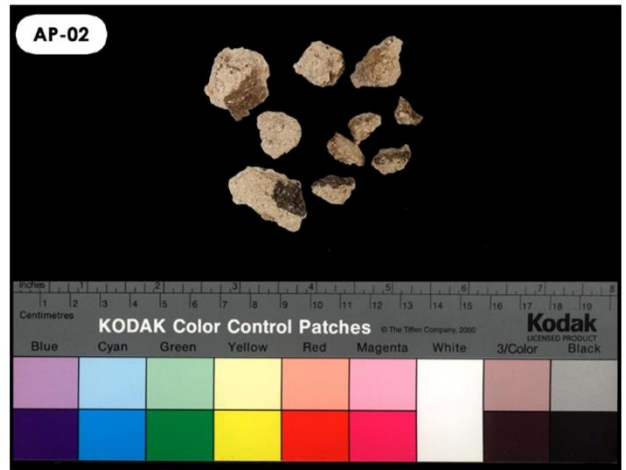
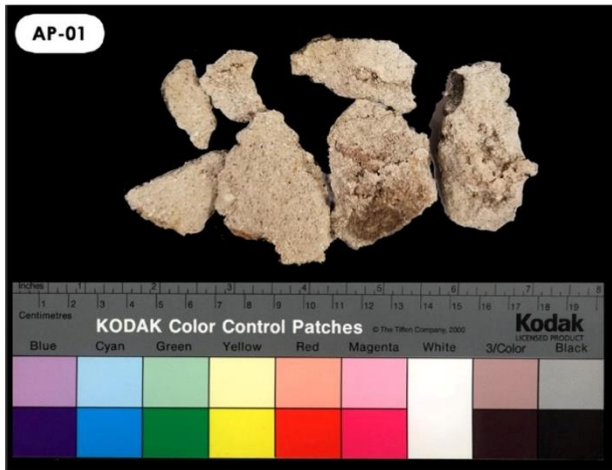


Figure 4-1. Photographic documentation of the samples before disaggregation.

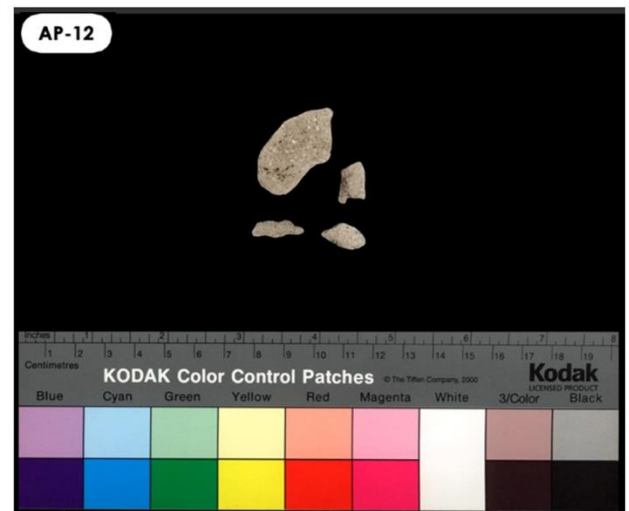
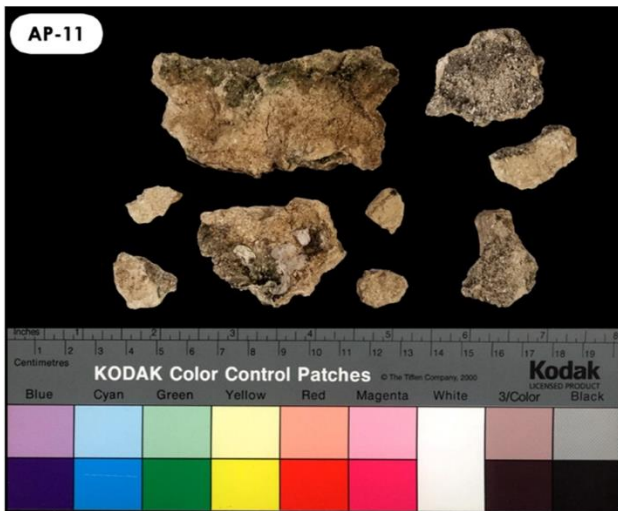
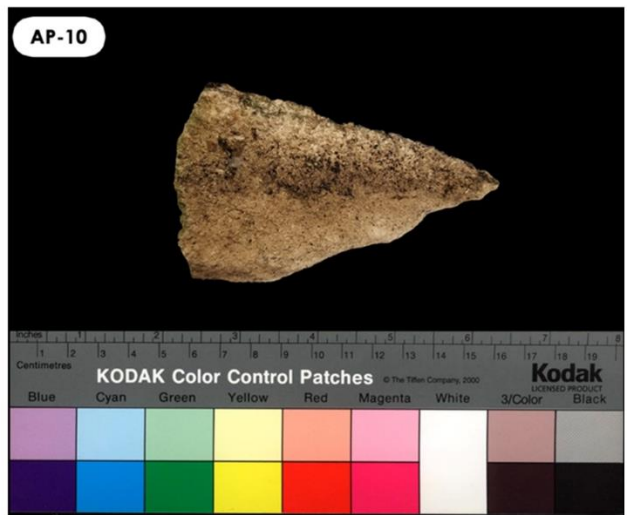
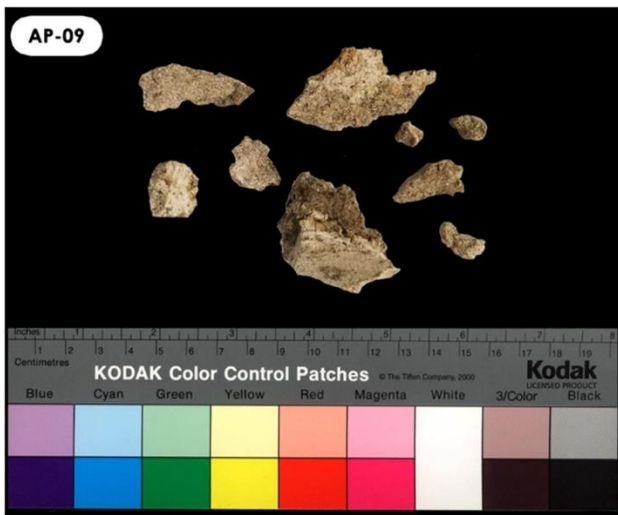
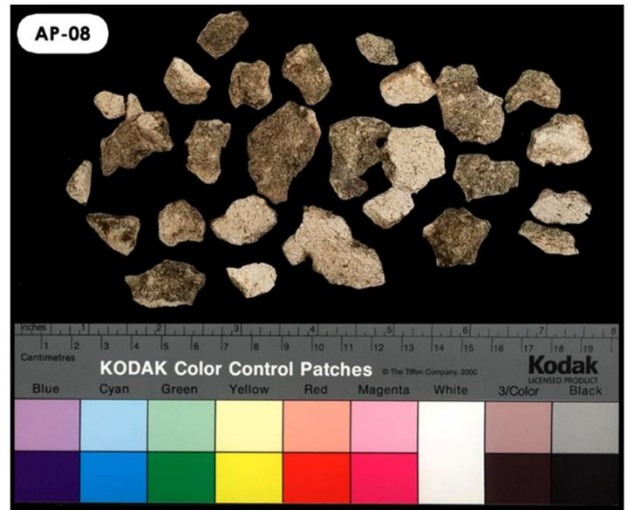
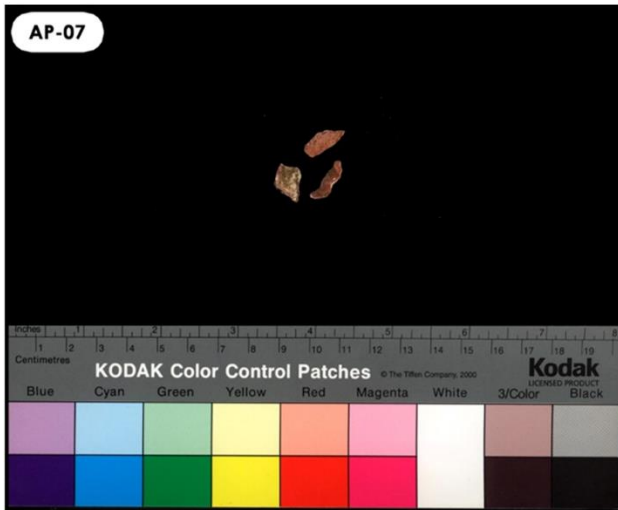


Figure 4-2. Photographic documentation of the samples before disaggregation (continuation).

4.2 STEREO MICROSCOPY

The observations made with stereo microscopy were used for supporting the preliminary data achieved through the visual inspections. The examination was carried out on polished cross sections and supplemental characteristics regarding the binder and aggregates were inspected.

Binder colour of the EVR mortar group appears to be varying between the brown tones, whereas the AP samples represented more greyish colours ranging between white to black (Tab. 4-2). The most abundant inclusion that is detected in all samples is lime lumps varying in sizes and shapes. In most of the samples, the lumps are present in round forms, which is considered as an indication of the lack of water or time during slaking while the conversion of calcium oxide, CaO, into calcium hydroxide, Ca(OH)₂ (Elsen, 2006; Adriano *et al.*, 2009; Cardoso *et al.*, 2014). On the other hand, the mortars deriving from the *sgraffito* decorations (AP-03, AP12U) has the nodules of lime that seem to have an angular appearance (Tab. 4-1) suggesting the use of crushed solid lime used as aggregates probably to achieve a whiter surface colour for the decorative needs. The samples show porous and heterogeneous character composing of aggregates of different angular morphology and sizes. The majority of the aggregates display angular to sub-angular shapes. There are large lithic fragments observed both in EVR and AP groups (Tab. 4-1). Differing from the others, sample AP-06 which has a black binder colour showed large fragments of coal and cracks were observed within the binder (Tab. 4-1).

Table 4-1. General aspect of the samples under stereo microscope.

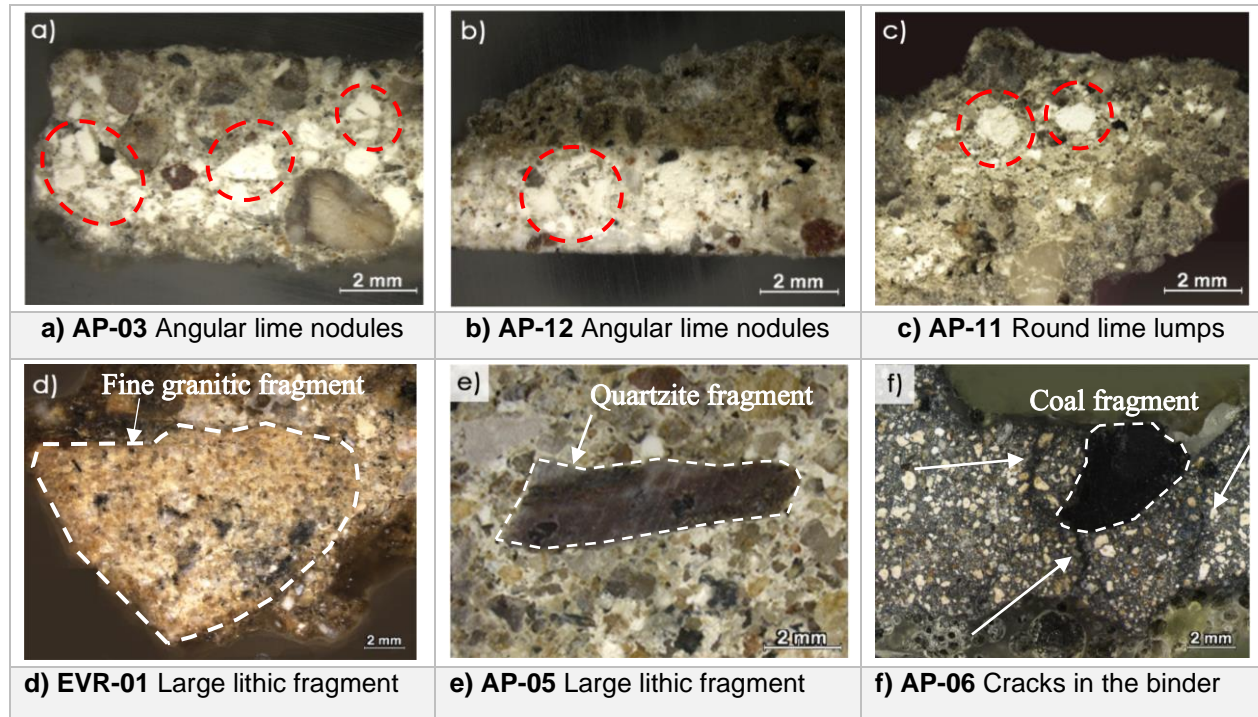
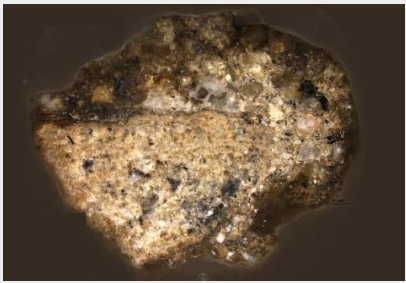
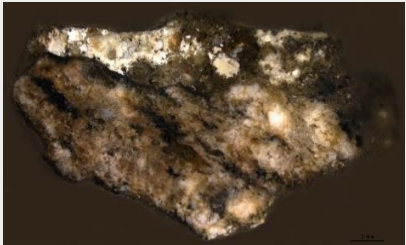
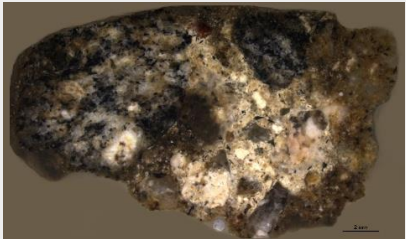
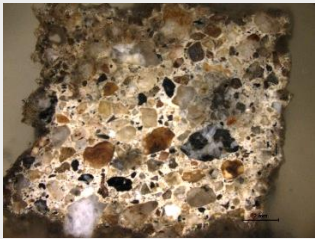
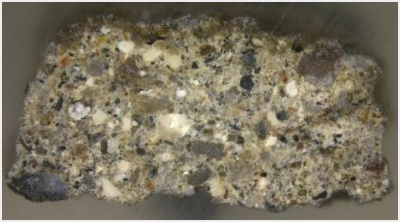
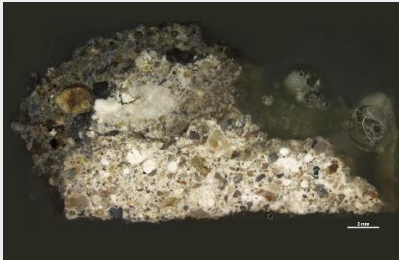
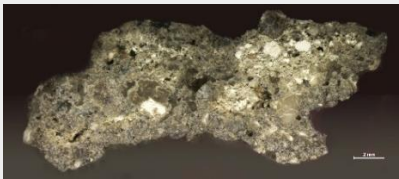
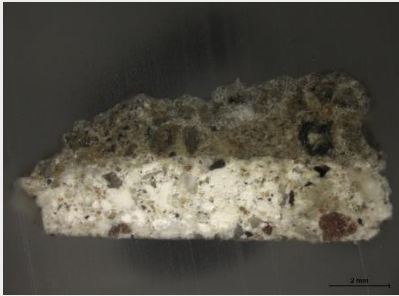


Table 4-2. Preliminary assessment and microscopic observations.

Sample	Function	Colour	Description	Cross section
EVR-01	Filler mortar from the XVI c. foundation	Brown	Aggregates sub-angular and angular, around 1 mm. Presence of large granitic fragments (15-20 mm). Small nodules of round lime lumps less than 1 mm in diameter.	
EVR-02	Filler mortar from the Roman foundation	Dark brown	Aggregates sub-angular, smaller than 1 mm. Small nodules of round lime lumps less than 1 mm in diameter. Presence of black elongated inclusions.	
EVR-03	Filler mortar from the Roman foundation	Brown	Aggregates sub-angular and angular, around 1 mm. Large nodules of lime lumps, 4 to 6 mm in diameter.	
EVR-04	Filler mortar from Roman foundation <i>Opus caementicium</i>	Dark brown	Aggregates sub-angular and angular, around 1 mm. Small nodules of lime lumps less than 1 mm in diameter. Presence of dark coloured lithic fragments.	
EVR-05	Filler mortar from Roman construction <i>Opus quadratum</i>	Dark brown	Aggregates sub-angular and angular, smaller than 1 mm. Small nodules of lime lumps less than 1 mm in diameter. Larger lithic fragments in yellowish colour.	
EVR-06	Filler mortar from the XVI c. foundation	Greyish brown	Aggregates angular, smaller than 1 mm. Nodules of sub-angular lime lumps around 1-2 mm.	

EVR-07	Filler mortar from the Roman foundation	Light brown	Aggregates sub-angular and angular (some around 2 mm). Has a light binder colour. Nodules of lime lumps around 1 mm in diameter.	
EVR-08	Filler mortar from the XVI c. foundation	Dark brown	Aggregates sub-angular and angular, smaller than 1 mm. Small nodules of lime lumps less than 1 mm in diameter. Presence of some lithic inclusions.	
AP-01	Render mortar from XVII c. restoration	Grey	Aggregates sub-angular and angular, around 1 mm. Small nodules of lime lumps. Has medium mechanical strength.	
AP-02	Render mortar from XVII c. restoration	Grey	Aggregates sub-angular and angular, around 1 mm. Small nodules of lime lumps. Presence of black elongated inclusions. Has medium mechanical strength.	
AP-03	Decoration mortar from <i>sgraffito</i> XVI? c.	Whitish/ Light grey	Aggregates sub-angular and angular, around 1-2 mm. Large nodules of lime lumps in angular forms, possibly crushed limestones. Has low mechanical strength.	
AP-04	Render mortar from XVI? c. construction	Grey	Aggregates sub-angular and angular, around 1-2 mm. Small nodules of lime lumps less than 1 mm in diameter. Has medium mechanical strength.	
AP-05	Render mortar from the later interventions of XIX c.	Grey	Aggregates sub-angular and angular, around 1-2 mm. Large nodules of lime lumps up to 5 mm. Presence of a large quartzite fragment 7 mm in length. Has chromatic layer over its surface. Shows medium mechanical strength.	

AP-06	Decoration mortar from the XIX c. fountain	Black	Aggregates sub-angular and angular, smaller than 1 mm. Large nodules of lime lumps up to 3 mm. Presence of a large coal fragment (6 mm). Visible cracks in the binder. Has high mechanical strength.	
AP-07	A ceramic fragment from the XIX c. fountain	Reddish	A piece of ceramic that is submerged inside the mortar to achieve a reddish surface colour. Used for decorative purposes. Brittle.	
AP-08	Decoration mortar from the XIX c. fountain	Light grey	Aggregates sub-angular and angular, around 1-2 mm. Nodules of lime lumps around 1-2 mm in diameter. Has low mechanical strength.	
AP-09	Decoration mortar from the XIX c. fountain	AP-09D Dark Grey	Aggregates sub-angular and angular, up to 2 mm. Has high mechanical strength. Inclusions of lithic fragments.	
		AP-09U Light grey	Aggregates sub-angular and angular, around 1 mm. Lime lumps up to 1 mm. Has medium mechanical strength.	
AP-10	Render mortar from the external façade of the pool from XIX c. fountain	AP-10D Grey	Aggregates sub-angular and angular, less than 1 mm. Has medium mechanical strength.	
		AP-10U Light grey	Aggregates sub-angular and angular, less than 1 mm. Lime lumps up to 1 mm. Has medium mechanical strength.	
AP-11	Render mortar from the XIX c. construction	Grey	Aggregates sub-angular and angular, around 1 mm. Nodules of lime lumps around 1-2 mm in diameter. Has medium mechanical strength.	
AP-12	Decoration mortar from <i>sgraffito</i> XVI? c.	AP-12D Grey	Aggregates sub-angular and angular, less than 1 mm. Has medium mechanical strength.	
		AP-12U White	Aggregates sub-angular and angular, less than 1 mm. Nodules of lime lumps in angular forms, possibly crushed limestones. Has low mechanical strength.	

4.3 OPTICAL MICROSCOPY

Optical microscopy was used on the thin sections for a better understanding of the texture (porosity and fractures), nature and identification of the aggregates (minerals, lithics, ceramics, *i.e.*) that would help to study possible provenances of the components. AP mortar samples were inspected under petrographic microscope for the identification of their aggregates (minerals, lithics) and their morphological characteristics as well as the textural features of their binder.

The majority of the samples displayed a similar mineralogical character based on their aggregate composition. The main mineral abundant in all samples were quartz in angular and sub-angular forms as well as feldspars (K-feldspar and plagioclase), amphiboles and micas (muscovite and biotite). Other minerals detected in some samples were pyroxene, olivine and calcite (AP-01, AP-02, AP-08, AP-09, AP-12) (Tab. 4-4). Quartz grains were found both as single grains and in association with feldspars as lithic fragments as a result of disaggregation of the granitic rocks. In terms of the morphology, render mortars (AP-01, AP-02, AP-04, AP-05, AP-10 and AP-11) showed larger grain sizes and bigger aggregate/binder ratios compared to the decoration mortars (AP-03, AP-06, AP-08, AP-09 and AP-12) which had smaller grains and more binder (Tab. 4-3).

Table 4-3. Petrographic images, representing render (a, b, c) and decorative (d, e, f) mortars.

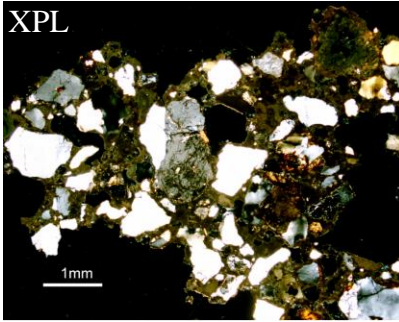
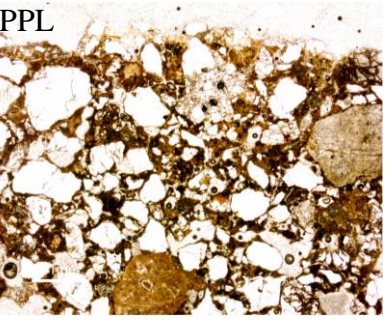
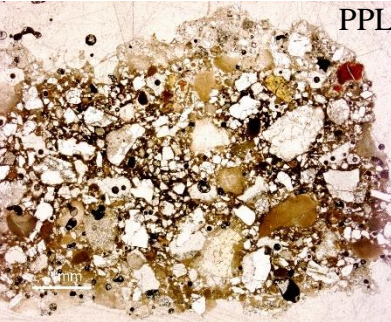
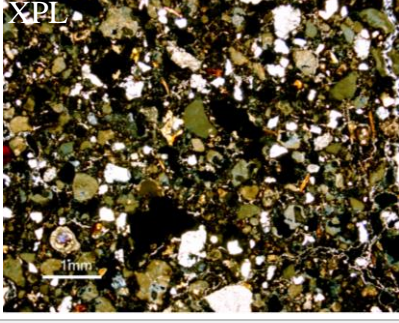
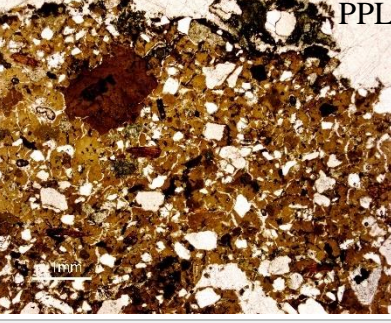
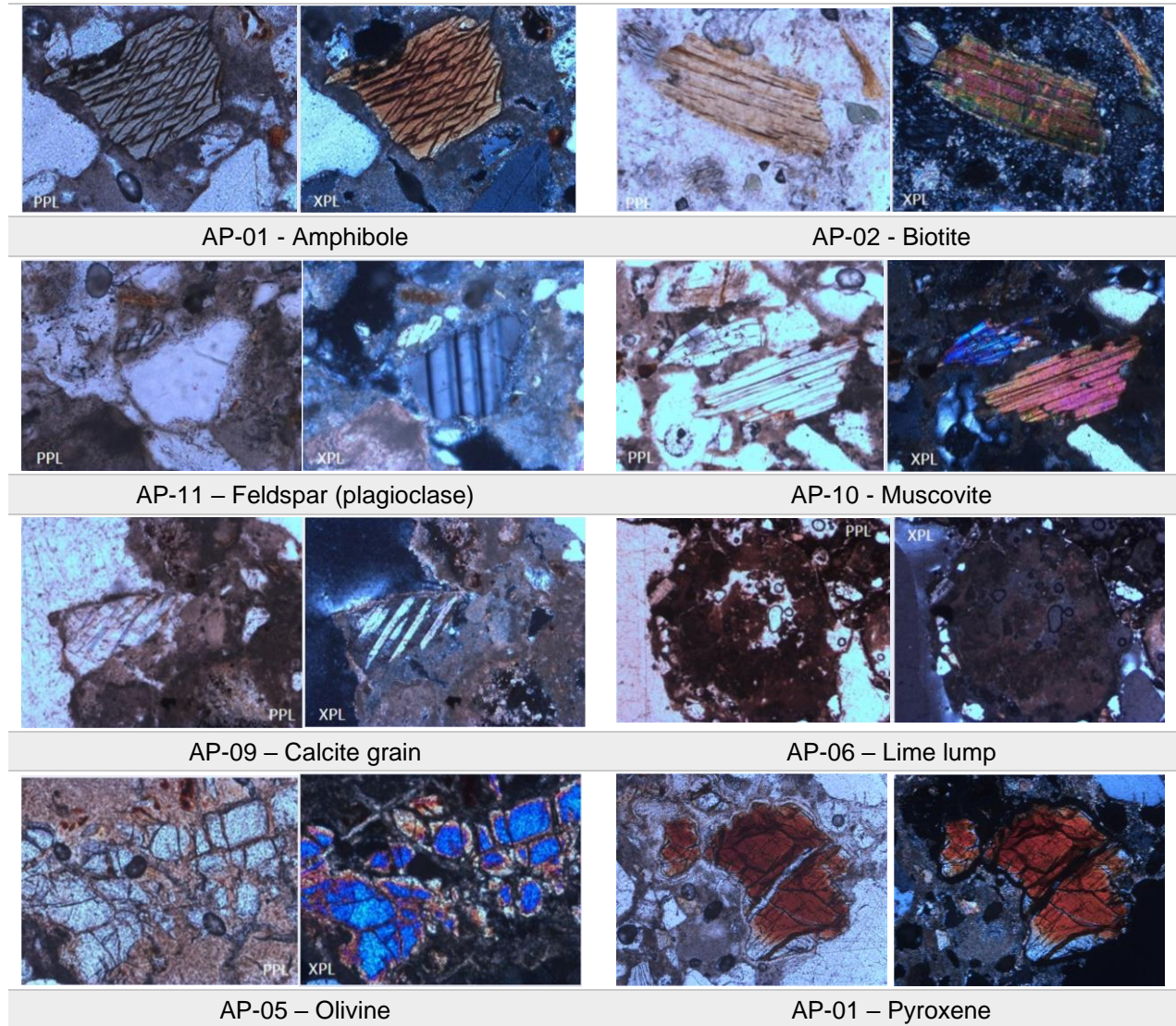
 <p>XPL</p>	 <p>PPL</p>	 <p>PPL</p>
<p>a) AP-04 Quartz grains both single and in association with feldspars and micas, lime lumps present</p>	<p>b) AP-05 Quartz, feldspars, micas, amphibole, rock fragments (quartzite) and lime lumps are present.</p>	<p>c) AP-01 Quartz, feldspars, micas, amphibole, weathered rock fragments and nodules of lime lumps are present.</p>
 <p>XPL</p>	 <p>PPL</p>	 <p>PPL</p>
<p>d) AP-06 Quartz, feldspars, micas, amphibole, numerous lime lumps are present. (grains smaller in size)</p>	<p>e) AP-03 Quartz, feldspars, micas, amphiboles and numerous nodules of lime lumps are present. (grains smaller in size and more binder)</p>	<p>f) AP-08 Quartz, feldspars, micas, olivine and large/small nodules of lime lumps are present. (grains smaller in size)</p>

Table 4-4. Images of the isolated minerals observed under XPL (cross polarized light) and PPL (plane polarized light).



Lime lumps were observed in all samples confirming the preliminary assessments by stereo microscopy. Within the binder of the decorative mortars (AP-03, AP-06, AP-08, AP-09 and AP-12) it was possible to observe carbonated grains which were not as distinguishable as they share a similar composition with the binder itself and did not define a very clear shape (Fig. 4-3). Such inclusions gave the binder a continuous and homogenous appearance. These grains could also be observed in the samples that had stratigraphy (AP-09, AP-10 and AP-12). Their lighter coloured layers (AP-09U, AP-10U and AP-12U) were more enriched with carbonated grains and had fewer aggregates. Their binder was more continuous. Whereas, the darker layers of these samples (AP-09D, AP-10D, AP-12D) were composed of more aggregates mostly smaller in sizes (< 0,5 mm) and had less amount of binder (Fig. 4-3).

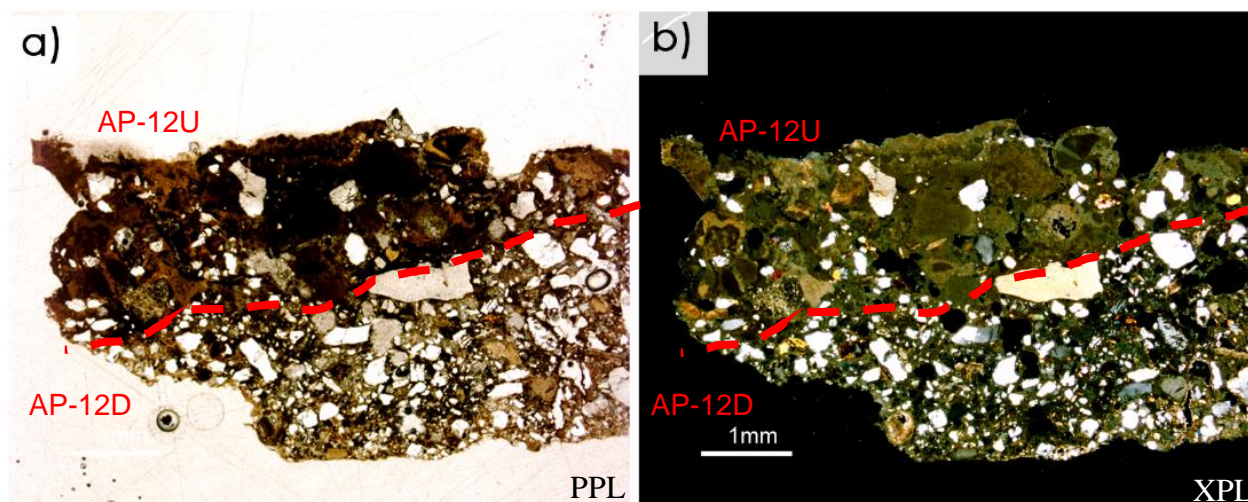


Figure 4-3. Representative petrographic images of AP-12, PPL(a) and XPL(b); AP-12U (referring the whiter layer); presence of carbonated grains within the binder forming a more homogenous appearance, AP-12D (referring the darker layer); has more aggregates and less binder.

4.4 X-RAY DIFFRACTION (XRD)

The mineralogical composition of both EVR and AP mortar groups were determined by means of powder X-ray diffraction. Samples that have stratigraphy were analysed separately for each layer. Experimentation was carried out both in global and fine fractions of the EVR mortar samples (Appx. 7-8).

The global fraction powders of the EVR mortar group indicate the predominance of quartz and feldspars (albite, anorthite, microcline and orthoclase) as the main constituents, associated with calcite in minor amounts. Among the foundation mortars, a rather high predominance of calcite was spotted in samples EVR-01 and EVR-08 and in trace amounts in EVR-02. Micaceous minerals (biotite and muscovite) and amphibole were also detected as accessory minerals. The amount of amphibole was significantly higher in samples EVR-05, EVR-07 and slightly lower in EVR-06, EVR-08 and not detected in EVR-01, EVR-02 and EVR-03. Vermiculite was also present in samples EVR-05, EVR-06 and in small amounts in EVR-01, EVR-02 and EVR-08. It was not detected in EVR-03, EVR-04 and EVR-07.

The analysis of the fine fractions of the EVR samples demonstrated an increase in proportions of calcite. Calcite abundance was more significant in the XVI century samples (EVR-01, EVR-06 and EVR-08) (Fig. 4-4) whereas, the Roman samples (EVR-02, EVR-03, EVR-04, EVR-05 and EVR-07) showed slightly smaller changes in the calcite amounts (Fig. 4-5). The mineralogical compositions of GF and FF powders are resumed in Tab. 4-5.

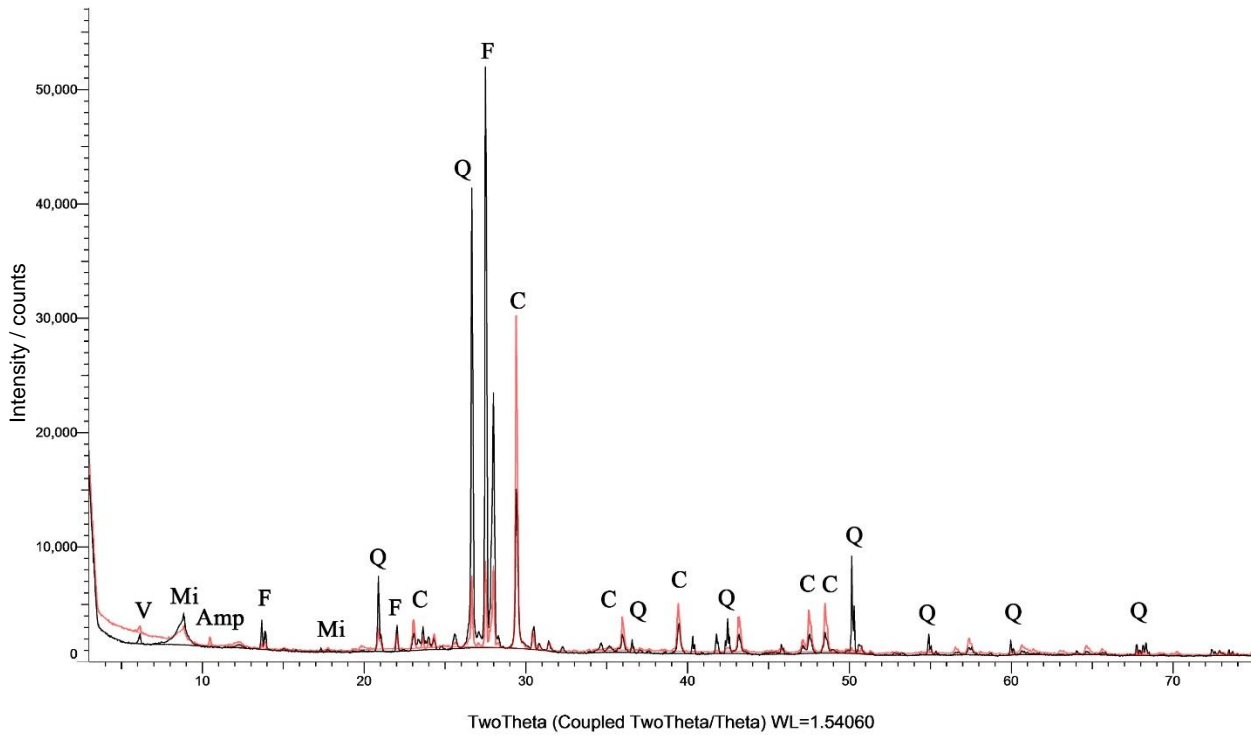


Figure 4-4. Representative XRD pattern of the XVI century filling mortar; diffractogram of EVR-01 GF (black), FF (red), (Q: quartz, C: calcite, F: feldspar, Mi: mica, Amp: amphibole, V: vermiculite)

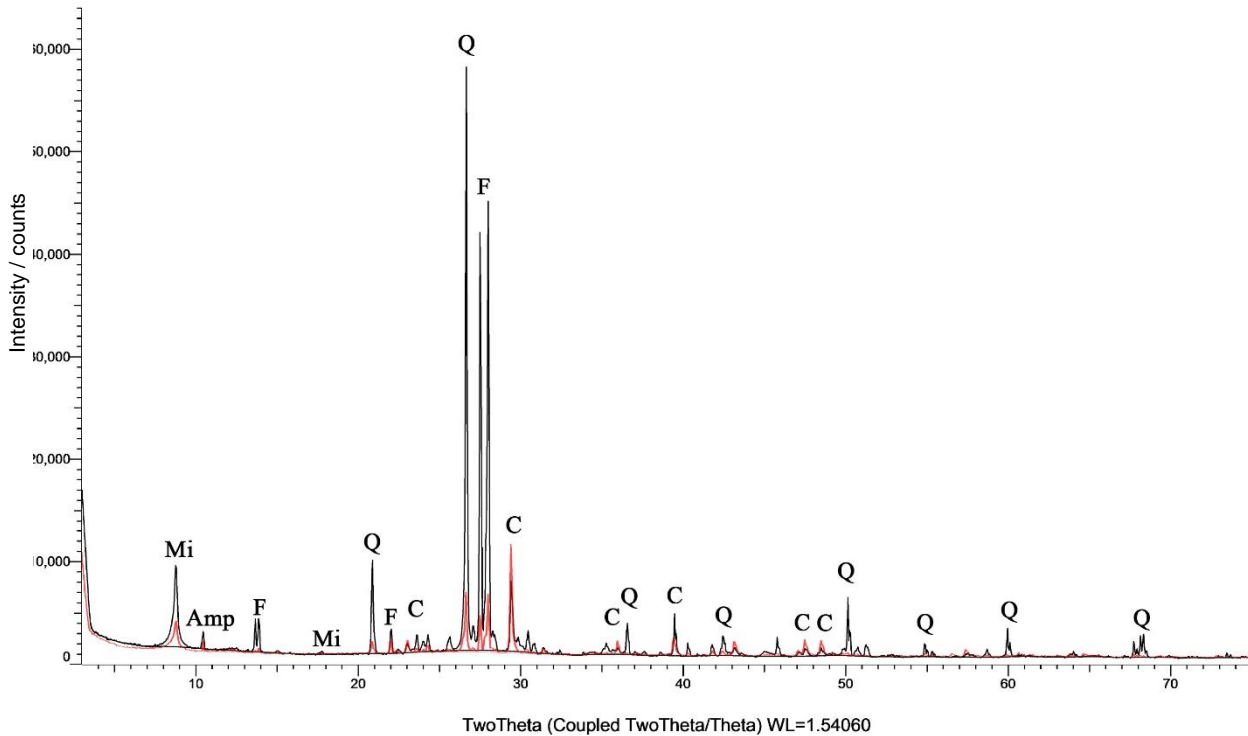


Figure 4-5. Representative XRD pattern of the Roman filling mortar; diffractogram of EVR-04 GF (black), FF (red), (Q: quartz, C: calcite, F: feldspar, Mi: mica, Amp: amphibole, V: vermiculite)

Table 4-5. Mineralogical compositions of the GF and FF powders of EVR samples by XRD analysis (Peak intensity: +++++, very abundant; +++, abundant; ++, present; +, small amount; -, undetected).

Sample		Quartz	Calcite	Feldspar	Mica	Chlorite	Amphibole	Vermiculite
EVR-01	GF	+++	++	++++	+	+	-	+
	FF	++	+++	++	+	+	+	+
EVR-02	GF	++++	+	+++	+	+	-	+
	FF	++	++	++	+	+	+	+
EVR-03	GF	++++	+	++++	++	+	-	-
	FF	++	+++	++	++	+	+	+
EVR-04	GF	++++	+	+++	+	+	+	-
	FF	++	+++	++	+	+	+	-
EVR-05	GF	+++	+	++++	+	+	+++	++
	FF	+	++	++	+	+	+++	++
EVR-06	GF	++++	++	+++	+	+	++	++
	FF	++	++++	++	+	+	++	++
EVR-07	GF	++++	+	+++	++	+	+++	-
	FF	++	+++	++	+	+	++	+
EVR-08	GF	+++	++	++++	+	+	++	+
	FF	++	++++	++	+	+	++	+

The results obtained from the AP group indicate the presence of quartz as the main constituent in most of the samples, associated with calcite and feldspars (albite, anorthite, microcline and orthoclase) (Appx. 7-8). Micaceous (biotite and muscovite), amphibole, olivine and chlorite were also identified in minor amounts as described in Tab.4-6. Calcite was more abundant in the samples having decorative purposes (AP-03, AP-06, AP-08 and AP-12U) apart from AP-09 whereas, the render mortars (AP-01, AP-02, AP-04, AP-05, AP-10, AP-11) showed lower amounts. Samples that have stratigraphy also revealed higher amounts of calcite in their lighter layers (AP-09U, AP-10U and AP-12U) in contrast to the calcite in the darker layers (AP-09D, AP-10D and AP-12-D) (Fig. 4-6 and Fig. 4-7).

The results also showed the presence of magnesium carbonates (magnesite and hydromagnesite) within the mortar compositions of certain samples of the AP group. The ones that showed clear indications of hydromagnesite were AP-06 and AP-09U whereas, AP-03 and AP-05 also had the same peaks but in lower intensities therefore less abundant. Magnesite was also identified clearly in sample AP-12U and in minor amounts in AP-03, AP-12D (Fig. 4-8). The indications of calcium and magnesium carbonates within the sample's composition suggest that dolomitic materials may have been preferred for the production of the aerial lime (Adriano *et al.*, 2009).

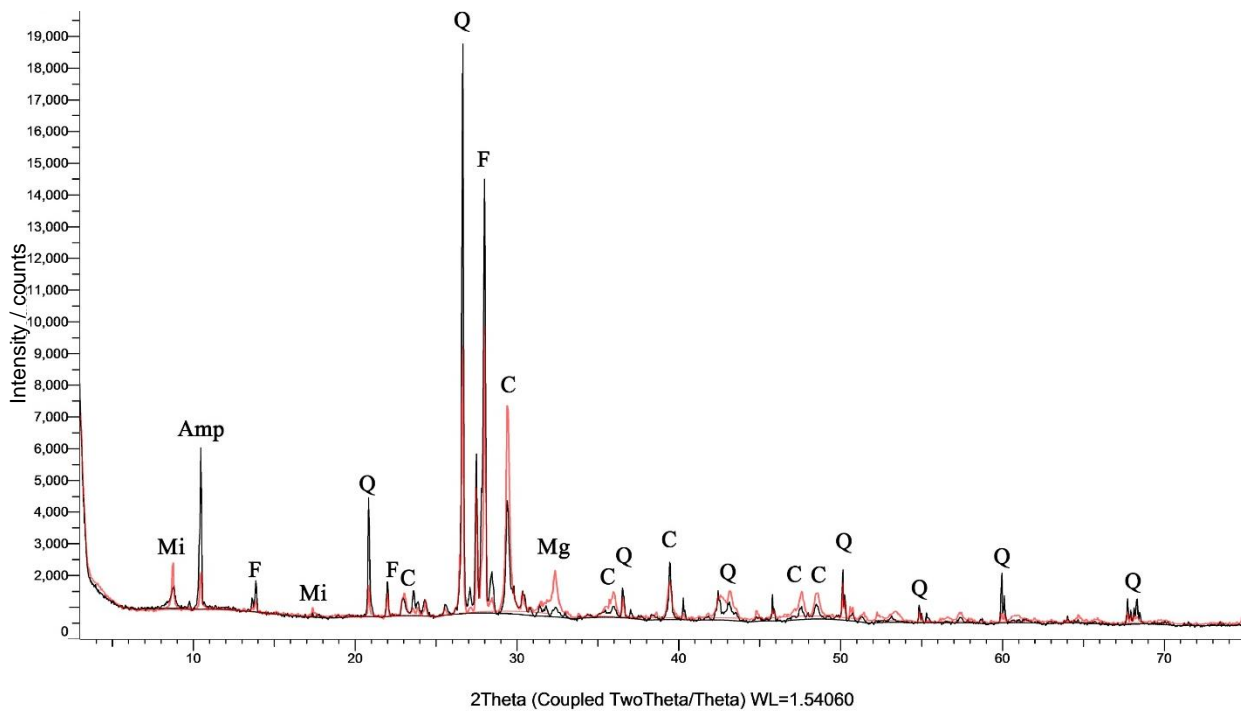


Figure 4-6. XRD Patterns of the stratigraphic layers of decorative mortar AP-12; Light coloured layer AP-12U (red), darker coloured layer AP-12D (black), (Q: quartz, C: calcite, F: feldspar, Mi: mica, Amp: amphibole, Mg: magnesite).

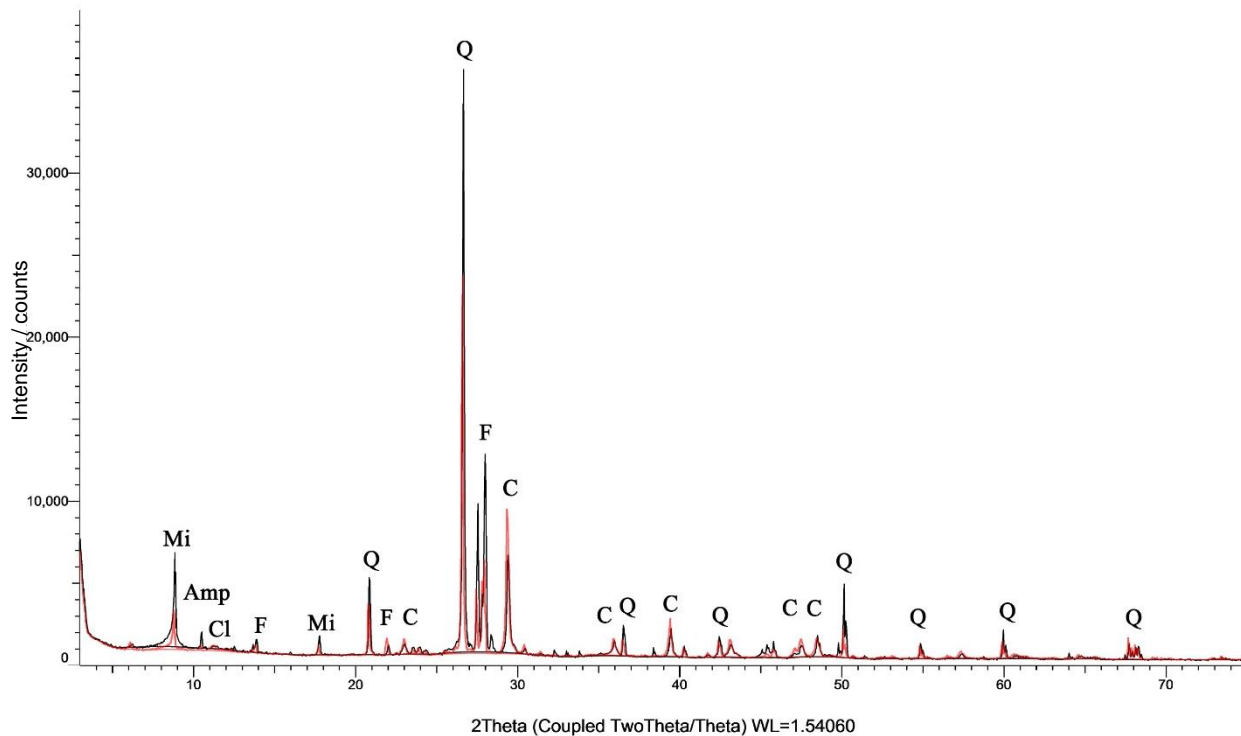


Figure 4-7. Patterns of the stratigraphic layers of the render mortar AP-10; Light coloured layer AP-10U (red), darker coloured layer AP-10D (black), (Q: quartz, C: calcite, F: feldspar, Mi: mica, Amp: amphibole, Cl: chlorite).

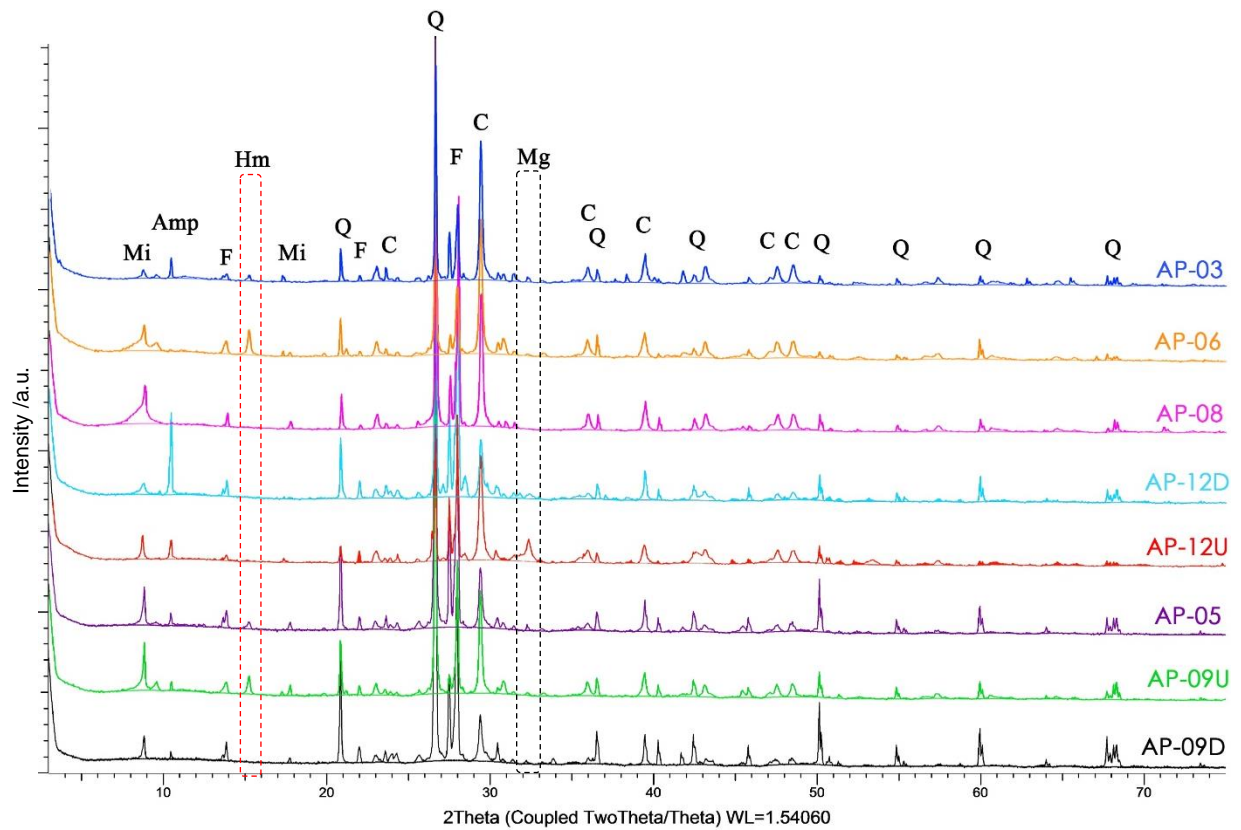


Figure 4-8. XRD Patterns of the samples with decorative use and AP-05 (Q: quartz, C: calcite, F: feldspar, Mi: mica, Amp: amphibole, Hm: hydromagnesite) (marked with red box), Mg: magnesite (marked with black box).

Table 4-6. Mineralogical compositions of the AP samples by XRD analysis (Peak intensity: +, small amount; ++, present; +++, abundant; +++, very abundant; -, undetected).

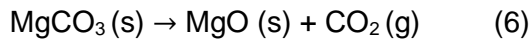
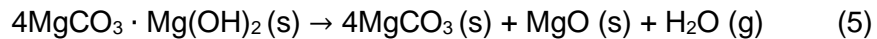
Sample	Quartz	Calcite	Feldspar	Magnesite	H. magnesite	Mica	Chlorite	Amphibole	Olivine
AP-01	+++	++	++++	-	-	+	+	+	+
AP-02	+++	++	++++	-	-	+	-	++	+
AP-03	++++	+++	+	+	+	+	-	+	+
AP-04	++++	++	+++	-	-	++	-	+	-
AP-05	++++	++	++	+	+	+	-	+	+
AP-06	++++	+++	++	+	++	+	-	-	+
AP-08	++++	+++	+++	-	-	+	-	-	-
AP-09U	++++	++	++	+	++	+	-	+	+
AP-09D	++++	+	++	+	-	+	-	+	-
AP-10U	++++	+++	++	-	-	+	+	+	+
AP-10D	++++	++	++	-	-	++	-	+	-
AP-11	++++	++	++	-	-	+	+	+	+
AP-12U	++++	+++	+++	++	-	+	+	+	+
AP-12D	++++	++	+++	+	-	+	-	++	+

4.5 THERMOGRAVIMETRIC ANALYSIS (TGA-DTG)

Thermal analysis revealed crucial information about the mortar composition by measuring the mass changes throughout a heating program, in an inert atmosphere. The thermogravimetric curve (TG) together with the derivative thermogravimetric curve (DTG) was used for the determination of the temperature ranges in which the weight changes occur. The TGA-DTG analysis was carried out on both AP and EVR groups (Appx. 9). The mass losses at each temperature range were calculated (in percentage) as shown in Tab. 4-7.

The temperature ranges were set as 40-120°C, 120-200°C, 200-650°C and 650-900°C according to significant mass losses. The weight loss at 40-120°C is attributed to the physically absorbed water and at 120-200°C to the loss of crystallization water from the hydrated salts (Elsen, Van Balen and Mertens, 2013; Leone *et al.*, 2016). Among all samples, the loss at 40-120°C varied between 0.04% (EVR-05) and 0.76% (AP-12U). The mass losses in the second range at 120-200°C differed between 0.04% (EVR-02) and 0.77% (AP-12U). The samples that have stratigraphy revealed a higher percentage of weight losses in their upper layers (AP-09U, AP-10U and AP-12U) compared to their lower layers between 120-200°C. Their weight losses were measured 0.61%, 0.62% and 0.77%, respectively.

At 200-650°C, the weight change is related to the loss of chemically bounded water. For the samples bearing hydromagnesite ($\text{Mg}_5(\text{CO}_3)_4(\text{OH})_2 \cdot 4\text{H}_2\text{O}$) and magnesite (MgCO_3), the range was divided into 3 sub-ranges according to the decompositions as represented by the equations (4), (5) and (6).



Equations (4) and (5) represent the dehydration of $(4\text{MgCO}_3(\text{s}) \cdot \text{Mg}(\text{OH})_2(\text{s}) \cdot 4\text{H}_2\text{O}(\text{l}))$ and dihydroxylation of $(4\text{MgCO}_3 \cdot \text{Mg}(\text{OH})_2(\text{s}))$ which happens between the temperature ranges 200-340°C for and 340-450°C, respectively. The last step refers to the decarbonation of magnesite according to the final equation (6) happening at the temperature range 450-550°C. Samples that showed the significant mass losses in these ranges were AP-03, AP-05, AP-06 and AP-09U compromising with the results achieved by the XRD analysis. Their weight losses were measured 1.59%, 1.17%, 3.45% and 2.59% on the first step (4), 2.93%, 2.62%, 10.07% and 6.78% on the second step (5) and 2.16%, 0.92%, 2.88% and 1.99% on the third step (6), respectively. The TG/DTG curves for samples AP-03, AP-05, AP-06 and AP-09U are shown in Fig. 4-9.

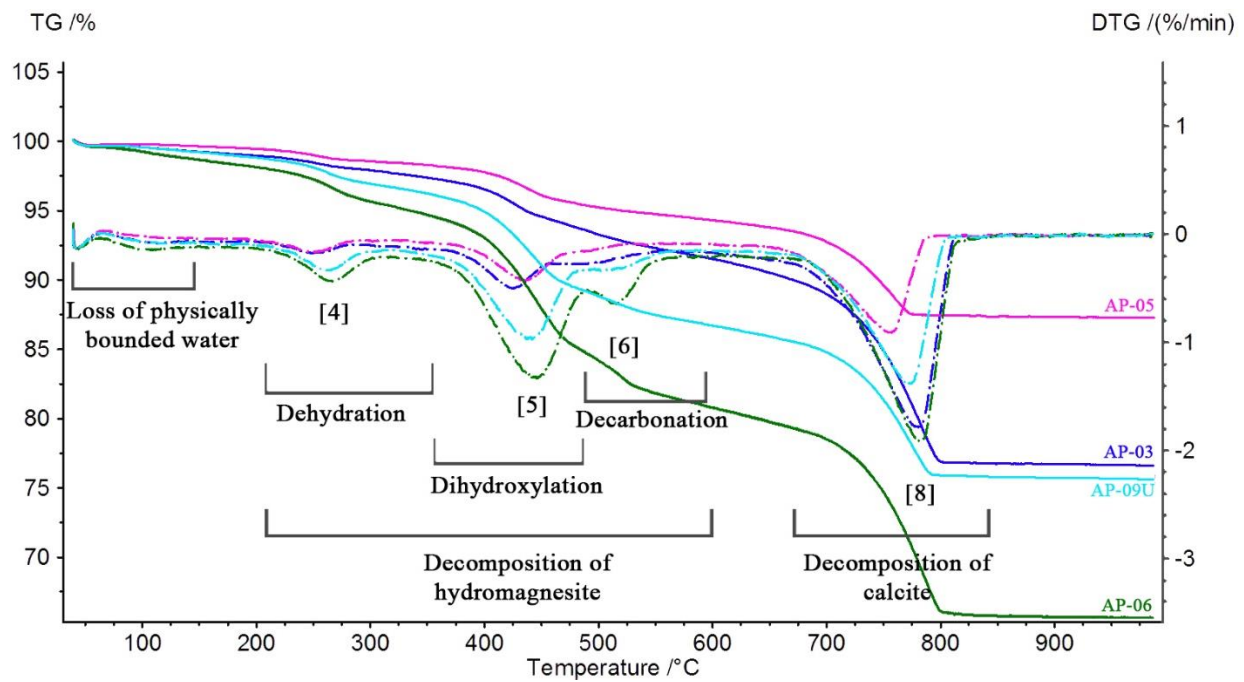


Figure 4-9. TG/DTG curves of samples AP-03 (blue), AP-05 (magenta), AP-06 (green) and AP-09U (cyan), continuous curves representing TG and dashed curve representing DTG data

Samples AP-12U and AP-12D were the two samples that contained magnesite without the presence of hydromagnesite as inferred by the XRD analysis. Both samples had their significant mass losses within the range 450-550°C due to the decomposition of magnesite ($MgCO_3$) as described above by equation (6). AP-12U revealed a larger percentage of mass loss of 14.25% bigger than AP-12D which has a loss of 5.54%, possessing a higher amount of magnesite within its composition. The TG/DTG curves for samples AP-12U and AP-12D are shown in Fig. 4-10.

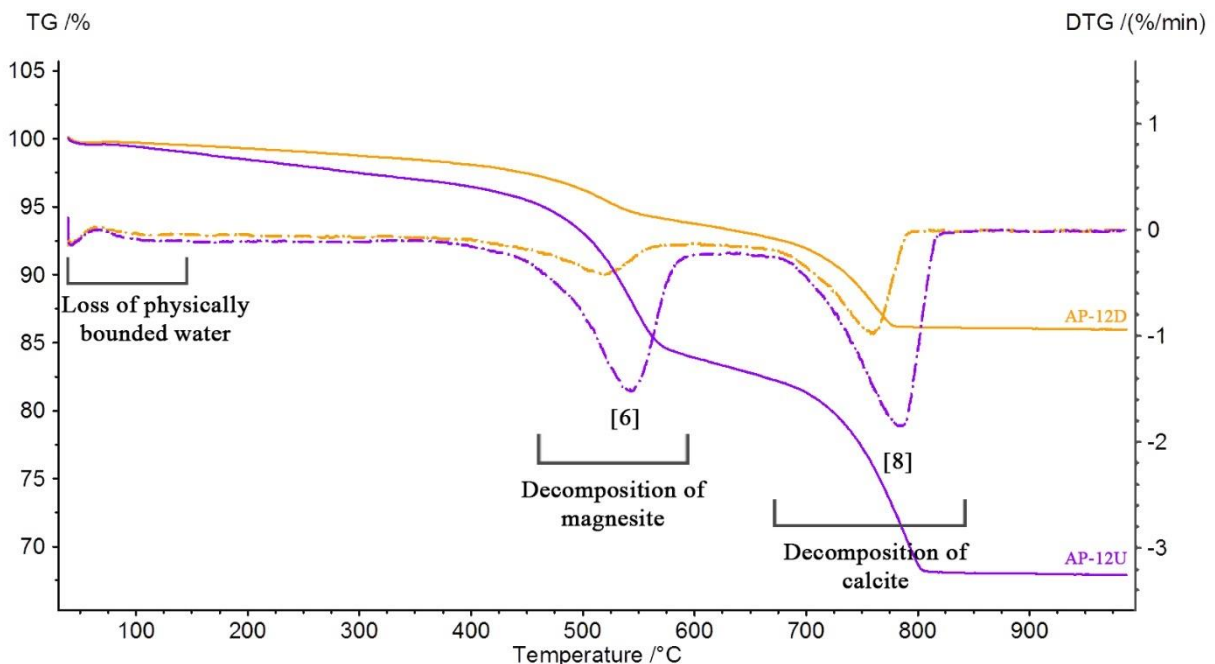
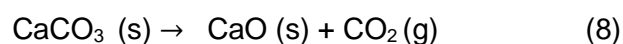
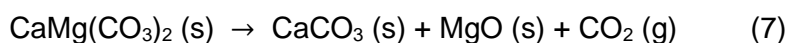


Figure 4-10. TG/DTG curves of samples AP-12U (purple), AP-12D (orange), continuous curves representing TG and dashed curve representing DTG data.

The significant mass losses of samples AP-03, AP-05, AP-06, AP-09U and AP-12 at the temperature ranges within 200-650°C suggest the use of materials with dolomitic nature was used for their production. Although not as significant, the remaining samples of the AP group (AP-01, AP-02, AP-04, AP-08, AP-09D, AP-10D, AP-10U and AP-11) also showed minor weight changes in the same range, possibly containing similar materials in smaller amounts (Tab. 4-7).

The dolomite decomposition occurs according to equation (7) and is followed by equation (8). The equation (8) represents the decomposition of calcium carbonate (CaCO₃) and occurs at the last measured temperature range that is set at 650-900°C.



In the temperature range at 550-650°C, all the samples of the AP group showed mass losses varying between 0.84% (AP-08) to 1.76% (AP-03). Their weight changes at the final temperature range (650-900°C) related to calcite decomposition differed between the lowest of 4.65% (AP-9D) and the highest of 19.44% (AP-08).

EVR mortar samples on the other hand, demonstrated mass losses only in the range at 650-900°C. Their losses varied between 0.65% to 8.92% which is a significantly narrower span compared to AP samples. The highest percentage of weight losses was achieved by the XVI century filling mortars (EVR-01, EVR-06 and EVR-08) with small variations of 8.92%, 8.49% and 8.30%, respectively. The TG/DTG curves for samples EVR-01, EVR-06 and EVR-08 are shown in Fig. 4-11. These thermograms also matched with the XVI century render mortars AP-04 and AP-11 (Appx. 9).

The filling mortars of the Roman period (EVR-02, EVR-03, EVR-04, EVR-05 and EVR-07) lost 0.65%, 2.22%, 3.04%, 4.67% and 3.83%, respectively. The comparison of the TG/DTG curves of the Roman mortars among each other allowed to detect their compositional similarities. The thermograms of the samples EVR-05 and EVR-07 which were acquired from the Torralva survey pit showed a clear match possibly deriving from a contemporary construction phase of the Roman time. Whereas, among the Cartuxa samples EVR-03 and EVR-04 were visibly similar compared to EVR-02 suggesting that they may be representative of two separate construction phases (Fig. 4-12). At the temperature range between 200-650°C the weight losses were without the presence of any peak in the DTG curves which could be related to the loss of dihydroxylation of the clay minerals.

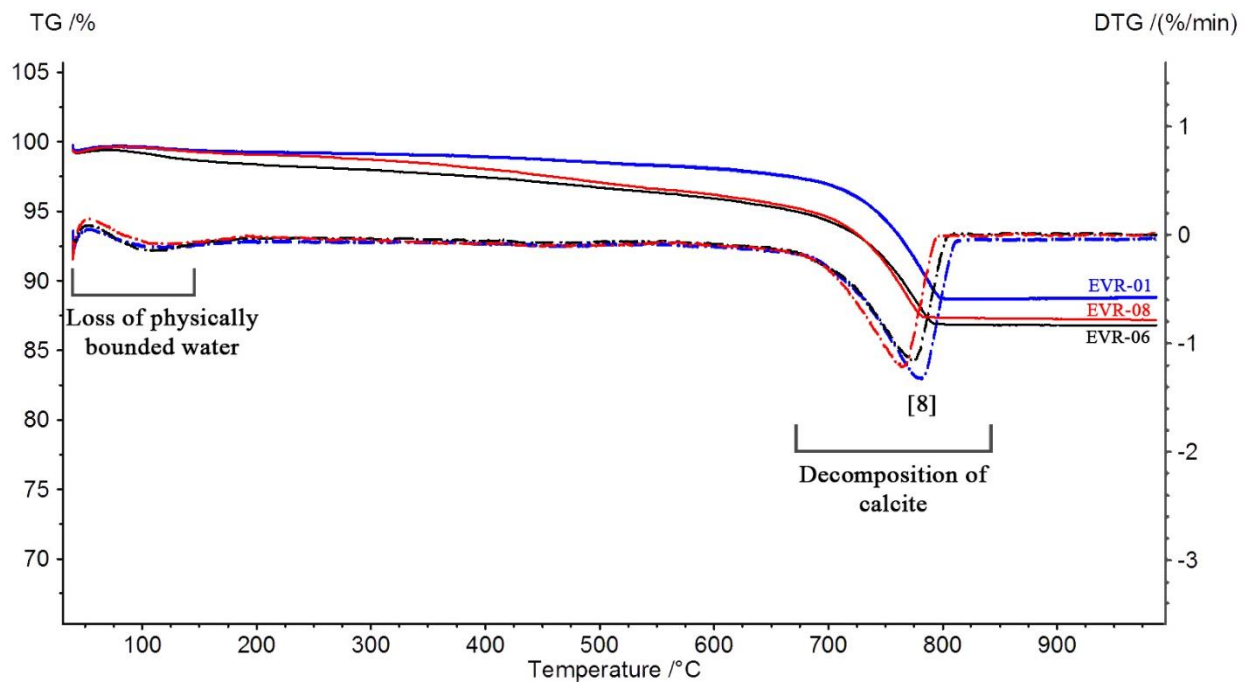


Figure 4-11. TG/DTG curves of XVI c. filling mortars; EVR-01 (blue), EVR-06 (black), EVR-08 (red); continuous curves representing TG and dashed curve representing DTG data.

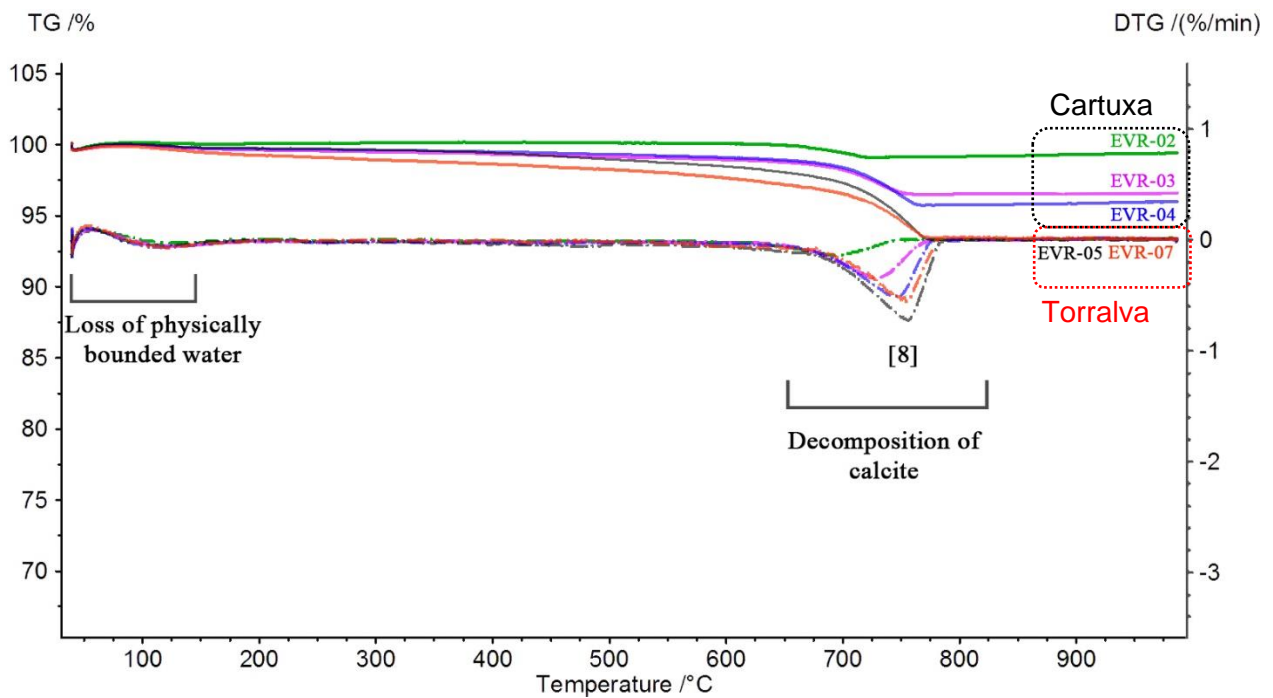


Figure 4-12. TG/DTG curves of the Roman filling mortars; EVR-02 (green), EVR-03 (magenta), EVR-04 (blue), EVR-05 (black), EVR-07 (red); continuous curves representing TG and dashed curve representing DTG data.

Table 4-7. TG/DTG temperature ranges (°C) and weight losses (%).

SAMPLES	Temperature ranges (°C) and weight losses (%)						
	40-120	120-200	200-650			550-900	
			200-450	450-550	550-650		
EVR-01	0.12	0.25		1.59		8.92	
EVR-02	0.15	0.04		0.12		0.65	
EVR-03	0.05	0.23		0.83		2.22	
EVR-04	0.07	0.18		0.78		3.04	
EVR-05	0.04	0.17		1.72		4.67	
EVR-06	0.71	0.58		3.05		8.49	
EVR-07	0.23	0.42		2.07		3.83	
EVR-08	0.50	0.39		3.51		8.30	
AP-01	0.51	0.40	1.83	1.28	1.33	10.71	
AP-02	0.47	0.33		3.20		10.75	
			200-350	350-450	450-550		
AP-03	0.61	0.47	1.59	2.93	2.16	1.76	13.81
			200-400	400-550			
AP-04	0.34	0.25	0.95	1.59		1.17	8.21
			200-350	350-450	450-550		
AP-05	0.32	0.29	1.17	2.62	0.92	0.96	6.43
			200-350	350-490	490-550		
AP-06	1.02	0.87	3.45	10.07	2.88	2.07	14.14
			200-400	400-550			
AP-08	0.31	0.24	1.23	2.06		0.84	19.44
AP-09D	0.33	0.22		2.66			4.65
			200-350	350-480	480-550		
AP-09U	0.60	0.61	2.59	6.78	1.99	1.55	10.18
AP-10D	0.49	0.43		3.66			8.75
AP-10U	0.65	0.62	2.36	1.55		1.50	13.61
			200-400	400-550			
AP-11	0.41	0.25	1.14	1.84		1.31	7.33
			200-350	350-650			
AP-12D	0.45	0.32	0.83		5.45		6.98
AP-12U	0.76	0.77	1.44		14.25		14.76

4.6 Scanning Electron Microscopy – Energy Dispersive X-ray Spectrometry (SEM-EDS)

The determinations about the chemical compositions and textural characteristics regarding aggregates and binder were made by SEM-EDS analysis. Polished cross sections were used for the experimentation to obtain the elemental mappings and point analysis. In all samples, the mineralogy of the aggregates was similar to each other whereas the binders differed significantly.

It was possible to identify the aggregates of quartz, feldspars and micas in all samples corroborating the result obtained by XRD and observations by optical microscopy. The elemental maps of the sample AP-02 are shown in Fig. 4-13. Quartz aggregates were detected by the strong predominance of silicon. Feldspars were identified from the association of silicon and aluminium together with either potassium forming potassium feldspars or sodium forming plagioclases. Micas were detected from the association of silicon, aluminium and potassium forming muscovite or with the addition of iron forming biotite. Their angular morphology was once again confirmed as being sub-angular to angular form as determined by previous tests.

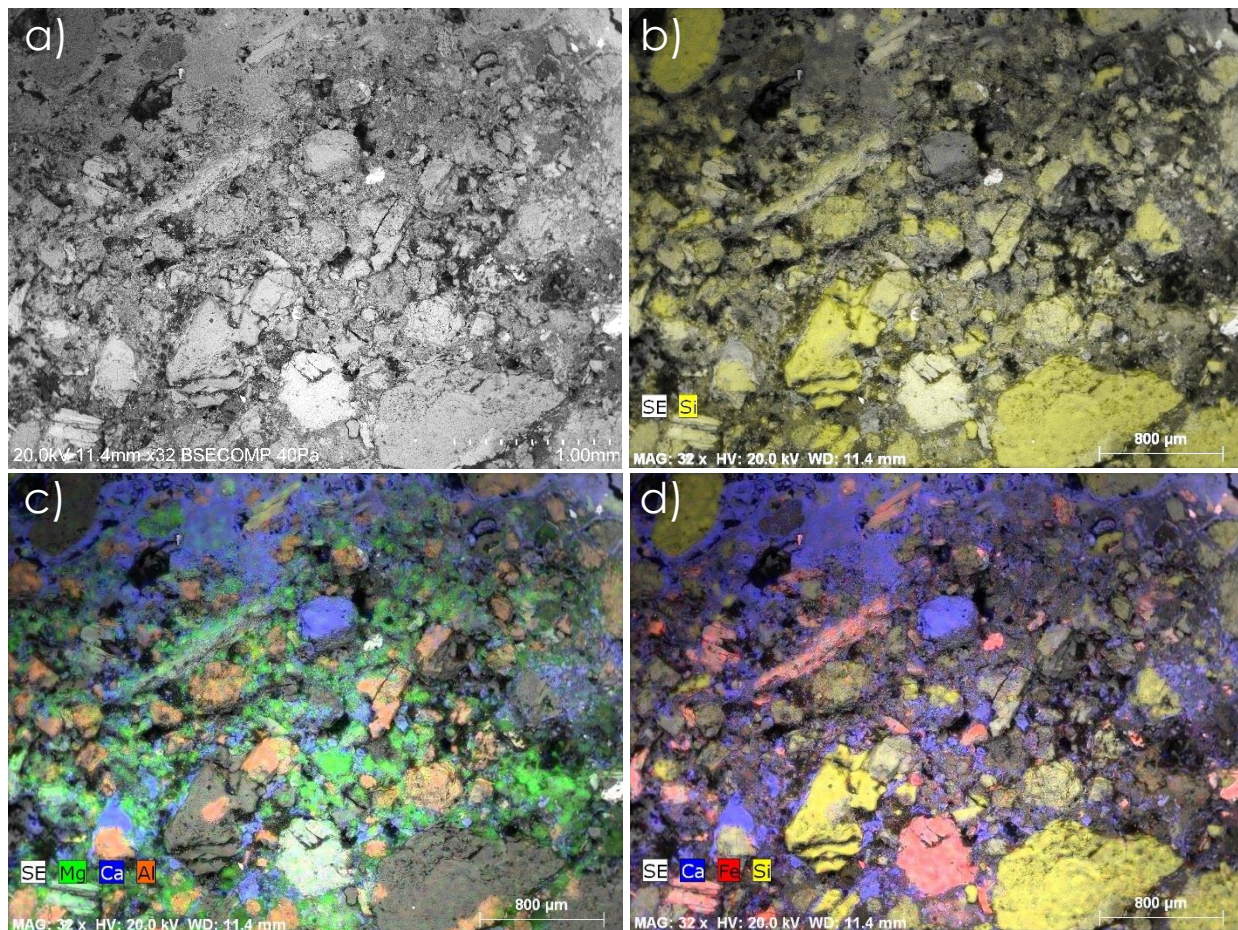


Figure 4-13. Elemental maps of AP-02; a) BSE image of the general composition, b) Siliceous aggregates within the composition c) Mg, Ca, Al elemental map, Al related to feldspars d) Ca, Fe, Si elemental map, Fe related to biotite. Yellow: Si, blue: Ca, green: Mg, orange: Al, red: Fe.

The presence of olivine was detected by SEM-EDS confirming the results obtained by XRD and optical microscopy. It was possible to identify olivine grains in all AP samples due to the association of silicon and oxygen with magnesium forming forsterite or with iron forming fayalite. Fig. 4-14 shows the forsterite grain in AP-03.

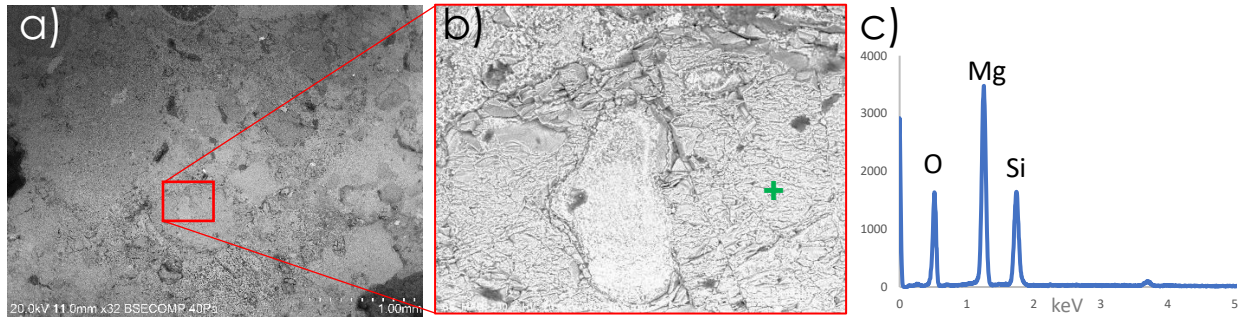


Figure 4-14. a-b) BSE image of AP-03, c) EDS spectra of the point analysis marked in (b).

In samples AP-03 and AP12U which are representing *sgraffito* decorations aggregates of crushed solid lime were detected. The white grains with angular forms that have been observed under the stereo microscope, were once again inspected under SEM-EDS. Their elemental compositions were enriched with Ca and O with a smaller amount of Mg and Si (Fig. 4-15).

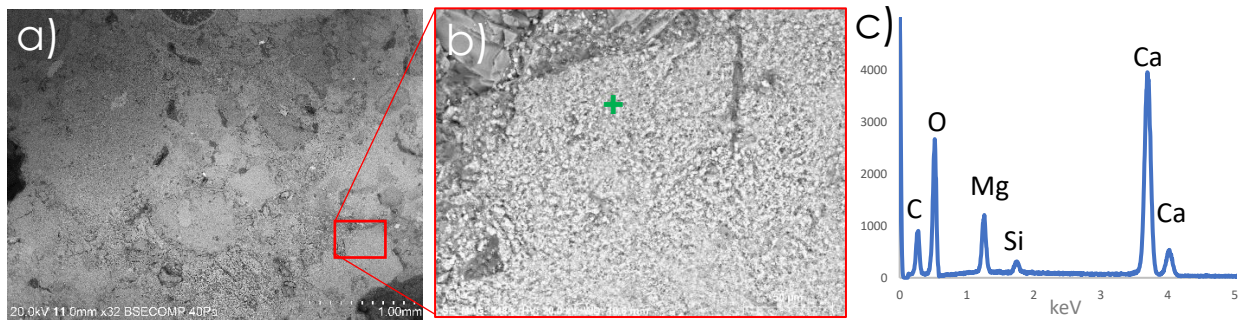


Figure 4-15. a-b) BSE image of AP-03, c) EDS spectra of the point analysis marked in (b).

On sample AP-06 which has a distinctive black colour, EDS analysis was carried out (Fig. 4-16). It was possible to detect coal fragments within the binder from the high concentration of C in association with O and S with some impurities of Mg, suggesting that the powdered coal fragments were added in the binder to give the black colour that was needed for decoration purposes.

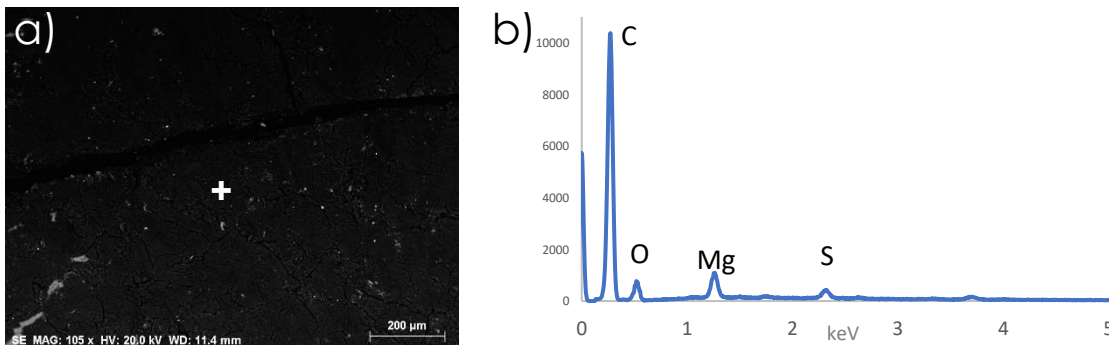


Figure 4-16. a) BSE image of AP-06, b) EDS spectra of the point analysis marked in (a).

The examinations in the binder matrix of the samples revealed different characteristics which allowed them to be separated into three groups in terms of their distinctive binder compositions. Although all samples of the AP group revealed the presence of both Mg and Ca in their binder composition, it was possible to detect proportional differences between the two elements. The first group is composed of AP group samples apart from AP-04 and AP-11. EDS elemental maps demonstrate the presence of both elements in which the distribution was not homogeneous. It was possible to detect some areas in the binder that are more enriched with calcium while others in magnesium in opposition with each other (Fig. 4-17). Calcite was detected mostly in crystal forms in the calcium enriched areas of the binder (Fig. 4-18). Whereas, magnesium was found in crystallized forms in some samples and less crystallized in the others explaining why it was not detected in all samples by XRD analysis (Fig. 4-19). The presence of calcite and magnesite apart from each other was considered as a possible indication of their recrystallization side by side after the thermal decomposition of the dolomitic stone used during the lime production (Cardoso *et al.*, 2014). Additionally, lumps are considered as the inclusions representing the lime used at the moment of the mortar production. Supporting the previous observations, lime lumps demonstrated a more homogeneous appearance compared to the distribution in the binder matrix (Fig. 4-18 a-b). The point analysis obtained in the lumps revealed the atomic ratio of Ca/Mg: ~1 which is suggesting the use of dolomitic limestone for the mortar production (Fig. 4-18 c-d).

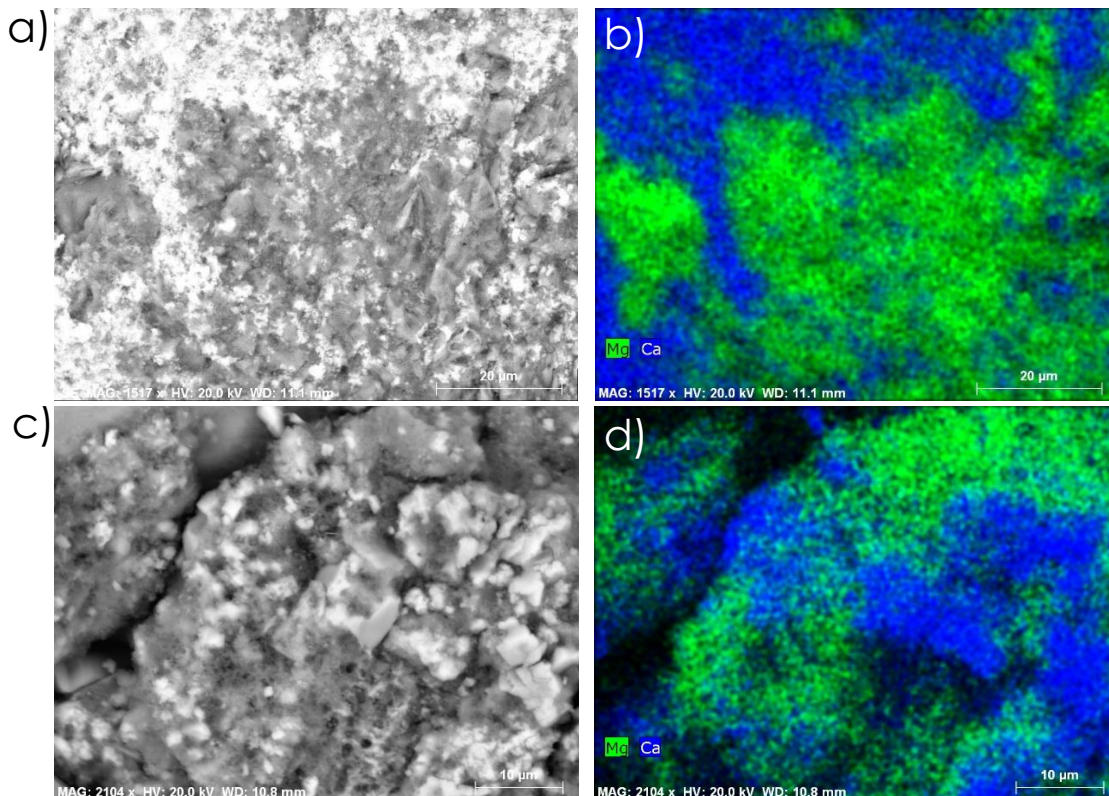


Figure 4-17. Representative image of binder microstructure; a-b) Sample AP-09U, c-d) Sample AP-01; BSE images on the left and elemental distribution maps of calcium (blue) and magnesium (green) on the right, respectively.

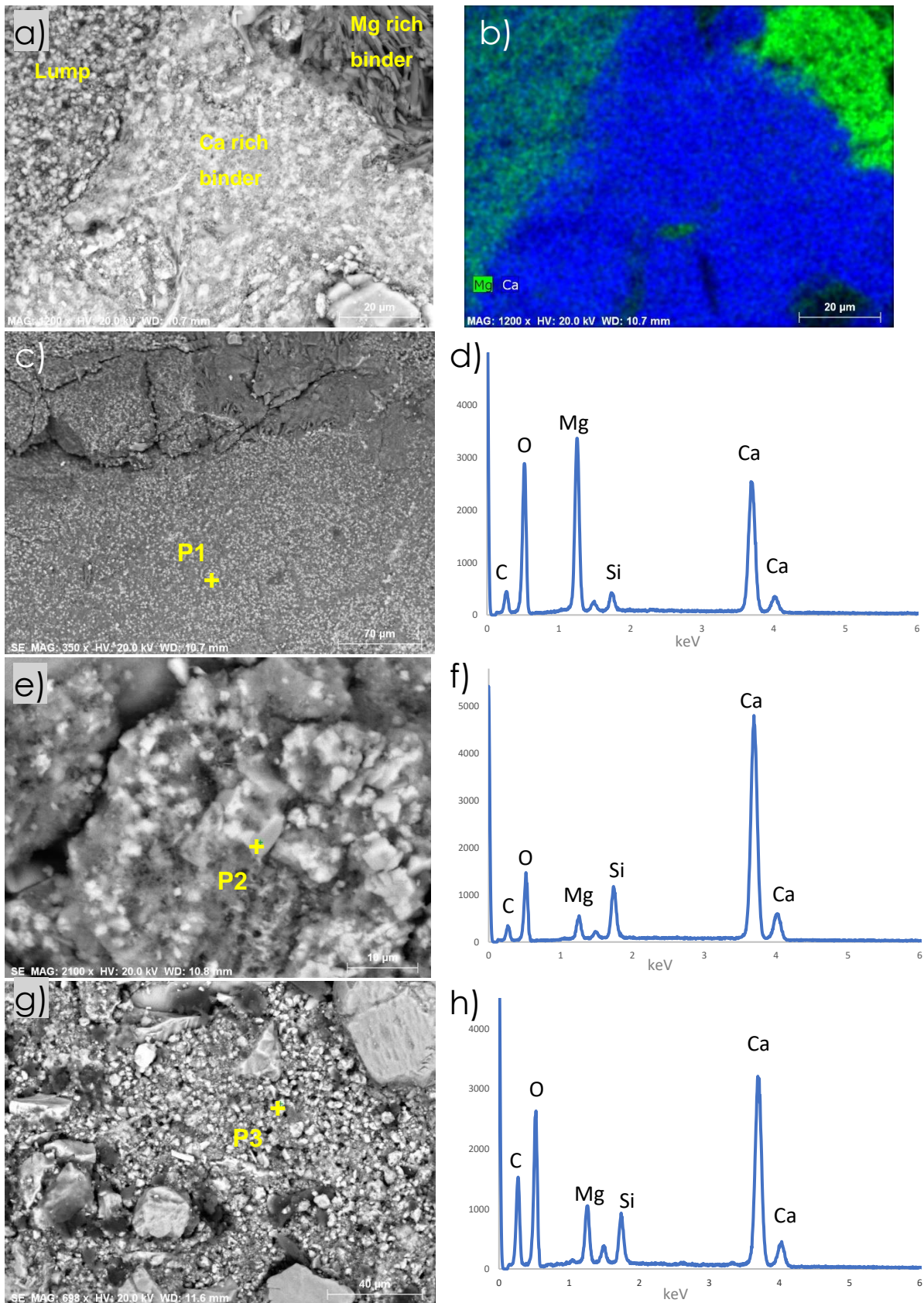


Figure 4-18. a) General aspect of lime lump and binder of AP-01; b) Elemental map of (a), c-h) Point analysis and corresponding EDS spectrum of lump (P1) in AP-01, Ca rich (P2) in AP-01 and Ca rich (P3) in AP-12, respectively.

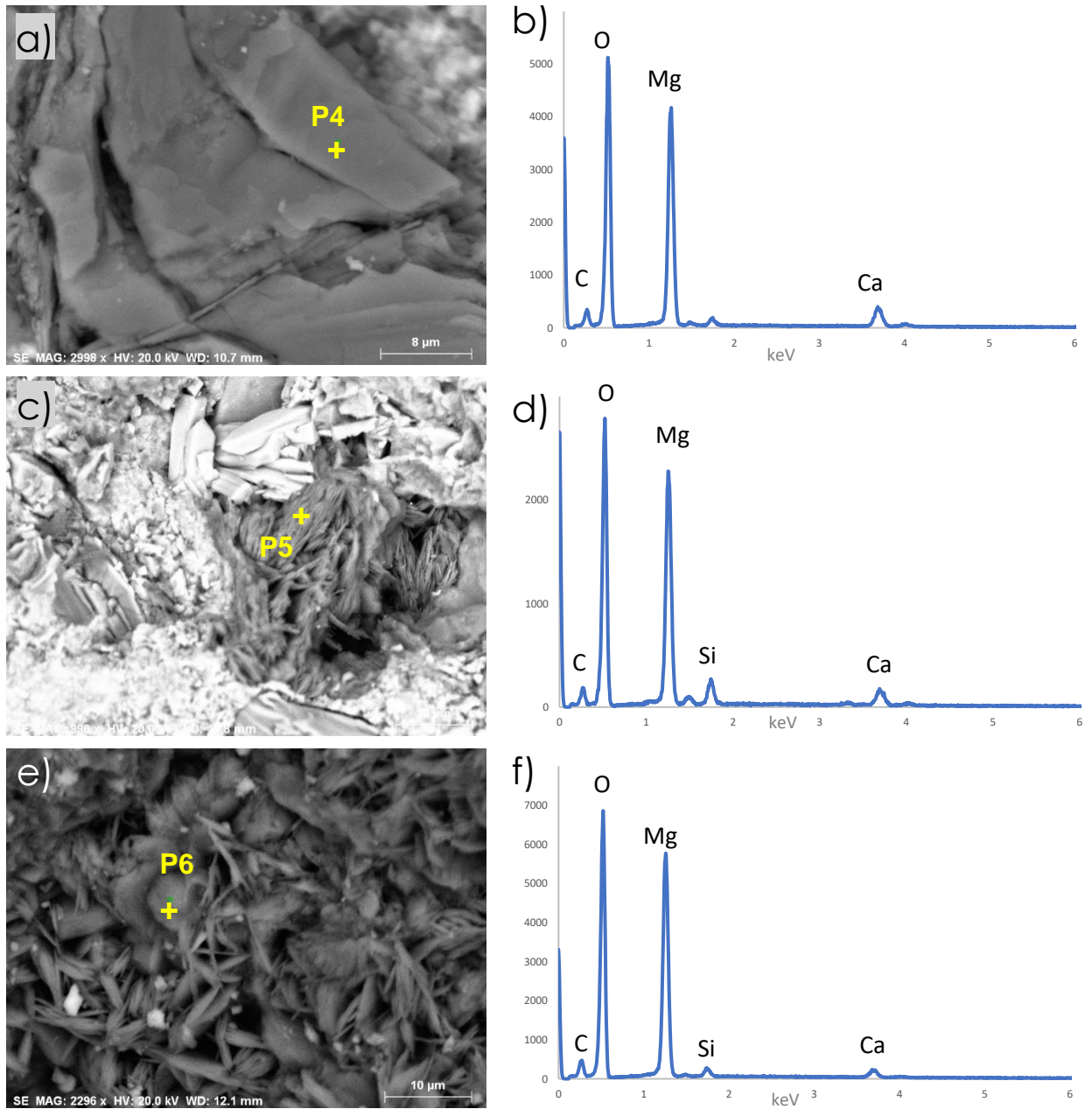


Figure 4-19. BSE image of the point analysis and corresponding EDS spectrums of the magnesite crystals within the binder matrix; a-b) AP-01, c-d) AP-03 and e-f) AP-05.

Samples AP-04 and AP-11 demonstrated different characteristics from the rest of the AP samples in terms of calcium and magnesium proportions within the binder matrix. From the elemental maps, it was possible to detect the areas which were more enriched in Ca or in Mg (Fig. 4-20). Point analysis was carried out on both areas and revealed the predominance of Ca over Mg content even in magnesium-rich zones. Lime lumps were also examined by the point analysis. The results displayed again the domination of calcium with the atomic ratios of Ca/Mg: ~7 for the lump in AP-04 and Ca/Mg: ~6 for the lump in AP-11. Both lime lumps suggest the use of calcitic lime with a small amount of magnesium impurities were used as the binder for these mortars.

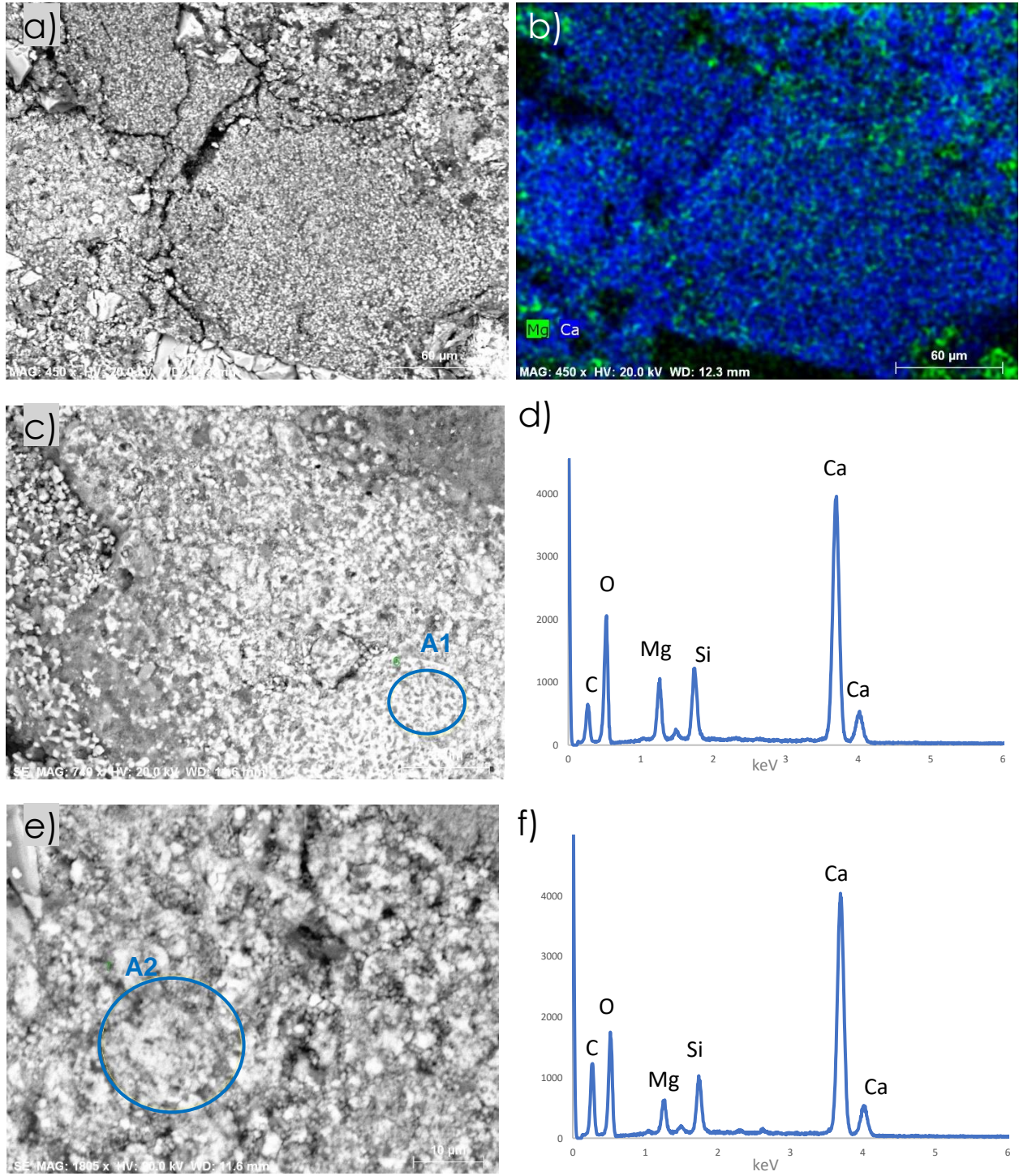


Figure 4-20. a) Representative image of binder microstructure of AP-11, b) Elemental map of (a) Ca and Mg, c-f) BSE image of the multipoint analysis in the binder of AP-04 and corresponding EDS spectrums of the (A1) Mg bearing area and (A2) Ca bearing area.

The third group that was defined in terms of their distinctive binder composition was EVR mortars. SEM-EDS analysis was carried out in samples EVR-01, EVR-04 and EVR-06. All three mortars represented a similar type of binder which displayed a soil/clayish matrix that is rich in Si, Al, Ca and Mg and with a small amount of calcitic lime. Point analysis was also performed. The binder of EVR-04, representing the Roman construction demonstrated a higher proportion of Ca, while the XVI century samples (EVR-01 and EVR-06) were more enriched in Mg (Fig. 4.21-22).

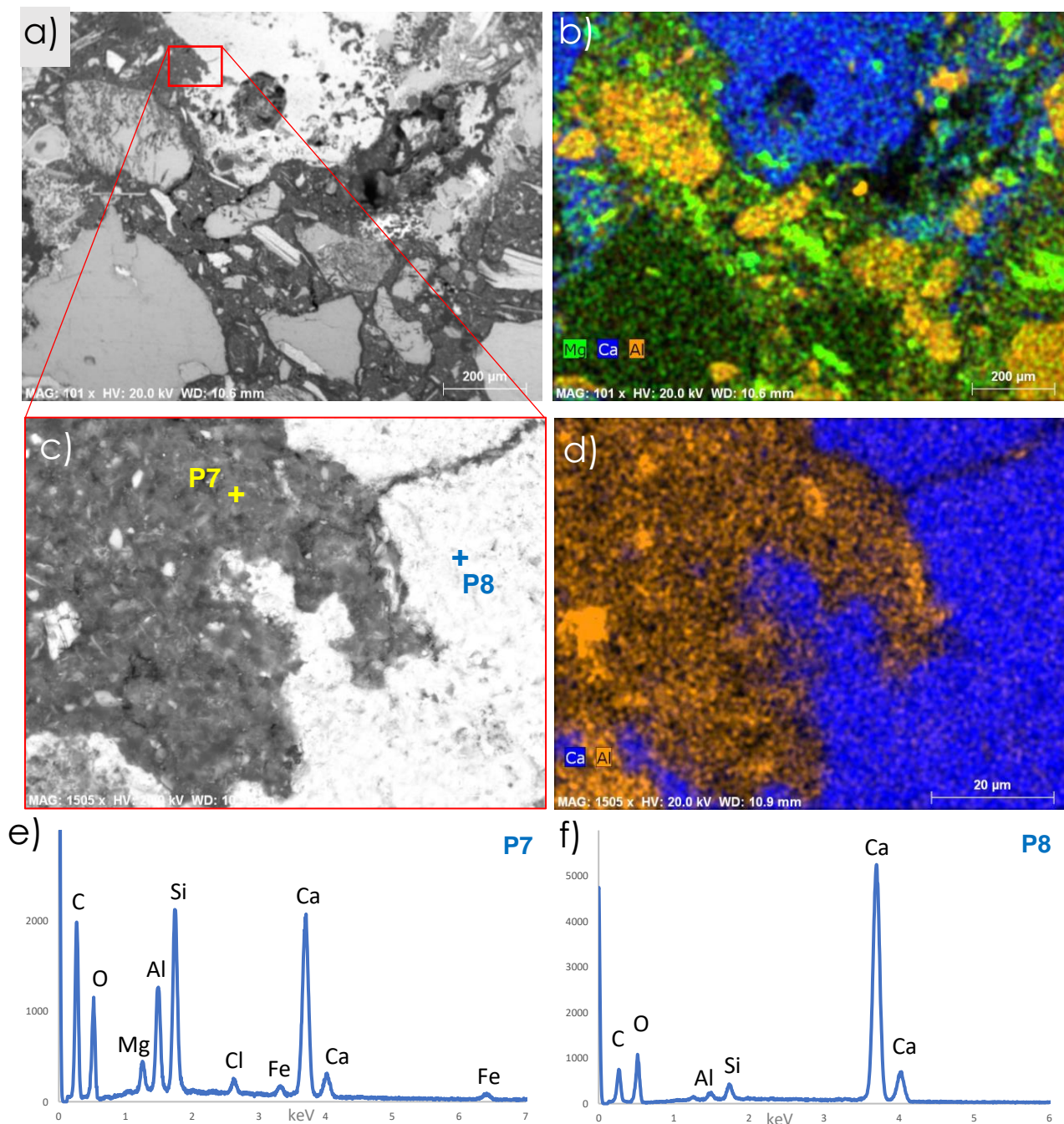


Figure 4-21. a) BSE image of the general composition of EVR-04 (Roman sample), b) Elemental map of (a) with Mg, Ca and Al, c) BSE image of a more focused on the binder area with calcitic lime on the right, d) Elemental map of (c) with Ca and Al, e-f) Point analysis P7 on the binder (e) and P8 on the calcitic lime binder (f).

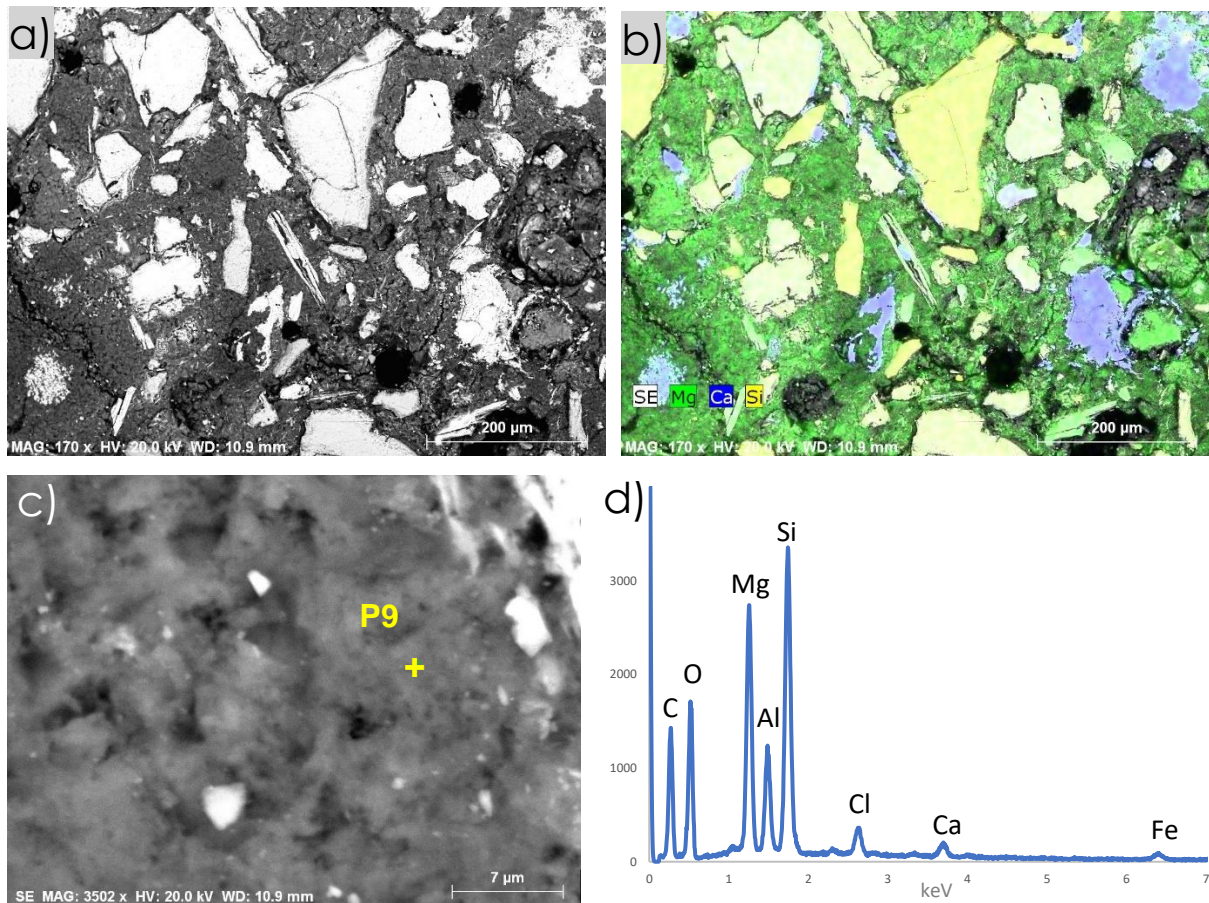


Figure 4-22. a) BSE image of the general composition of EVR-06 (XVI century sample), b) Elemental map of (a) with Mg, Ca and Si, c) BSE image of a more focused on the binder area, d) Point analysis P9 on the binder (c).

4.7 ACID ATTACK AND GRANULOMETRIC ANALYSIS

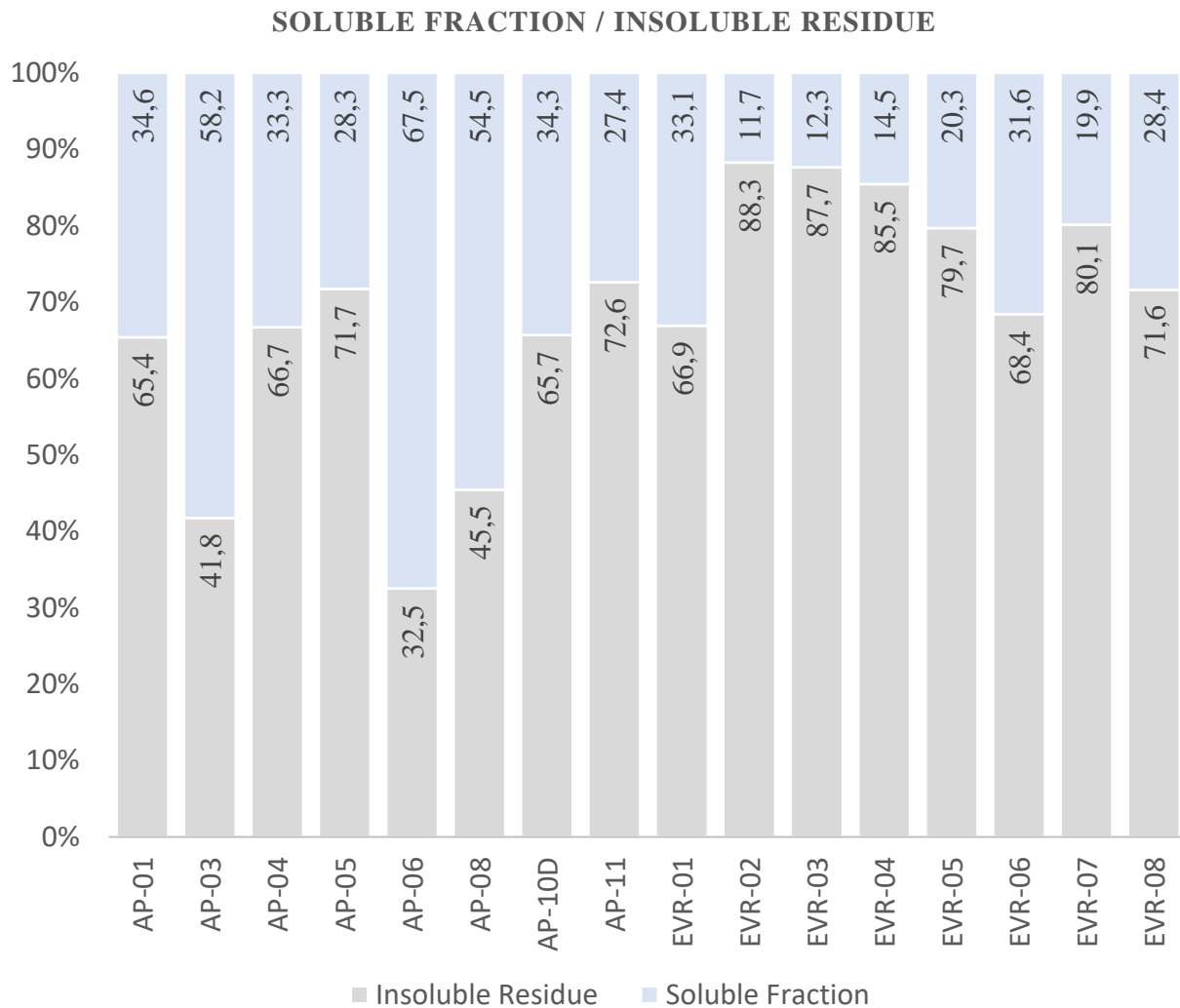
Acid attack with an aqueous solution of hydrochloric acid (1:3) was performed for the determination of the amount of the soluble fraction and insoluble residue. The soluble fraction represents the binder content, soluble salts, organic matter and carbonated aggregates while the insoluble residue constitutes the silicious aggregates within the samples (Silva *et al.*, 2006). The analysis was conducted in duplicate as described in Appx. 10 and the mean values were calculated as plotted in Tab. 4-8. In the cases where there was not enough material (AP-02, AP-07, AP-09, AP-10U and AP-12) analysis could not be performed or performed only once as in the sample AP-03. The percentages of the insoluble residue varied between 32,5% and 88,3% whereas the soluble fractions ranged from 11,7% to 67,5%.

The decorative mortar samples (AP-03, AP-06 and AP-08) displayed the lowest percentages of the insoluble residues which are below 50%. They were the only samples that showed a higher amount of soluble fraction against the insoluble residues due to the presence of crushed solid lime

and high concentration of lime lumps (AP-03, AP-08) and organic fragments (AP-06) in their compositions. Since the soluble fraction of these samples did not only represent the binder, the ratio of binder:aggregate could not be determined.

Samples of the Roman period (EVR-02, EVR-03, EVR-04, EVR-05 and EVR-07) presented the highest percentage of insoluble residues ranging from 79,7 % up to 88,3 %. Samples EVR-05 and EVR-07 from Torralva and EVR-02, EVR-03 and EVR-04 from Cartuxa displayed similar values to each other allowing them to be grouped by their locations, agreeing with the results of the TGA analysis. The soluble fraction:insoluble residue ratio of the Torralva samples were 1:4 while Cartuxa samples varied between 1:6 and 1:8. The filler mortars from the XVI century and the render mortars displayed the values of the insoluble residue ranging between 65,04 % and 72,6 %, having similar binder:aggregate ratios of either 1:2 or 1:3.

Table 4-8. Mean values obtained from the soluble and insoluble fractions after the acid attack.



The sieving of the insoluble residues allowed to determine the grain size distributions of the aggregates as plotted in Appx.11. It was possible to identify the predominant fraction for each sample by their distribution patterns. Filler mortars from the Roman period (EVR-02, EVR-03, EVR-04, EVR-05 and EVR-07) had the highest amount of fraction between 2,0 and 1,0 mm which is categorized as very coarse sand by Wentworth, 1922 (Fig. 4-23). Even though having the highest fraction at the same range, the Roman mortars from Torralva pit (EVR-05 and EVR-07) displayed a different distribution pattern, allowing them to be grouped together as in the previous observations. Filler mortars of XVI century (EVR-06 and EVR-08) displayed a finer grain pattern by having the highest fraction between 0,125 and 0,063 mm categorized as very fine sand (Blott and Pye, 2001). Distinctively, EVR-01 which is also a filler mortar from the XVI century presented a very similar distribution pattern to the Roman samples.

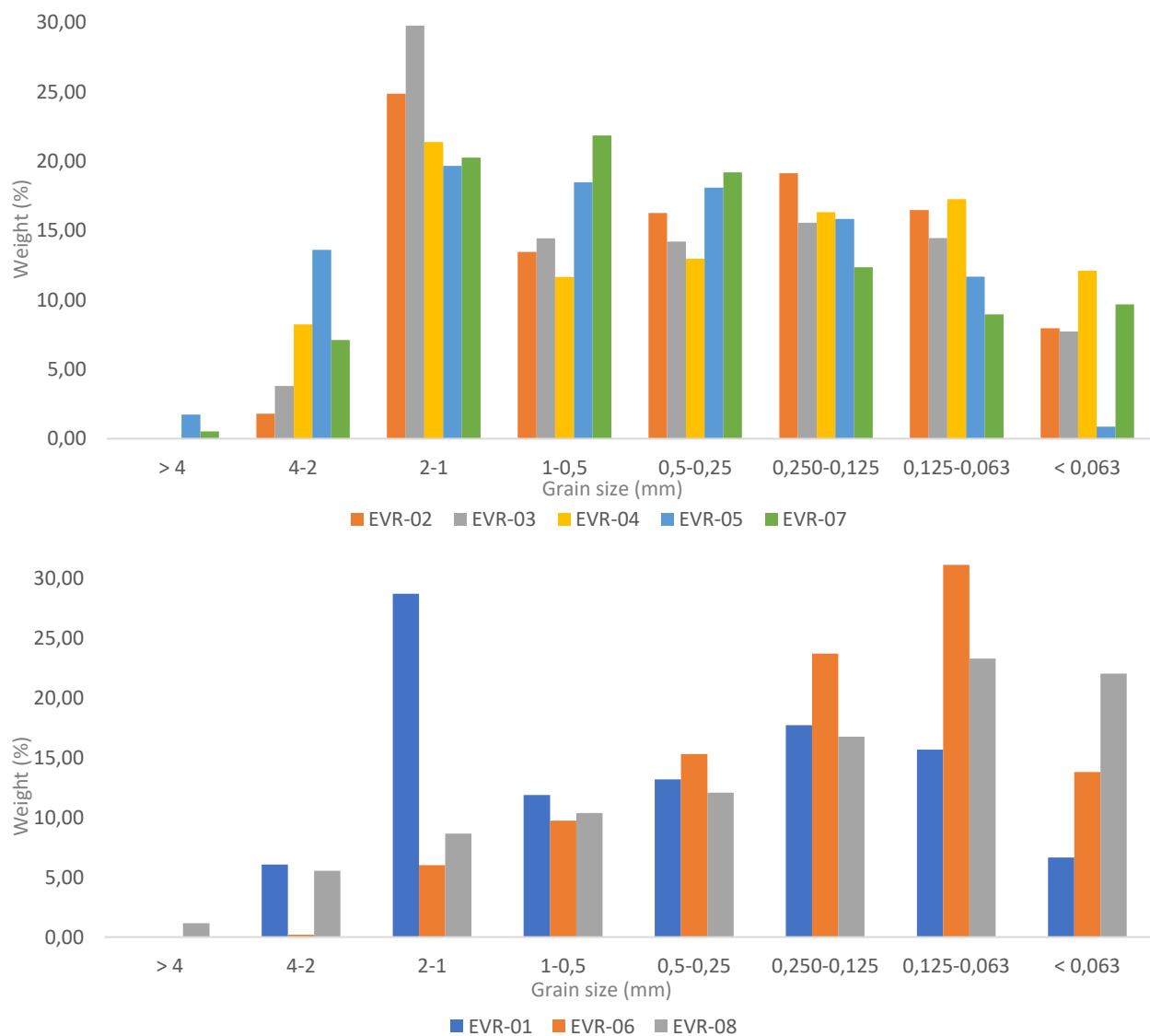


Figure 4-23. Grain size distributions of filler mortars from Roman period (upper) and XVI century (lower).

The results of the render mortars represented a finer grain size distribution pattern compared to Roman mortars. The highest fractions observed in the decorative samples were between 0,5-0,250 mm for AP-06 and AP-08 and 0,250-0,125 mm for AP-03 (Fig. 4-24). However, the lack of greater size fractions may be due to the dissolution of the carbonated aggregates during the acid attack. The rest of the render mortars displayed a grain distribution with the highest size fractions between 1,0-0,5 mm for AP-04 and AP-05, 0,5-0,250 mm for AP-10D, 0,250-0,125 mm for AP-1 and 0,125-0,063 mm for AP-11. Using the statistics software GRADISTAT developed by Blott and Pye, 2001 samples were analyzed according to their textural groups, fraction modality and sorting. The results are described in Tab. 4-9.

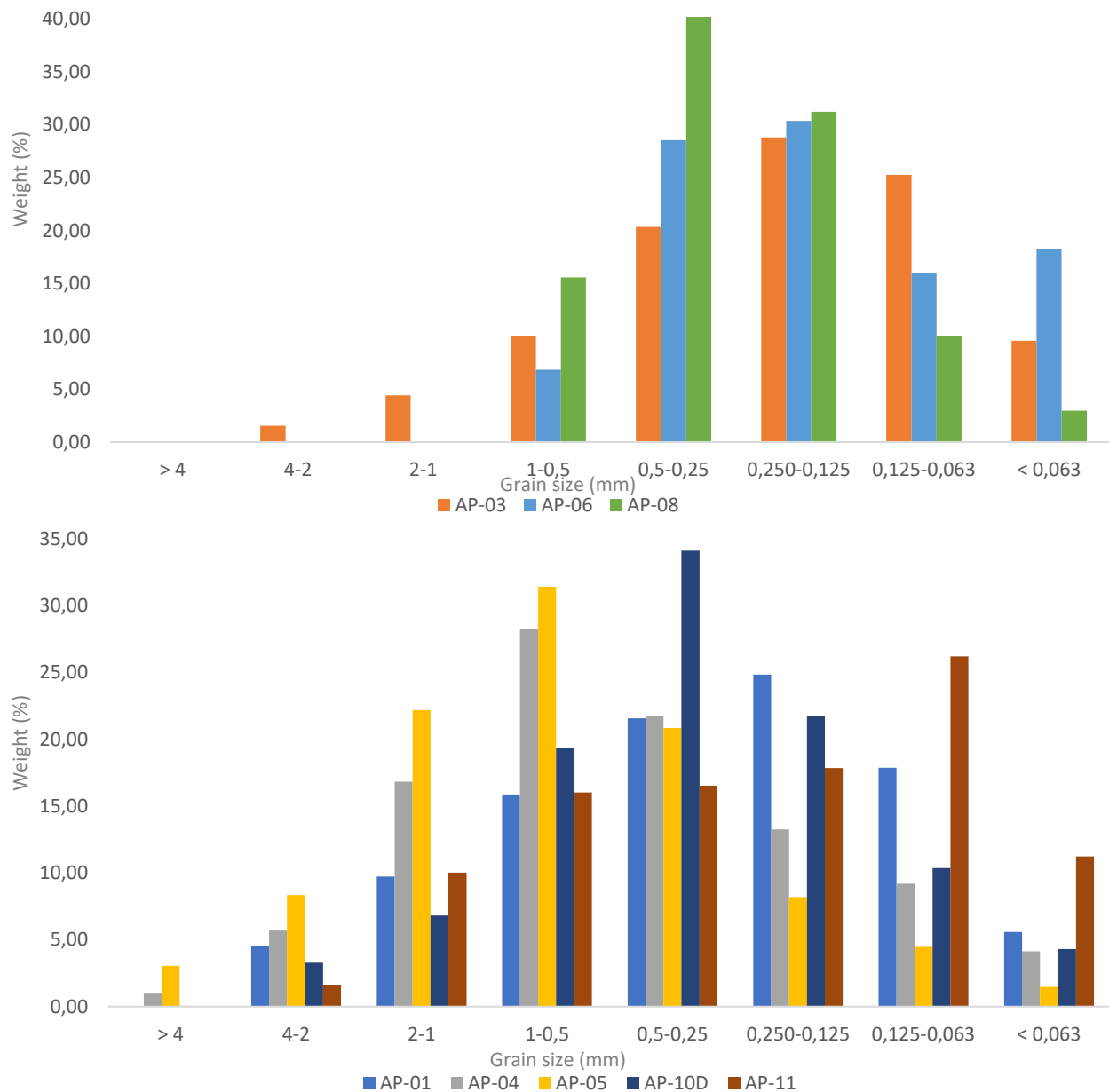


Figure 4-24. Grain size distribution curves of render mortars; decorative mortars (upper) and render mortars (lower).

According to the results obtained from the GRADISTAT samples are represented by 6 different textural groups that are sand, slightly gravelly sand, gravelly sand, muddy sand, slightly gravelly muddy sand and gravelly muddy sand. Almost all samples are poorly sorted apart from EVR-04, EVR-07 and EVR-08 that are very poorly sorted and AP-08 which is moderately sorted. Roman samples from Cartuxa (EVR-02, EVR-03 and EVR-04) and EVR-01 display a rather bimodal fraction trend whereas all the others are unimodal. Using the statistics software GRADISTAT the triangular gravel:mud:sand diagram is built (Fig.4-25).

Table 4-9. Description of the insoluble residue.

Sample	Mode	Predominant fraction (mm)	Sorting	Textural group
EVR-01	Bimodal	2,000 - 1,000 (28,76 %) 0,250 - 0,125 (17,74 %)	Poorly sorted	Gravelly sand
EVR-02	Bimodal	2,000 - 1,000 (24,88 %) 0,250 - 0,125 (19,13 %)	Poorly sorted	Slightly gravelly sand
EVR-03	Bimodal	2,000 - 1,000 (29,79 %) 0,250 - 0,125 (15,57 %)	Poorly sorted	Slightly gravelly sand
EVR-04	Bimodal	2,000 - 1,000 (21,40 %) 0,125 - 0,063 (17,27 %)	Very poorly sorted	Gravelly muddy sand
EVR-05	Unimodal	2,000 - 1,000 (19,66 %)	Poorly sorted	Gravelly sand
EVR-06	Unimodal	0,125 - 0,063 (31,17 %)	Poorly sorted	Slightly gravelly muddy sand
EVR-07	Unimodal	1,000 - 0,500 (21,87 %)	Very poorly sorted	Gravelly muddy sand
EVR-08	Unimodal	0,125 - 0,063 (23,33 %)	Very poorly sorted	Gravelly muddy sand
AP-01	Unimodal	0,250 - 0,125 (24,84 %)	Poorly sorted	Slightly gravelly sand
AP-03	Unimodal	0,250 - 0,125 (28,81 %)	Poorly sorted	Slightly gravelly sand
AP-04	Unimodal	1,000 - 0,500 (28,22 %)	Poorly sorted	Gravelly sand
AP-05	Unimodal	1,000 - 0,5000 (31,42 %)	Poorly sorted	Gravelly sand
AP-06	Unimodal	0,250 - 0,125 (30,35 %)	Poorly sorted	Muddy sand
AP-08	Unimodal	0,500 - 0,250 (40,20 %)	Moderately sorted	Sand
AP-10D	Unimodal	0,500 - 0,250 (34,12 %)	Poorly sorted	Slightly gravelly sand
AP-11	Unimodal	0,125 - 0,063 (26,20 %)	Poorly sorted	Slightly gravelly muddy sand

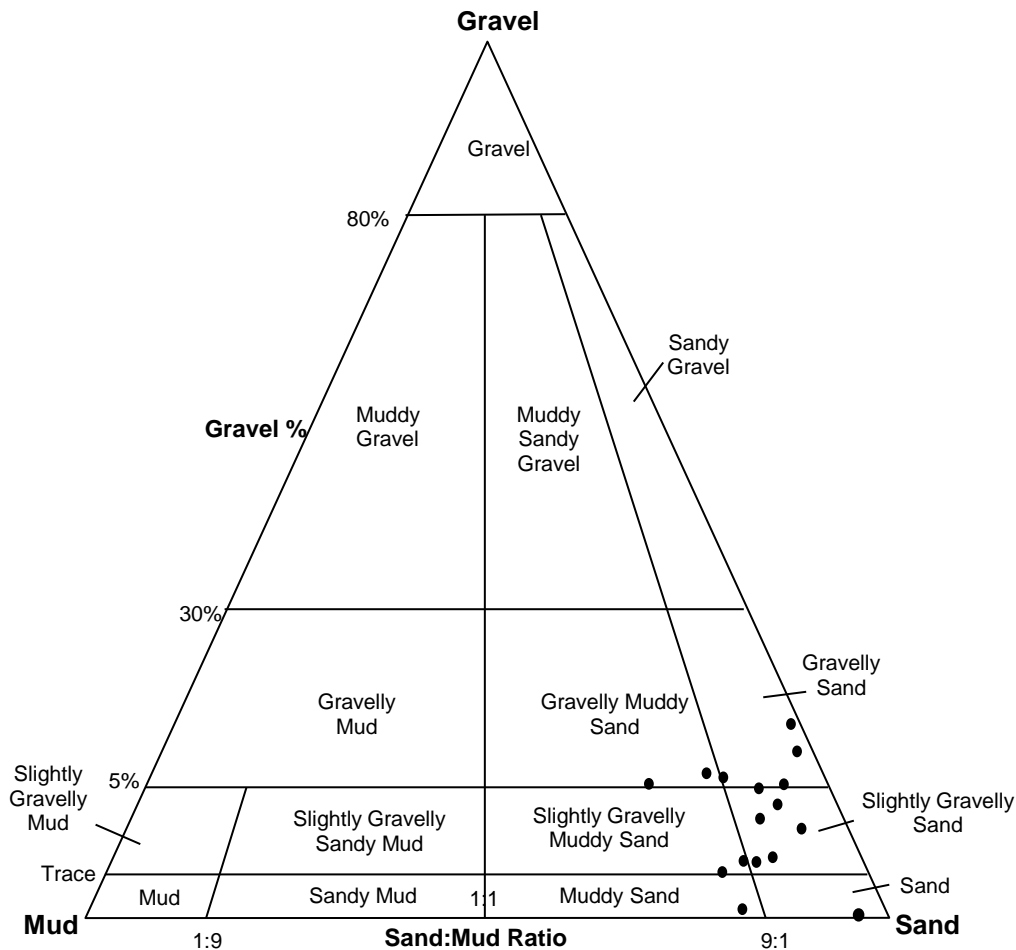


Figure 4-25. Gravel:mud:sand diagram from GRADISTAT.

After the acid attack with the aqueous solution of hydrochloric acid, the remaining insoluble residue was examined under the stereo zoom microscope for the determination of their morphological and mineralogical characteristics (Appx. 12). In all fractions, quartz was detected as the dominant mineral in transparent (hyaline) and white (milky) forms. Feldspars, micas (biotite and muscovite), small fragments of gabbro, quartzite and granitoid rocks were also detected. Grains are observed mostly in angular and sub-angular forms complementing the previous observations. Their angular morphology suggests short distance travel from the original outcrop. According to the observations under the microscope and together with XRD analysis, all samples demonstrate a uniform mineralogical composition which also correlates with the local geology of the Évora Massif which is composed of granitoid rocks with minor gabbro intrusions (Moita *et al.*, 2009).

5 DISCUSSION

The mortars of the aqueduct of Água da Prata were analysed with a multi analytical approach for the determination of their composition (binders, aggregates and additives). The samples chosen from diverse construction periods and structural needs were compared to point out their similarities and differences. The study revealed the properties of the Roman and XVI century filler and render mortars, XVII century restoration mortars and later interventions produced both for rendering and decorative purposes. The results were discussed to build up a chronological sequence of the aqueduct. The analysis provided evidence of the possible provenance of the raw materials preferred for the production of the mortars, their technologies and manufacturing processes. The information was examined to understand if the ancient receipts of the Roman builders as described by Vitruvius were followed or either reformulated to adapt to the new needs or changed based on the availability of resources.

On the basis of the characteristics and functional purposes, samples were firstly divided into 3 main groups as filler, render and decorative mortars to be able to discuss the variations of their compositions in relation to their functions. The 1st group is the filler mortars composing of 2 subgroups related to their periods, Roman and XVI century. The 2nd group composed of the render from the XVI and XVII centuries, the inner layers of the samples with stratigraphy were also discussed among this group. Finally, the 3rd is the decorative group which is also divided into 2 subgroups based on their periods. XVI century is representing *sgraffito* decorations and XIX century deriving from the monumental fountain, as explained in Tab. 5-1. The grouping is used for the assessment of the results of different functional needs and also for comparisons of periods within the same functions.

Table 5-1. Division of groups used for the discussion of the results

Group 1		Group 2			Group 3	
Filler mortars		Render mortars			Decorative mortars	
Roman	XVI cent.	XVI cent.	XVII cent.	XIX? cent.	XVI cent.	XIX cent.
EVR-02	EVR-01	AP-04?	AP-01	AP-09D	AP-03	AP-05
EVR-03	EVR-06	AP-11	AP-02	AP-10D	AP-12?	AP-06
EVR-04	EVR-08					AP-08
EVR-05						AP-09U
EVR-07						AP-10U

5.1 RAW MATERIALS

The results from the visual observations, Optical Microscopy (OM), Thermographic Analysis (TGA-DTG), Scanning Electron Microscopy-Energy Dispersive X-ray Spectrometry (SEM-EDS) and X-ray Diffraction (XRD) together led to the identification of the raw materials. The results are discussed according to the two main components of the mortars that are binder and aggregates.

5.1.1 Binder

On the basis of the results obtained by OM, XRD, TGA-DTG and SEM-EDS three types of binder groups were determined which can broadly be categorized as earthy/clayish, calcitic lime and dolomitic lime.

The first group refers to the foundation mortars which have an earthy/clayish binder matrix which also bears a small amount of calcitic lime. According to the microscopic observations, all samples belonging to this group have a distinctive brown binder colour. As observed by SEM-EDS analysis, the binder is heterogeneous with clayish areas enriched in Si together with Al, Ca and Mg, and other areas where carbonated binder prevails (Ca enrichment). In sample EVR-04 which is representing the Roman mortars, point analysis on lime revealed the presence of higher content of Ca in comparison to Mg agreeing with the use of calcitic lime. On the other hand, in the XVI century sample EVR-06, the point analysis represented rather higher contents of Mg over Ca. Although in smaller amounts, the presence of calcitic lime within the binders was also confirmed by the XRD analysis of the binder enriched fractions (Appx. 8).

The second group is defined as the render mortars of different periods. Their binder composition is mainly calcite but there is also the presence of magnesium carbonate in smaller amounts. Among this group, AP-04 and AP-11 are the two samples representing the XVI century render mortars. As confirmed by SEM-EDS analysis, the binders of both samples possess a high content of Ca with less amount of Mg and Si. Additional point analysis on the spots which bear higher amount of Mg also revealed the predominance of Ca over Mg (Fig. 5-1). The thermograms of the two samples are also very similar allowing them to be correlated together in the same historical phase (Appx. 9). AP-01 and AP-02 are the two mortars dating back to the XVII century from the period of renovations by Francisco Ferreira (CME-DCP, 2019). On the basis of SEM-EDS elemental mapping, both samples have Ca-rich and Mg-rich zones in opposition to each other. The point analysis on each spot revealed again the predominance of Ca over Mg (Fig. 5-1). In their thermograms, slight variations are detected between 200-550°C which is a range for magnesite and hydromagnesite decomposition (Appx. 9). However, such compounds were not

detected in XRD analysis possibly due to their presence in small amounts and low crystallinity. Although AP-01 and AP-02 are mortars on top of each other, the similarities in their binders allow them to be grouped in the same historical period. Samples AP-09 and AP-10 collected from the monumental fountain are the samples with stratigraphy. Their inner layers (AP-09D and AP-10D) are also classified in this group as render mortars since they are used for surface regularization. They both display a calcitic composition and the presence of magnesite or hydromagnesite was not detected by SEM-EDS or TGA analysis. The distinctions of the binder in their inner and outer layers may be due to their production in different historical periods.

The third group is decorative mortars and display binder properties of dolomitic lime. All mortars of this group possess significant weight losses between 200-550°C in the range for magnesite and hydromagnesite decomposition by TGA analysis (Appx. 9). As observed by SEM-EDS, they show Ca-rich and Mg-rich zones in opposition to each other like in the XVII century samples. The difference allowing them to be grouped separately is due to the point analysis which reveals the predominance of Mg over Ca considerably higher in comparison to the other samples (Fig. 5-1) suggesting the use of dolomitic limestone for their production. Although their construction period varies from XVI to XIX centuries decorative mortars share rather similar binder compositions.

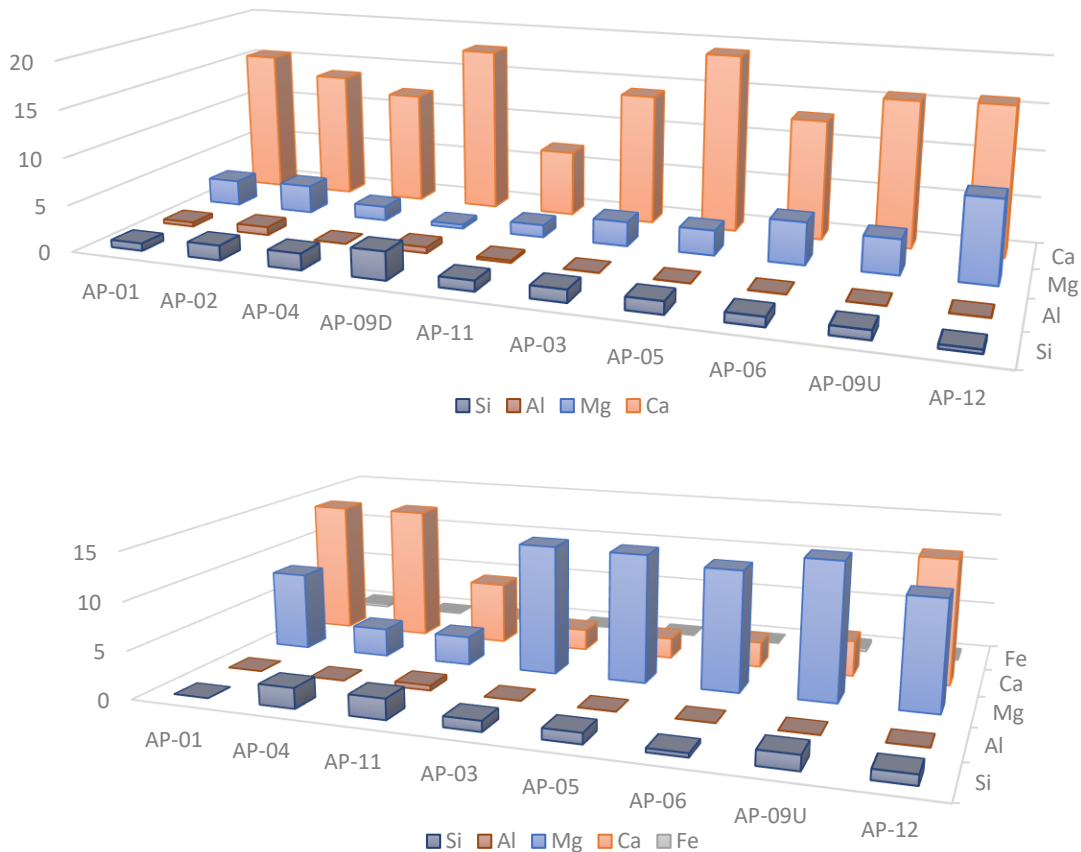


Figure 5-1. EDS analysis of Ca rich (upper) and Mg rich (lower) points within the binder of the samples (%).

5.1.2 Aggregates

Based on the analytical results, mortars from all groups present a uniform aggregate composition. No ceramic fragments were observed in any of the groups.

As confirmed by the analysis most of the aggregates are silicious in nature. Quartz is the predominant mineral both in transparent and milky forms. Feldspars are detected as K-feldspars and plagioclases by OM and XRD analysis. They are found in all samples and sometimes in association with quartz grains as rock fragments. Micas, both biotite and muscovite are also detected in all samples. So as in feldspars, micas too are found in single forms and sometimes in association with other grains as rock fragments (granitic grain). The presence of amphiboles particularly hornblendes are also verified by XRD analysis and OM. In terms of the angular morphology, aggregates are found mostly in sub-angular and angular forms indicating a short distance of transportation of the sediments from the geological source. In almost all samples olivine and pyroxene were detected through OM.

In the samples AP-03 and AP-12, the presence of crushed lime as aggregate is detected. The results are confirmed with the complementary analysis by OM, SEM-EDS, TGA and Acid Attack although, it could not be performed on AP-12 due to the lack of material. During the acid attack, other decorative samples (AP-06 and AP-08) also lost more than half of their initial weights similar to AP-03 due to the dissolution of lime nodules or fragments within their composition. Acid attack analysis was not performed on the samples that have stratigraphy (AP-09, AP-10 and AP-12), due to the lack of material but such inclusions were also detected in the lighter layers of these samples (AP-9U, AP-10U and AP-12U) by optical microscopy. In TGA analysis the thermograms of (AP-03, AP-06, AP-08, AP-9U, AP-10U and AP-12U), the calcite decomposition occurred at around a temperature of 780°C as observed in their DTG curves slightly higher than the rest of the samples (Appx. 9). Such phenomenon is representative of the higher levels of crystallinity or bigger grain sizes of the calcium carbonates (Földvári, 2011), therefore supporting the hypothesis. Among the mortars of the EVR group, in the XVI century samples (EVR-01, EVR-06 and EVR-08) decomposition of calcite occurred at rather higher temperatures in comparison to the Roman samples although not as significant as the mortars with decorative purposes (Appx. 9).

5.2 PROVENANCE

For the determination of the provenance of the raw materials, the mineralogical data obtained through the analysis was combined with the geological context of Évora and its surroundings. As described in the geological maps, the vicinity of the city is mainly composed of granites and granodiorites. Locally, there are zones with the presence of gabbro and diorite inclusions (Fig. 5-2). Such mineralogical context is parallel to what has been observed through the analytical techniques.

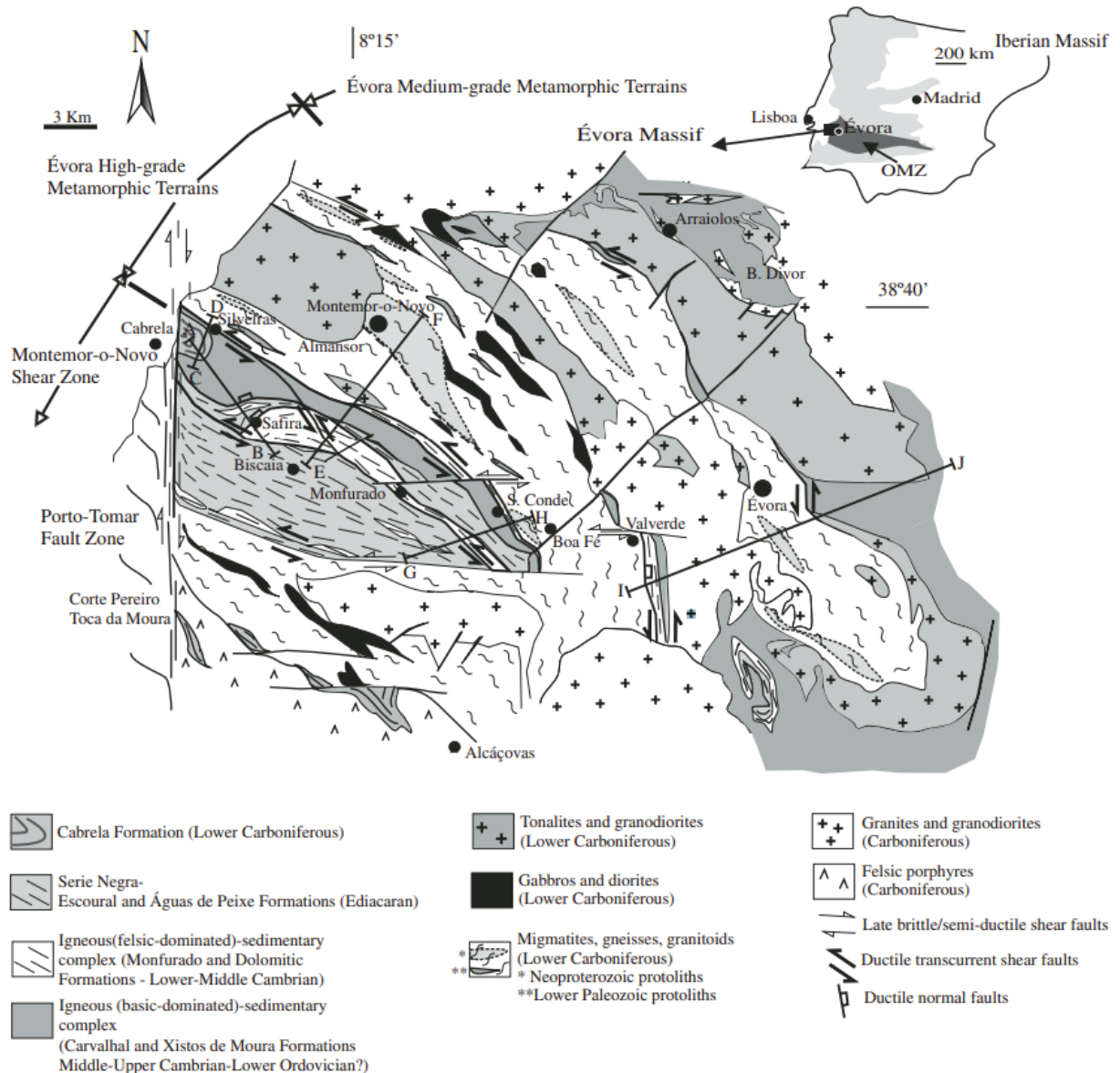


Figure 5-2. Geological map of Évora and its surroundings (Moita *et al.*, 2009)

The mineralogical composition of the aggregates is mainly quartz, feldspars and micas. Grains are found mostly in sub-angular and angular forms and sometimes in association with each other as rock fragments. Such morphology is indicative of a short distance of transportation of the aggregates meaning that the source is found in the vicinity. The possible provenance which corresponds to the mineralogical composition is the local granites of the Évora massif. Additionally, the presence of Mg and Fe rich grains like amphiboles, olivine and pyroxene indicate the gabbro inclusions of Alto de São Bento quarry may have been the possible resource of the raw materials for the acquisition of the aggregates. Such outcome also matches the study of the historical mortars from Santa Maria Church of Évora by Adriano *et al.*, (2009) which is another masonry construction of the XVI century.

In terms of the binder, the analysis indicates the use of clayish binder with small amount of calcitic lime (as in the Roman period) or the use of calcitic or dolomitic lime for the mortar production. Although with some impurities the use of calcitic lime was detected in XVI century render mortars (AP-04 and AP-11), XVII century render mortars (AP-01 and AP-02) and the inner sections of layered mortars (AP-09D and AP-10D). However, the decorative mortars of the XVI century (AP-03 and AP-12) and the mortars of the interventions of the XIX century (AP-05, AP-06, AP-08, AP9U and AP-10U) demonstrate properties of the use of dolomitic lime. Such difference reveals that the raw materials to produce the binder for diverse constructive needs were acquired from at least two different sources. It is assumed that such selection was done intentionally since the XVI century samples demonstrate different binder characteristics for render (AP-04 and AP-11) and decoration needs (AP-03 and AP-12). The dolomitic nature of AP-03 and AP-12 also correlate with the binder properties of Santa Maria Church in Évora (Adriano *et al.*, 2009) suggesting that dolomitic lime may have been a choice of an elaborate mortar production of the XVI century.

Although the correlation of the lime properties of the binder with the geological data is often challenging as the carbonates in the binder are no longer representing the exact original composition (Lammel and Lehrberger, 2007) it is assumed that the local sources may have been preferred. The possible sources in the vicinity of Évora are located in the south of Montemor-o-Novo marked in the geological map as igneous-sedimentary complex with dolomitic formations (Fig. 5-2). Another source with calcitic and dolomitic nature in the region is located also in the south of Évora in Viana do Alentejo, but in a greater distance which is around 30km. There are also two other possible zones with calcitic and dolomitic nature as shown in Fig. 5-3 as Zone 1 and Zone 2 that are rather in closer distances. This region is particularly known for the active kilns for the production of lime, nowadays.

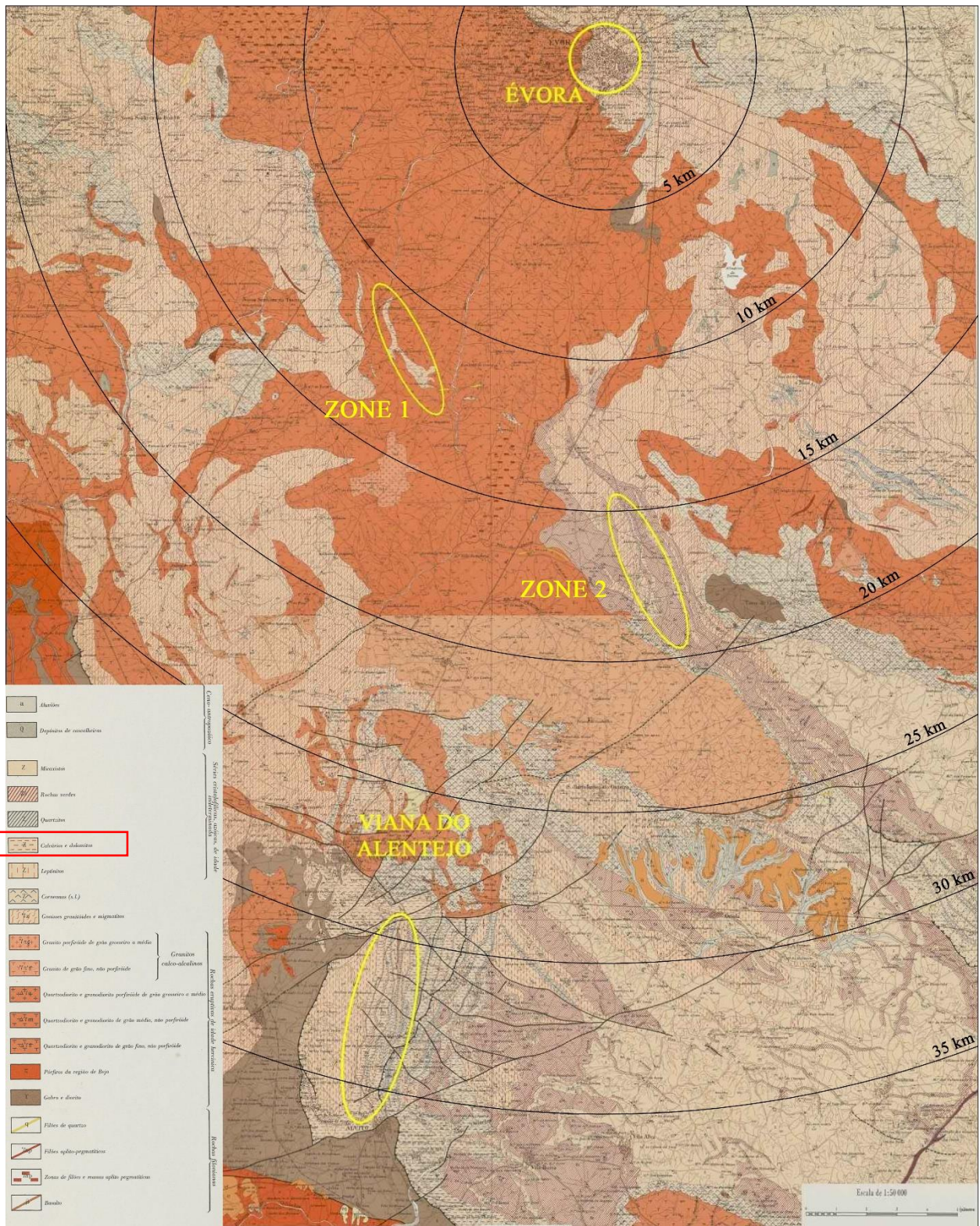


Figure 5-3. Geological scheme from Évora (40-A) and Viana do Alentejo (40-C) geological maps in 35 km of radius between Évora and Viana do Alentejo , scale of 1/50000 (taken and adapted from Laboratório Nacional de Energia e Geologia (LNEG), <http://geoportal.lneg.pt/geoportal/mapas/index.html>).

5.3 PRODUCTION TECHNOLOGY

In addition to the selection of the raw materials, identifying the preparation methods of the mortars reveal crucial information to observe the technical knowledge of the builders to achieve the desired construction needs. The study to understand the production technology is applied on the representative mortars from different periods so to compare the distinctions and similarities of the diverse building practices.

Based on the results of the analytical techniques, the compositional differences of the mortars vary depending either on the different construction phases or structural needs. The simplified compositions are calculated through Jedrzejewska method using the estimated percentages of carbonates by the TGA data together with residue analysis (Jedrzejewska, 1960). Tab. 5-2 explains the simplified compositions of the mortars, samples that are not listed are due to the lack of information about the silicious aggregates since the acid attack was not performed as the quantity of the material was lacking. Samples that possess magnesite and hydromagnesite, thus the use of dolomitic lime was calculated from the corresponding weight losses in the 200-650°C range in TGA analysis.

In the simplified compositions, the foundation mortars of the Roman period show a higher amount of siliceous aggregates, in Cartuxa over 85% and in Torralva 80%. These contents are much higher in comparison to other mortars since the binders of these samples have a clayish matrix meaning that the silicious grains of the binder were not dissolved by acid attack and are included in the calculation. Consequently, the calcite content of the Roman samples is lower (<10%) in comparison to other mortars possibly also due to the effect of dissolution through time. The production recipe changes in the XVI century by the reduced the amount of the silicious aggregates (around 70%) within the composition. The calcite content is increased by around 20%. Both foundation and render mortars of the XVI century display similar compositional percentages proving that the similarities in the production receipts are related to the same historical phases. The calcite content of the decoration mortars AP-03, AP-06 and AP-08 remained inconclusive since the calculated calcite content includes both calcium bearing aggregates and binder.

Despite the material variations of the binders, render mortars from different periods display similar binder:aggregate ratios ranging between 1:3 and 1:4. Such proportion partially correlates with the ancient practices as suggested by Vitruvius in *De Architectura*. The ideal proportion advised in his treatise, in the case of using pit sand is 1:3 (Book II, Chapter V, Vitruvius). No ceramic additives were detected in any of the mortars since all the Roman samples had structural

functions and none of them were in direct contact with water. The practice of ratios and additives may have been inherited from ancient treaties.

Table 5-2. Simplified compositions of the mortars (%) using Jedrzejewska method (Jedrzejewska, 1960).

SAMPLES	Silicious Aggregates ¹	Calcite ²	Magnesite ³	Hydromagnesite ⁴	Soluble fraction ⁵
EVR-01	67*	20	-	-	13
EVR-02	88*	2	-	-	10
EVR-03	88*	5	-	-	7
EVR-04	85*	7	-	-	8
EVR-05	80*	10	-	-	10
EVR-06	68*	19	-	-	13
EVR-07	80*	9	-	-	11
EVR-08	72*	19	-	-	9
AP-01	65	24	3	-	8
AP-03	42	31**	4	7	16
AP-04	67	19	3	-	11
AP-05	72	15	2	6	5
AP-06	33	32**	6	24	5
AP-08	46	44**	4	-	6
AP-10D	66	20	-	-	14
AP-11	73	17	3	-	7

(1) Silicious Aggregates = insoluble residue after attack with the aqueous solution of HCl (1:3).

(2) Calcite = CaCO₃ content determined by TGA

(3) Magnesite = MgCO₃ content determined by TGA

(4) Hydromagnesite = hydromagnesite content determined by TGA.

(5) Soluble fraction = 100 – Σ (Aggregate + Calcite + Magnesite + Hydromagnesite)

*Silicious aggregates includes silica bearing grains of the binder due to its clayish matrix

**Calcite includes binder+calcium carbonate bearing aggregates

Samples were also studied in terms of their level of hydraulicity. Even though they lack ceramic fragments, they possess a certain level of clay minerals that support the mortars with hydraulic properties agreeing with the XRD analysis in the binder enriched fractions of the EVR sample group (Appx. 9). Based on the results obtained by TGA analysis, the ratio between carbon dioxide (CO₂) to structurally bound water (H₂O) in relation to carbon dioxide (CO₂) can be calculated to relate it to the hydraulic degree of the mortars (Moropoulou *et al.*, 2005). The ratios were calculated by excluding the magnesite and hydromagnesite contents. Results were plotted and two clusters were obtained (Fig. 5-4).

The Roman mortars of the foundation with the exception of EVR-02 all represented hydraulic properties. Possibly due to their clayish binder matrix, even without the addition of ceramic fragments, they appeared to have hydraulic properties naturally. Since they are mortars prepared to be used underground such degree of hydraulicity correlates with the expected performance. EVR-02 stayed outside the cluster which may be due to heterogeneity of the sample. The second cluster describing a medium level of hydraulicity included the XVI century foundation mortars and render mortars from all periods. Since these group of mortars were prepared to be used in the outdoors, such level of hydraulicity may have been provided for the resistance against rainwater. The remaining samples that did not fit in any of the two clusters were the decorative mortars both from the *sgraffito* decoration and the monumental fountain. The non-hydraulic degree of the decoration mortars agrees with the fact that no hydraulic property was expected from them.

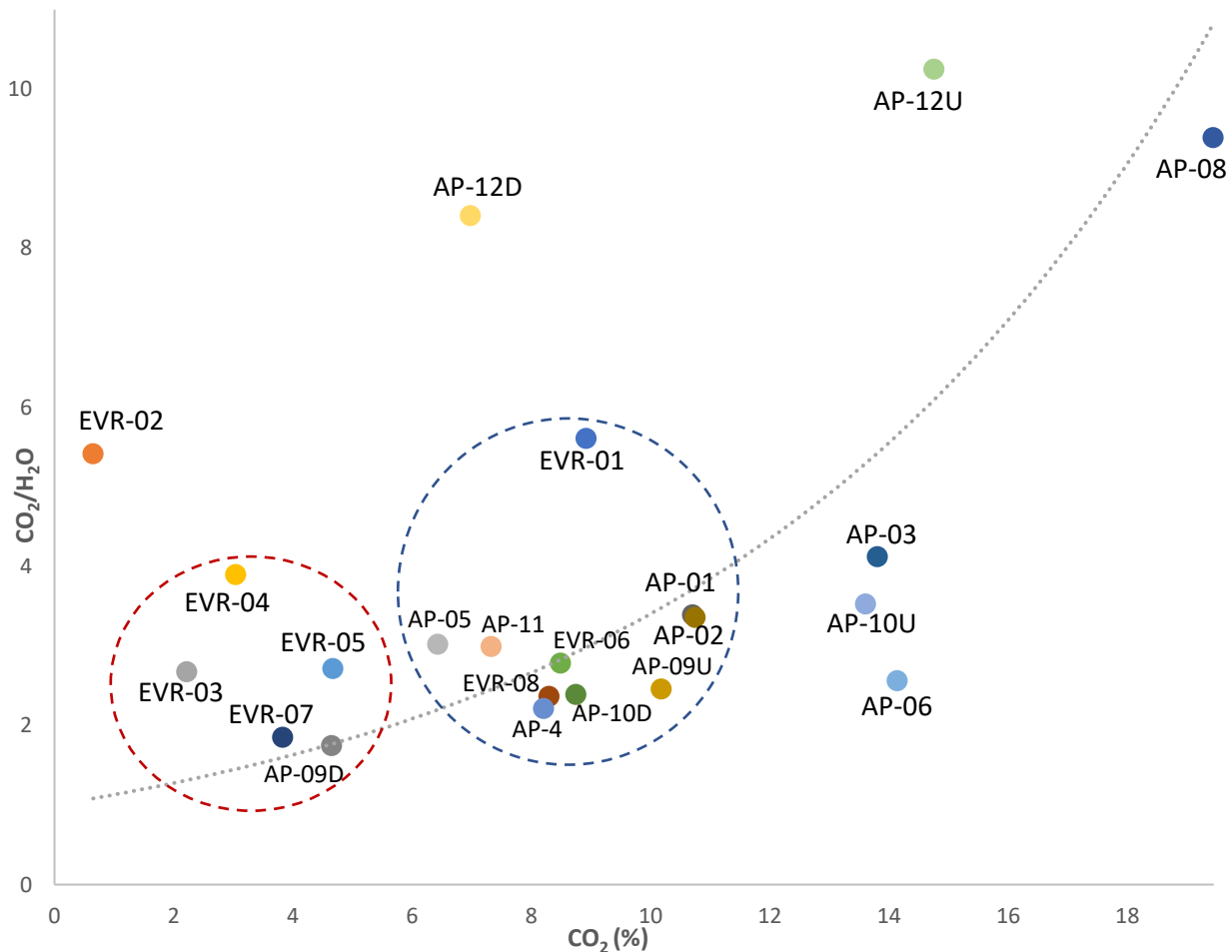


Figure 5-4. Carbon Dioxide / Structurally Bound Water versus Carbon Dioxide (%).

6 CONCLUSION

The aim of the study was to provide a better understanding of the aqueduct Água da Prata in correlation with the chronological sequence through the investigation of its mortars. It was also essential to characterize the materials in terms of their binder, aggregates and determination of the ratios used for their production. Such information is crucial to develop the restoration mortars that are compatible with the existing materials to implement a successful conservation and restoration work.

A total of 20 samples representing the Roman and XVI century foundations, the XVI century renders and decorations, the XVII century renders and the XIX century decoration mortars were examined through a multi analytical approach. They were analysed by using Optical Microscopy (OM, stereo zoom and petrographic microscope), X-ray Diffraction (XRD), Scanning Electron Microscopy coupled with Energy Dispersive X-ray Spectroscopy (SEM-EDS), Thermogravimetric Analysis (TGA-DTG), Acid Attack and Granulometric Analysis. Their chemical and mineralogical determinations were obtained for the designation of the repair mortars and assessment of the raw materials together with their provenance. The manufacturing receipts of the historical mortars and their production techniques were also hypothesized.

On the basis of the results obtained, samples were grouped into 3 main groups; 1) Filler mortars from foundations with sub-groups for the Roman and XVI century, 2) Render mortars (including XVI and XVII centuries) and 3) Decoration mortars with subgroups for XVI and XIX centuries. Within the groups and sub-groups, the characteristic properties of the mortars demonstrated similarities. A clear difference was observed in terms of the binder properties of the mortars from different construction periods and structural needs. Whereas, their aggregates demonstrated a uniform mineralogical composition at all historical phases.

The first group of samples which are the filler mortars collected from the foundations revealed a clay like binder matrix composed of Si, Al, Mg, Ca and Fe together with small amount of calcitic lime. Such composition of the binder gave the mortars hydraulic properties without the addition of ceramic fragments or pozzolanic additives. This characteristic feature is directly connected with the expected performance of the mortars since they were prepared to support the structure under the soil, naturally in a moist environment and needed to have a certain level of resistance against humidity compared to the mortars used in the upper structure.

The second group of samples is the render mortars from the XVI (AP-04 and AP-11), XVII (AP-01 and AP-02) centuries and the inner layers of XIX century mortars (AP-09D and AP-10D). They demonstrated similar characteristics among each other in terms of binder properties by the use of calcitic lime with some impurities which indicates the probable use of the same source for the acquisition of raw materials. Their binder:aggregate ratios vary between 1:2 and 1:3. Among the XIX century mortar group, their inner layers of the samples with stratigraphy (AP-09D and AP-10D) revealed distinctive characteristics from their upper layers (AP-09U and AP-10U). Similar to the render mortars of the XVI and XVII centuries, AP-09D and AP-10D revealed the use of calcitic lime for their binder suggesting that the layering of these samples (AP-09 and AP-10) may be representative of the different construction phases. The hydraulicity level of this group is calculated as a medium degree expectedly lower than the foundation mortars but still corresponding to a certain level. This characteristic feature can be correlated with the expected performance of the mortars since they were prepared to be used in the open air, naturally in contact with outdoor conditions and needed to have a certain level of resistance against the rainwater.

The third group of samples is the decorative mortars of the XVI century and all mortars of the XIX century with the exception of the inner layers (AP-09D and AP-10D). The binder material of this group demonstrated dolomitic properties indicating the use of a different source for the acquisition of the raw materials. Within the composition of the decorative mortars, the addition of crushed lime was determined. Such additives were detected especially in the lighter coloured samples possibly to achieve a whiter appearance on the finished surfaces therefore used as pigments. None of the samples in this group represented hydraulic properties possibly because such property was already obtained with the render mortars in the inner layers so as in (AP-09D and AP-10D) and no additional performance was expected from the decorative mortars.

The grouping of the mortars according to their binder characteristics allowed to correlate the different constructive purposes with the selection of binder material as the distinctive feature. The clayish binder with a small amount of calcitic lime was representative for sub-terranean mortars, whereas calcitic lime for rendering and dolomitic lime for decorative needs. Among the XVI century mortar group, the selection of binder material is clearly visible indicating the intentional choice of the builders in this period. In comparison with the Santa Maria Church of Évora, which is considered as a fine example of XVI century's building practices, the use of dolomitic lime has also proven with analytical studies (Adriano *et al.*, 2009). The difference of binder properties of the XVI century render and decoration mortars may be hypothesized as the choice of dolomitic lime is related to a more elaborate production as in the decorative mortars of the aqueduct and the mortars of Santa Maria Church of Évora. Such grouping was not achieved in the XIX century

render and decoration mortars since both of them displayed the use of dolomitic lime. The choice of the dolomitic raw material in the mortars of this century may have been a specific decision since they were the productions of a certain intervention activity in the XIX century which aimed the decoration of the monumental fountain located inside the Fortress of Santo António. Therefore, sample AP-05 that was used for rendering purposes was also a production of decorative intervention activity.

In terms of aggregate composition all samples shared a uniform mineralogical pattern composing of mainly quartz, feldspars and micas together with Mg and Fe rich minerals like amphiboles, olivine and pyroxenes. The single grains which were predominant in angular and subangular forms were sometimes in association with each other as rock fragments. The morphology is indicative for a short distance of transportation of the aggregates (also the use of crushed materials) meaning that the geological source (outcrops) is found in the vicinity. The possible provenance which corresponds to the mineralogical composition is the local granites of the Évora massif as described in the geological maps by Moita *et al.*, (2009). The presence of Mg and Fe rich minerals (olivine and pyroxene) in the samples agrees with the gabbro intrusions of Alto de São Bento as a proximal source of the raw materials which also correlates with the study of the historical mortars from Santa Maria Church of Évora (Adriano *et al.*, 2009). Both structures are considered prestigious masonry constructions of the XVI century.

The study provides the assessment of the mortars from the aqueduct of Água da Prata which is one of the most recognized landmarks of Évora with its national and universal heritage value. The archaeometric study carried out on the historical mortars allowed to obtain crucial information about the materials used for the production of the mortars and the selection of different raw materials in relation to the expected performance for the sub-terranean, upper structure and decorative needs. Such characterization is necessary to create compatible repair mortars as an important part of the development of a sustainable conservation methodology for the restoration work of the monument which is planned to be made in the future. Another important outcome of the work is that it provides essential information to enlighten the historical background of the structure dating back to Roman periods which also contributes to the previous researches (Bilou and Santos, 2019) on Aqueduto da Água da Prata which plays an essential role in the cultural and social life of Évora.

7 BIBLIOGRAPHY

- Adriano, P., A. Santos Silva, R. Veiga, J. Mirão, and A. E. Candeias. 2009. “Microscopic Characterisation of Old Mortars from the Santa Maria Church in Évora.” *Materials Characterization* 60(7):610–20.
- Artioli, Gilberto and Roberta Oberti. 2019. “Introduction: The Role of Modern Mineralogy in Cultural Heritage Studies.” *European Mineralogical Union Notes in Mineralogy* 20:1–11.
- Artioli, Gilberto, Michele Secco, and Anna Addis. 2019. “The Vitruvian Legacy: Mortars and Binders before and after the Roman World.” *European Mineralogical Union Notes in Mineralogy* 20:151–202.
- Berking, Jonas. 2018. “Water Management in Ancient Civilizations: Editorial.” *Water Management in Ancient Civilizations*. Berlin studies of the Ancient World. 53:1-7.
- Bilou, Francisco. 2010. A Refundação do Aqueduto da Água da Prata, em Évora, 1533-1537. Edições Colibri, Évora, Portugal.
- Bilou, Francisco., Santos, José Rui. 2019. “A Origem Romana do Aqueduto da Água da Prata: Entre a Tradição ‘Sertoriana’ e os Vestígios Arqueológicos Romanos.” O Aqueduto da Água da Prata e O Património Hidráulico de Évora. CME.:15-22. ISBN: 978 972 8509 66 8.
- Blott, S. J. and Pye, K. 2001. “Gradistat: A grain size distribution and statistics package for the analysis of unconsolidated sediments.” *Earth Surface Processes and Landforms*. 26(11):1237–1248. doi: 10.1002/esp.261.
- Borsoi, G., A. Santos Silva, P. Menezes, A. Candeias, and J. Mirão. 2019. “Analytical Characterization of Ancient Mortars from the Archaeological Roman Site of Pisões (Beja, Portugal).” *Construction and Building Materials* 204:597–608.
- Buxó, Ramon. 2008. ‘The Water Management in an Ancient Greek-Roman City (I): An Example in the North-east of Spain’. *Water Culture and Water Conflict in the Mediterranean Area*, 83:9–16.
- Cardoso, I., M. F. Macedo, F. Vermeulen, C. Corsi, A. Santos Silva, L. Rosado, A. Candeias, and J. Mirao. 2014. “A Multidisciplinary Approach to the Study of Archaeological Mortars from the Town of Ammaia in the Roman Province of Lusitania (Portugal).” *Archaeometry* 56(1):1–24.
- Claro, Sylvie. 2019. “Aquaeducto: proposta de percurso para a Água da Prata.” Master Thesis. University of Evora, Department of Architecture. Evora.
- CME-DCP. 2018. “Relatório Das Sondagens Arqueológicas Na Herdade Da Cartuxa e Torralva.”, Programa de Conservação e Consolidação do Aqueduto da Água da Prata. Evora.

- CME-DCP. 2019. “Requalificação Do Aqueduto Da Água Da Prata Em Évora.”, Programa de Conservação e Consolidação do Aqueduto da Água da Prata. Evora.
- Conde, Antonia. and Magalhaes, Olga. 2008. “Abordagem educativa de um monumento: o Aqueduto de Évora.” *Puertas a la lectura*, (20):91–112.
- De Feo, Giovanni., Angelakis, Andreas N., Antoniou Georgios., El Gohary, Fatma., Haut, Benoit., Passchier, Cees., Zheng, Xiao Yun. 2013. “Historical and technical notes on aqueducts from prehistoric to medieval Times.” *Water (Switzerland)*, 5(4):1996–2025. doi: 10.3390/w5041996.
- Elsen, Jan. 2006. “Microscopy of Historic Mortars-a Review.” *Cement and Concrete Research* 36(8):1416–24.
- Elsen, Jan, Koenraad Van Balen, and Gilles Mertens. 2013. “Hydraulicity in Historic Lime Mortars: A Review.” *RILEM Bookseries* 7(September):125–39.
- Ergenç, Duygu and Fort González, Rafael. 2017. “Preliminary Investigation of the Preparation of Repair Mortars for the Temple of Diana, Mérida, Spain.” *Ge-Conservacion* 1(11):42–49.
- Ergenç, Duygu and Fort González, Rafael. 2019. “Multi-Technical Characterization of Roman Mortars from Complutum, Spain.” *Measurement* 147:106876.
- Fahlbusch, Henning. 2010. “Water in human life: Technical innovations in hydraulic engineering in the last 5000 years.” *ICID J.* 49, 1–16.
- Fahlbusch, Henning. 2010. “Water Engineering and Management in the Classical Civilizations.” *Water management through time: Learning from history*. Editor: Enrique Cabrera Chapter 4:77-116. CRC press. ISBN: 13:978-0-203-83673-6.
- Földvári, Mária. 2011. “Handbook of the Thermogravimetric System of Minerals and Its Use in Geological Practice.” Vol. 213, Central European Geology. Budapest: Geological Institute of Hungary.
- Hodge, A. Trevor. 2000. “Aqueducts.” *Handbook of Ancient Water Technology.*, Editor: Örjan Wikander. Die Deutsche Bibliothek. Köln. Chapter 5:39–68. ISBN: 90 04 11123 9.
- Hodge, A. Trevor. 2013. “Aqueducts and Water Supply.” *A Companion to the Archaeology of the Roman Republic*, Chp.18:285–295. doi: 10.1002/9781118557129.
- ICCROM. 1981. “Mortars, cements and grouts used in the conservation of historic buildings.” *Symposium 3*, (pp. 1-424). Rome.
- Jedrzejewska, Hanna. 1960. “Old Mortars in Poland : A New Method of Investigation.” 5(4):132–38.

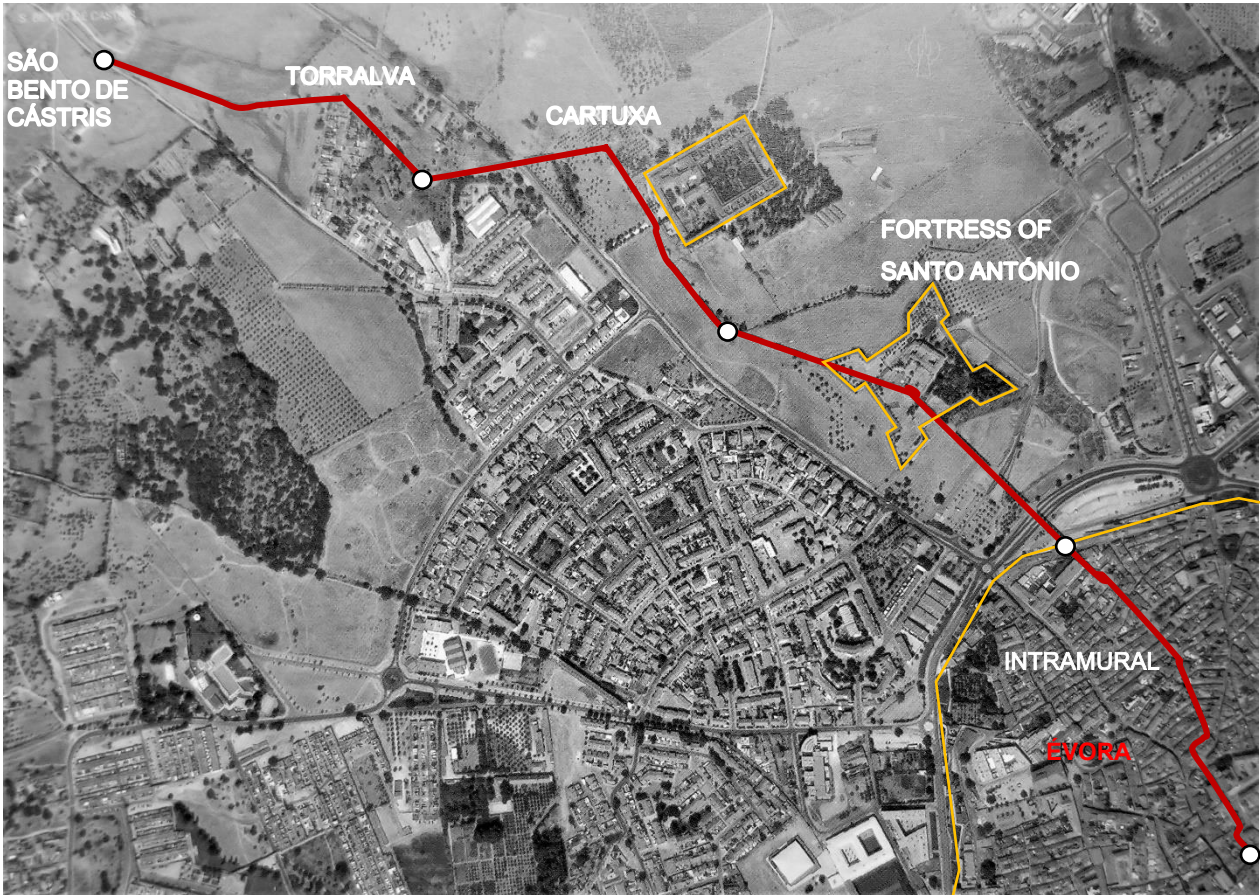
- Lammel, M. and G. Lehrberger. 2007. "Identification of the Carbonate Sources and Quarries for Historical Lime-Mortars in Teplá." Vol 9.
- Leone, Gemma, Alessandra De Vita, Agnese Magnani, and Claudio Rossi. 2017. "Thermal and Petrographic Characterization of Herculaneum Wall Plasters." *Archaeometry*, 59(4):747–761. doi: 10.1111/arcm.12275.
- Leone, Gemma, Alessandra De Vita, Agnese Magnani, and Claudio Rossi. 2016. "Characterization of Archaeological Mortars from Herculaneum." *Thermochimica Acta* 624:86–94.
- Lindqvist, Jan Erik., Johansson, Sölve. 2015. "Sub-Hydraulic Binders in Historical Mortars." (2):224–230.
- Martinez, Alberto. 2019. "Aquaduto da Água da Prata em Évora." O Aqueduto da Água da Prata e O Património Hidráulico de Évora. CME.:87-101. ISBN: 978 972 8509 66 8.
- Matias, Gina, Paulina Faria, and Isabel Torres. 2014. "Lime Mortars with Ceramic Wastes: Characterization of Components and Their Influence on the Mechanical Behaviour." *Construction and Building Materials* 73:523–34.
- Mays, W. Larry. 2009. "A Brief History of Water Technology During Antiquity: Before the Romans". Ancient Water Technologies." Springer. London.:1-28. ISBN: 978-90-481-8632-7.
- Mays, W. Larry. 2009. "A Brief History of Roman Water Technology." Ancient Water Technologies. Springer. London.:115-138. ISBN: 978-90-481-8632-7.
- Middendorf, B., J. J. Hughes, K. Callebaut, G. Baronio, and I. Papayianni. 2005. "Investigative Methods for the Characterisation of Historic Mortars - Part 2: Chemical Characterisation." *Materials and Structures/Materiaux et Constructions* 38(282):771–80.
- Miriello, Domenico, Donatella Barca, Andrea Bloise, Annamaria Ciarallo, Gino M. Crisci, Teresa De Rose, Caterina Gattuso, Flavia Gazineo, and Mauro F. La Russa. 2010. "Characterisation of Archaeological Mortars from Pompeii (Campania, Italy) and Identification of Construction Phases by Compositional Data Analysis." *Journal of Archaeological Science* 37(9):2207–23.
- Miriello, Domenico, Andrea Bloise, Gino M. Crisci, Raffaella De Luca, Bruno De Nigris, Alberta Martellone, Massimo Osanna, Rossella Pace, Alessandra Pecci, and Nicola Ruggieri. 2018. "New Compositional Data on Ancient Mortars and Plasters from Pompeii (Campania – Southern Italy): Archaeometric Results and Considerations about Their Time Evolution." *Materials Characterization* 146(September):189–203.
- Moita, Patrícia, José F. Santos, and M. Francisco Pereira. 2009. "Layered Granitoids: Interaction between Continental Crust Recycling Processes and Mantle-Derived Magmatism. Examples from the Évora Massif (Ossa-Morena Zone, Southwest Iberia, Portugal)." *Lithos* 111(3–4):125–41.

- Monteiro, M. F. M. 2012. “Passado presente, futuro ” Congresso Internacional Mosteiros Cistercienses: Alcobaça 14 a 17 Junho 2012:1–9.
- Moropoulou, A., A. Bakolas, and S. Anagnostopoulou. 2005. “Composite Materials in Ancient Structures.” *Cement and Concrete Composites* 27(2):295–300.
- Oguz, Cem. Turker, Fikret. and Kockal, Niyazi Uğur. 2014. “Construction materials used in the historical roman era bath in Myra.” *Scientific World Journal*, 2014. doi: 10.1155/2014/536105.
- Pavía, S., B. Fitzgerald, and R. Howard. 2005. “Evaluation of Properties of Magnesian Lime Mortar.” *WIT Transactions on the Built Environment* 83(January):375–84.
- Perreira, Marizia. 2012. “O património natural do Aqueduto da Água da Prata – um valor a preservar.” *Atas do Ciclo de Conferências ‘Água e Património’*, Convento dos Remédios, Évora. pp. 37–39.
- Raith, Michael M., Peter Raase, and Jürgen Reinhardt. 2011. “Guide to Thin Section Microscopy.” ISBN 978-3-00-033606-5 (PDF)
- Riccardi, Maria Pia, Marco Lezzerini, Federico Carò, Marco Franzini, and Bruno Messiga. 2007. “Microtextural and Microchemical Studies of Hydraulic Ancient Mortars: Two Analytical Approaches to Understand Pre-Industrial Technology Processes.” *Journal of Cultural Heritage* 8(4):350–60.
- Rizzo, G., Laura Ercoli, B. Megna, and Maria Parlapiano. 2008. “Characterization of Mortars from Ancient and Traditional Water Supply Systems in Sicily.” *Journal of Thermal Analysis and Calorimetry* 92(1):323–30.
- Rodríguez-Navarro, Carlos. 2012. “Binders in Historical Buildings: Traditional Lime in Conservation.” *Seminarios SEM* 9:91–112.
- Salema, Sofia. 2008. “Architecture Surfaces Conservation: (Re) Discovering Sgraffito in Portugal.” *1st Historical Mortars Conference*.
- Schnabel, Lorraine. 2008. “Mortar Analysis Part 1: Mortar-Making Materials.” *APT Bulletin* 39(1):1.
- Silva, A. Santos., M. Paiva, J. Ricardo, M. Salta, A. M. Monteiro, and A. E. Candeias. 2006. “Characterization of Roman Mortars from the Archaeological Site of Tróia (Portugal).” *Materials Science Forum* 514–516(PART 2):1643–47.
- Silva, A. Santos, J. M. Ricardo, M. Salta, P. Adriano, J. Mirão, A. Estêvão Candeias, and S. Macias. 2006. “Characterization of Roman Mortars from the Historical Town of Mertola.” *Proceedings of the International Conference on Heritage, Weathering and Conservation, HWC 2006* 1:85–90.

- Snežžana Miljanić, Leo Frkanec, Tomislav Biljan, Zlatko Meić Mladen Žinić. 2007. “Recent Advances in Linear and Nonlinear Raman Spectroscopy I.” *Journal of Raman Spectroscopy* 38(April):1538–53.
- Stefanidou, Maria, Vasiliki Pachta, Stavroula Konopissi, Fotini Karkadelidou, and Ioanna Papayianni. 2014. “Analysis and Characterization of Hydraulic Mortars from Ancient Cisterns and Baths in Greece.” *Materials and Structures/Materiaux et Constructions* 47(4):571–80.
- Struers. 2014. *Mineralogical specimen preparation*. Retrieved from: <https://www.als.com.tr/?wpfb_dl=135> in August 2020.
- Stuart, Barbara H. 2007. “*Analytical Techniques in Materials Conservation*.” John Wiley & Sons, England. ISBN: 0-470-01280-3
- Sürmelihiindi, Gül, Cees W. Passchier, Orhan N. Baykan, Christoph Spötl, and Paul Kessener. 2013. “Environmental and Depositional Controls on Laminated Freshwater Carbonates: An Example from the Roman Aqueduct of Patara, Turkey.” *Palaeogeography, Palaeoclimatology, Palaeoecology* 386:321–35.
- Tapete, Deodato, Stefano Morelli, Riccardo Fanti, and Nicola Casagli. 2015. “Localising Deformation along the Elevation of Linear Structures: An Experiment with Space-Borne InSAR and RTK GPS on the Roman Aqueducts in Rome, Italy.” *Applied Geography* 58:65–83.
- Valdez Madrid, Dulce Elizabeth. 2019. “Characterisation of Mortars Associated with the Hydraulic System of Roman Villa Horta da Torre.” Master Thesis. University of Evora, ARCHMAT. Evora.
- Válek, Jan, John J. Hughes, and Caspar J. W. P. Groot. 2013. “Historic Mortars: Characterisation, Assessment and Repair.” *RILEM Bookseries* 7(January).
- Varella, Evangelia. 2013. “*Conservation Science for the Cultural Heritage - Applications of Instrumental Analysis*.” Vol. 79., Springer. DOI 10.1007/978-3-642-30985-4.
- Vecchiattini, Rita. 2003. “The Use of Dolomitic Lime in Historical Buildings: History, Technology and Science.” *Construction* (January).
- Whotrips, 2020. “The door to the house is at the Évora Aqueduct”. viewed 27 November 2020. <<https://whotrips.com/2020/06/08/a-porta-da-casa-e-no-aqueduto-de-evora/>>.

8 APPENDICES

Appendix 1. Sections of the aqueduct of Água da Prata as described in the study.



Appendix 2. Photos of the aqueduct from Torralva section (Taken by the author in Sept. 2020).



Appendix 3. Photos of the aqueduct from Cartuxa section, the monumental archway. (Top, taken by author in Sept. 2020; bottom, taken by Whotips, 2020).



Appendix 4. Photos of the aqueduct from Cartuxa section. (Top, taken by Whotips, 2020; bottom, taken by the author in Sept. 2020).



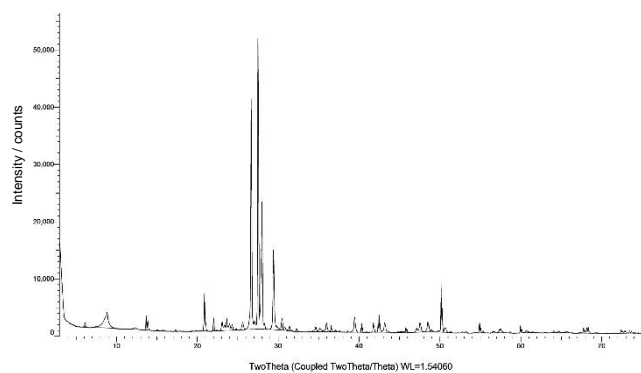
Appendix 5. Photos of the aqueduct from Fortress of Santo António section (Taken by author in Sept. 2020).



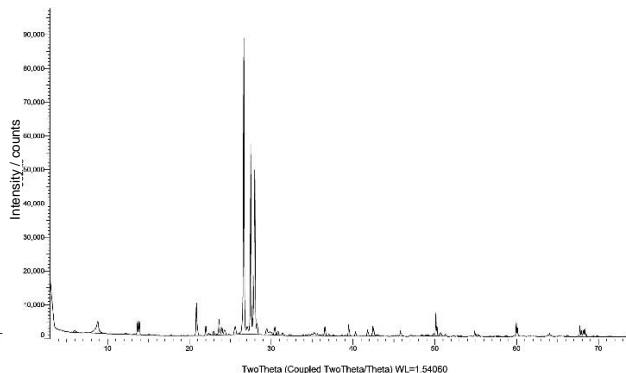
Appendix 6. Photos of the aqueduct from Intramural section, (Taken by Whotips, 2020).



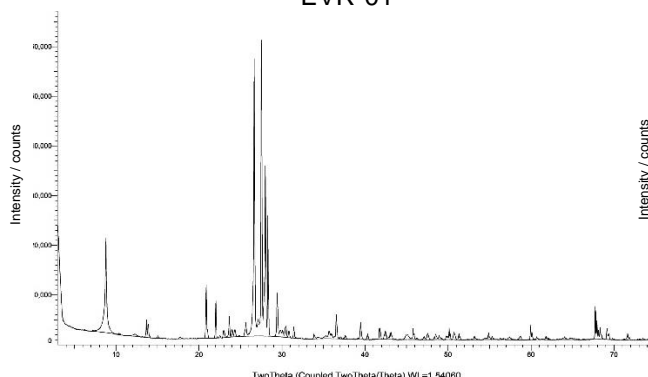
Appendix 7. X-ray diffractograms of the powdered samples from the aqueduct of Água da Prata (Global Fractions)



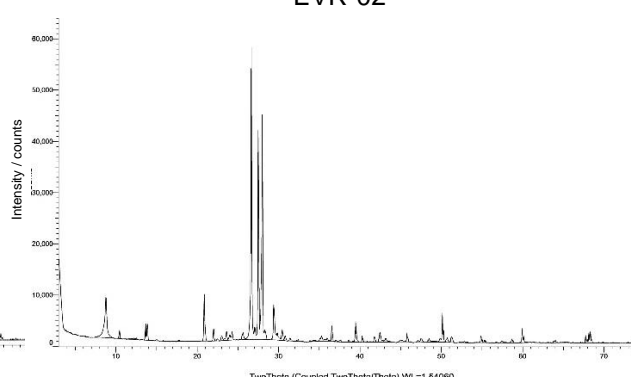
EVR-01



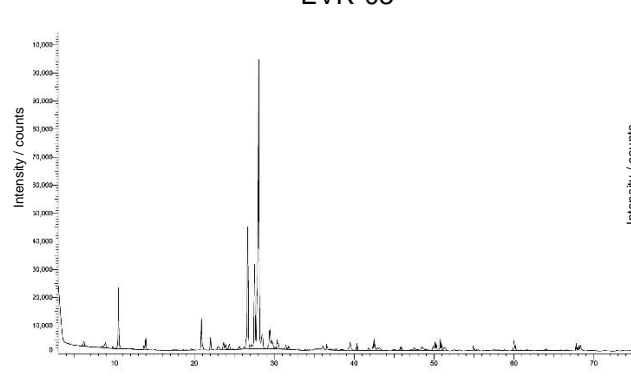
EVR-02



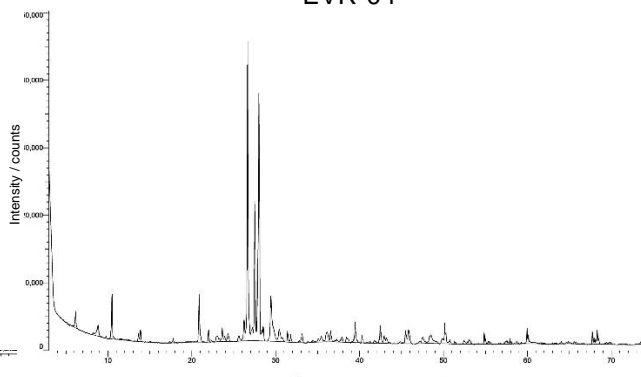
EVR-03



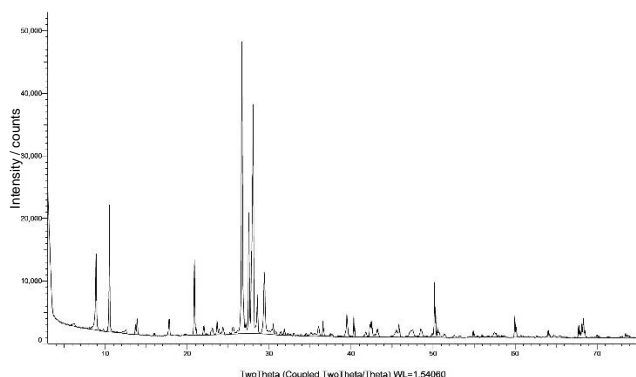
EVR-04



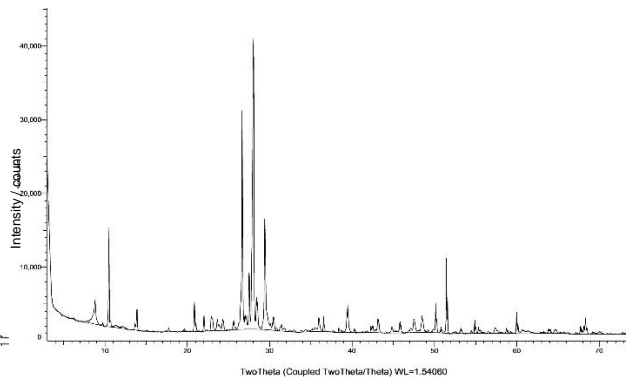
EVR-05



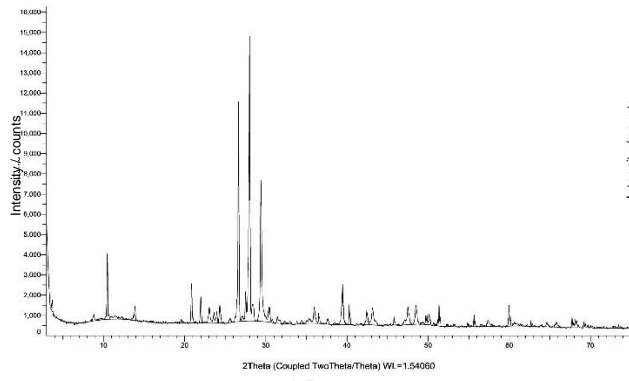
EVR-06



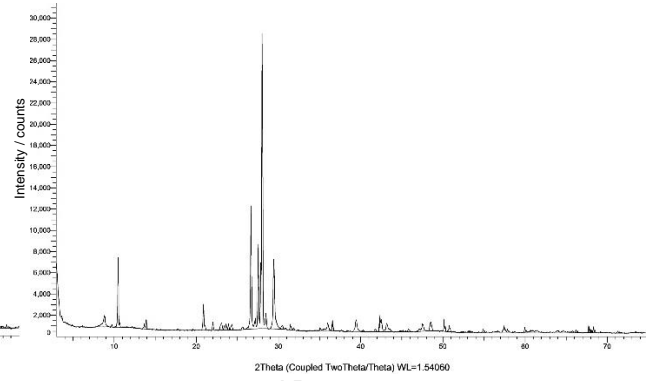
EVR-07



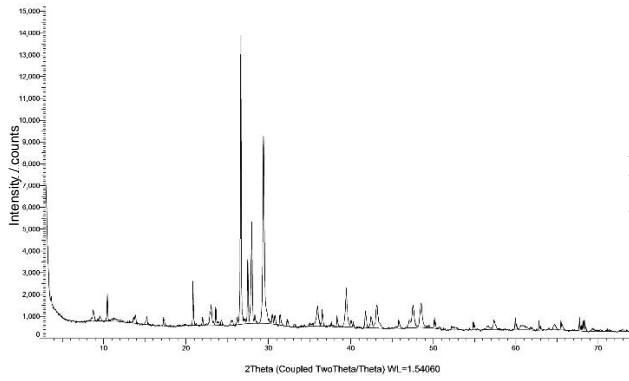
EVR-08



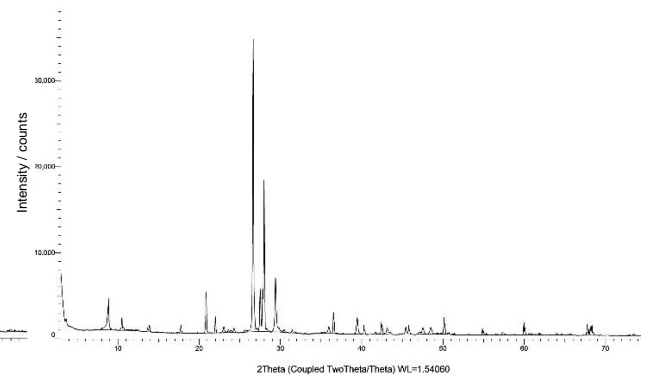
AP-01



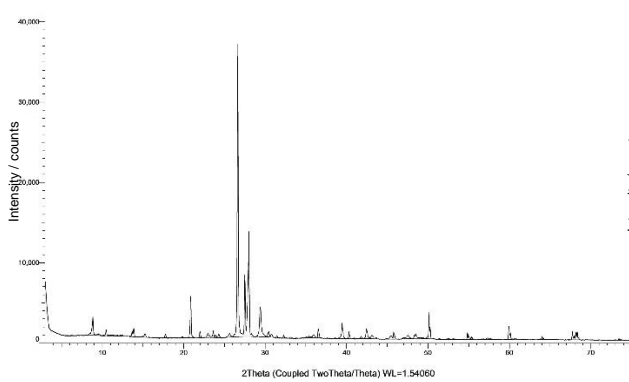
AP-02



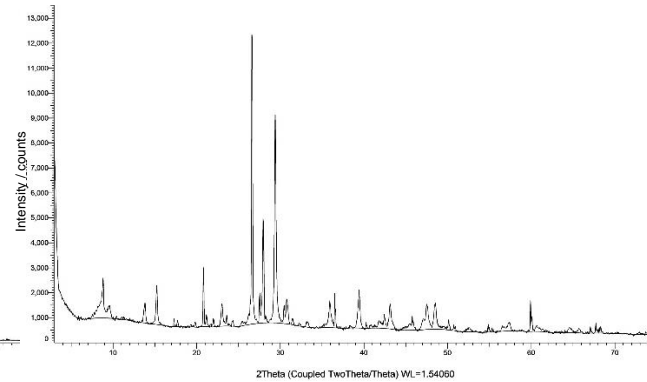
AP-03



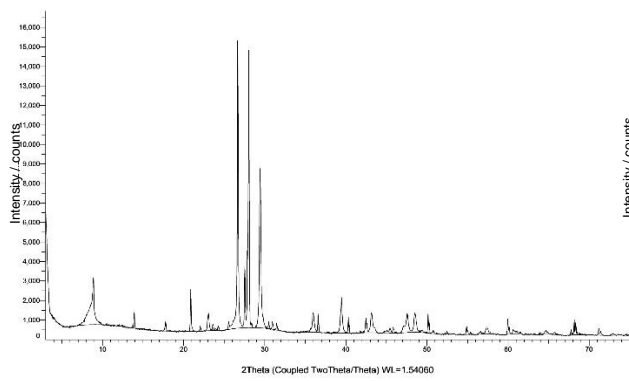
AP-04



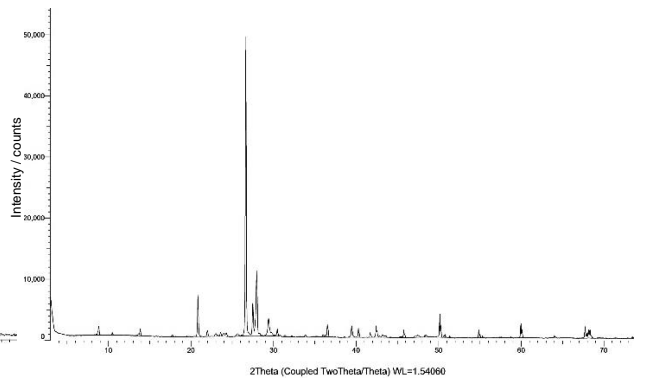
AP-05



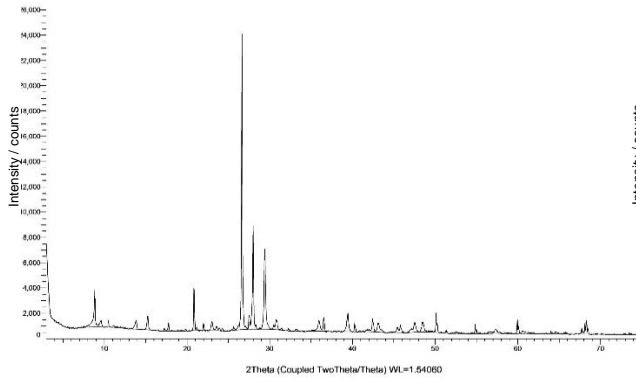
AP-06



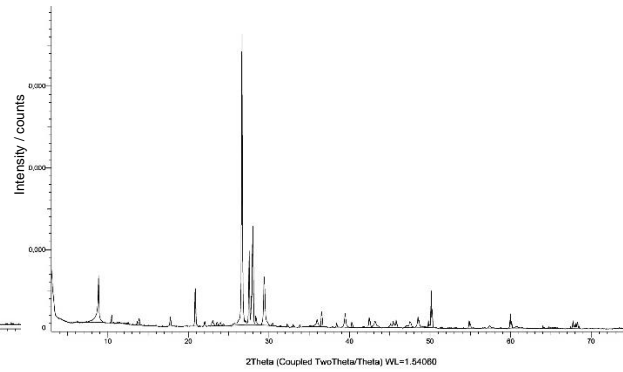
AP-08



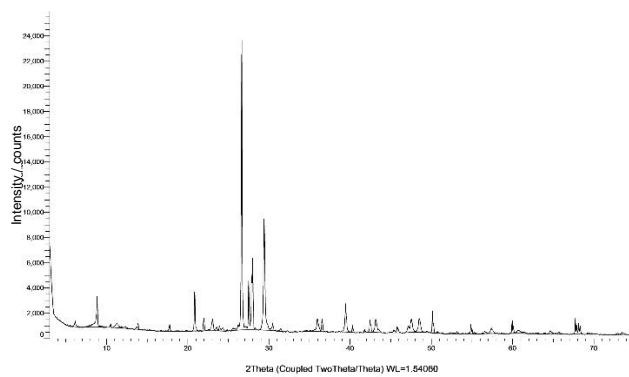
AP-09D



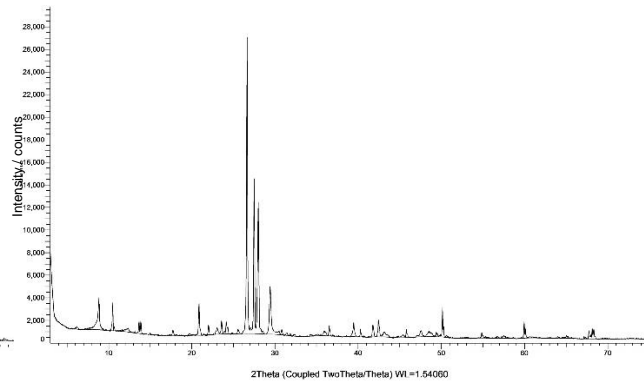
AP-09U



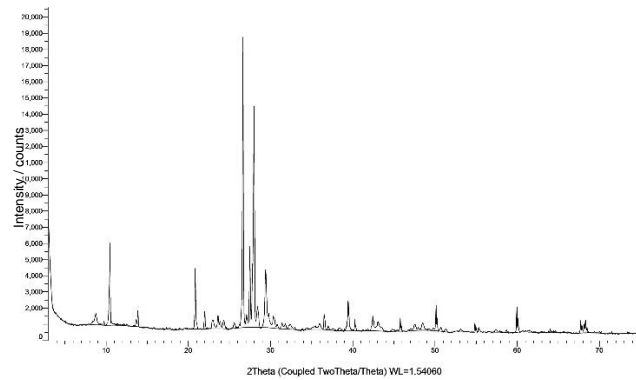
AP-10D



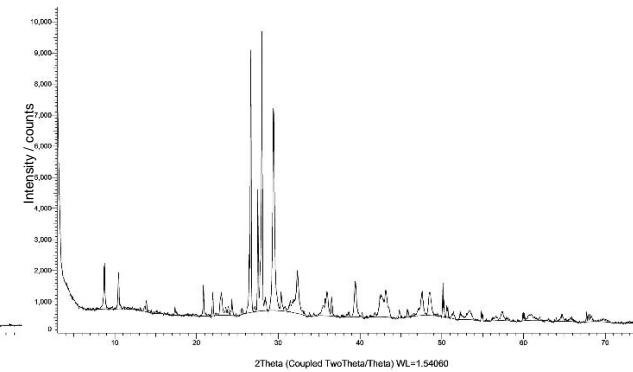
AP-10U



AP-11

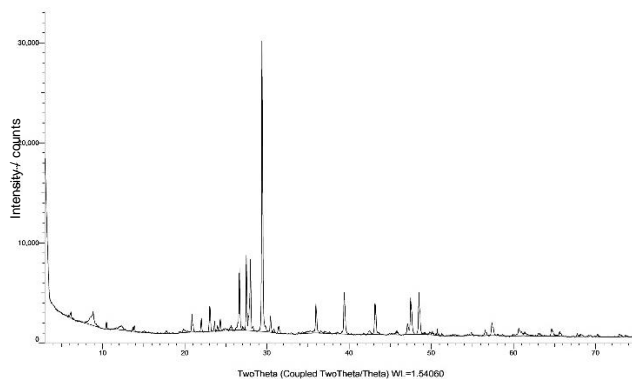


AP-12D

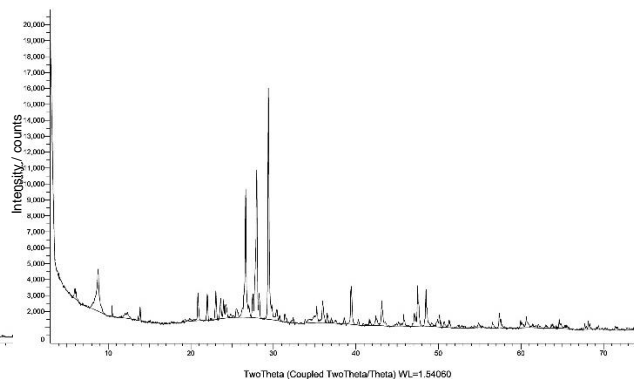


AP-12U

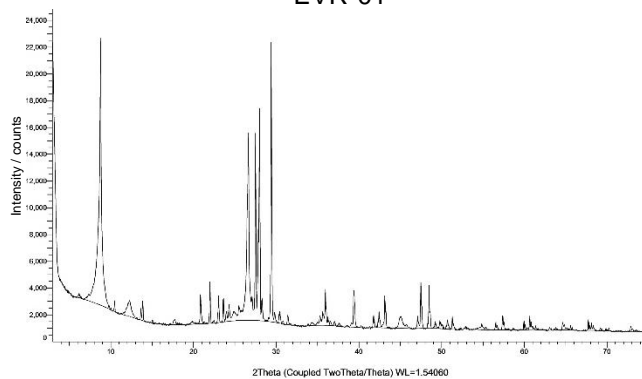
Appendix 8. X-ray diffractograms of the powdered samples from the aqueduct of Água da Prata (Fine Fractions)



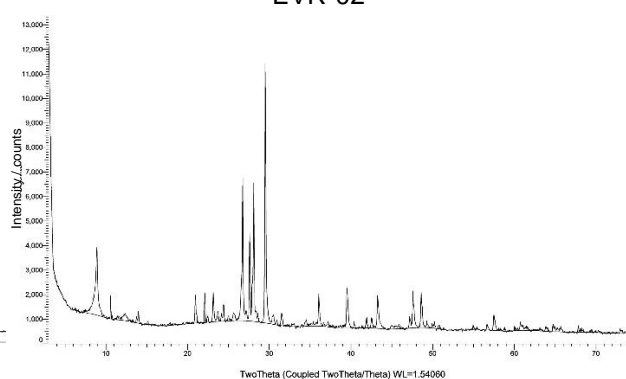
EVR-01



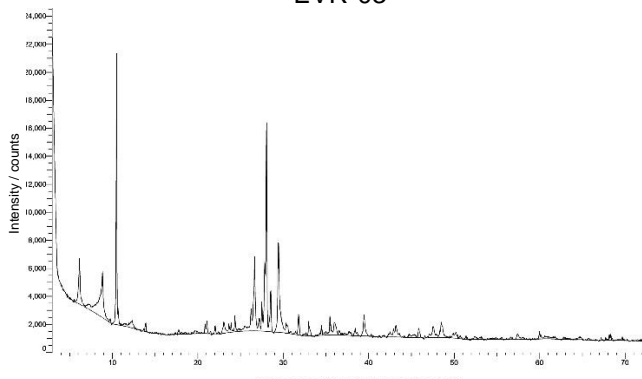
EVR-02



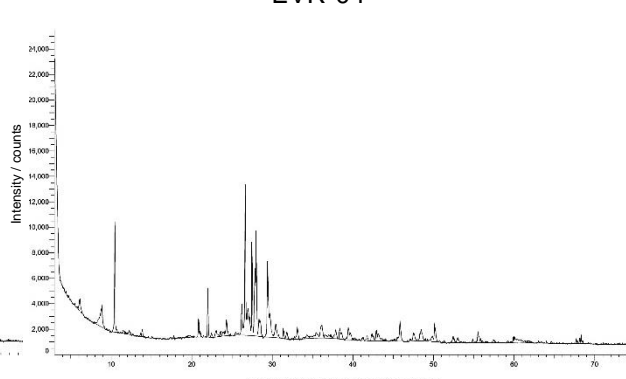
EVR-03



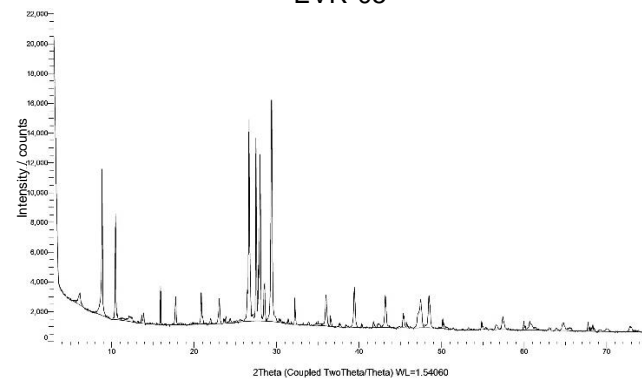
EVR-04



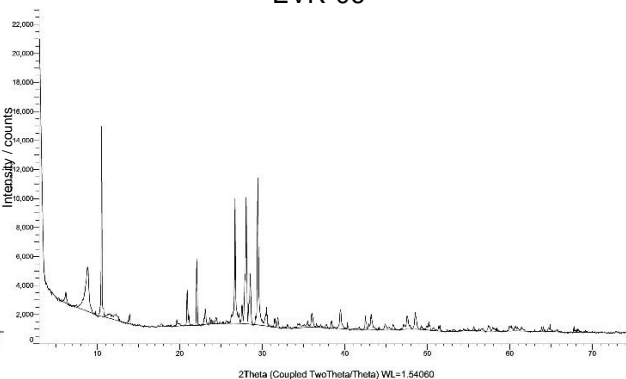
EVR-05



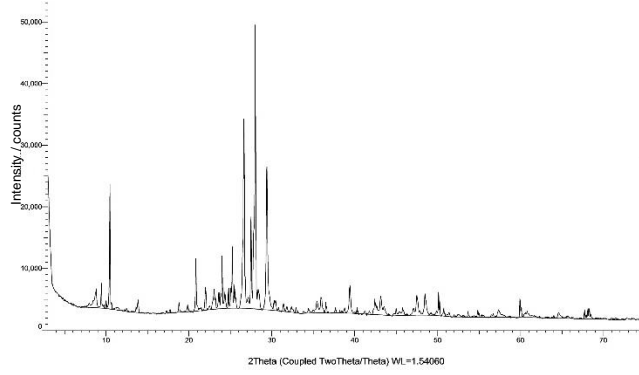
EVR-06



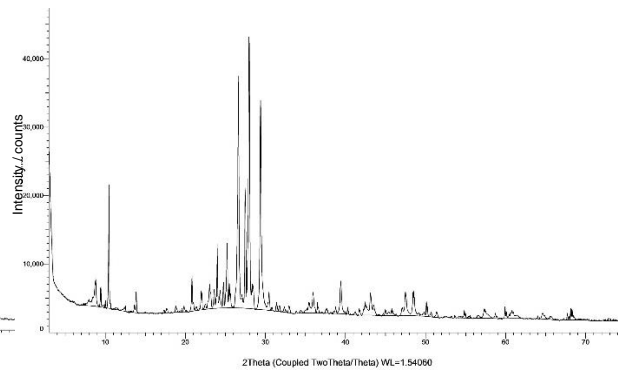
EVR-07



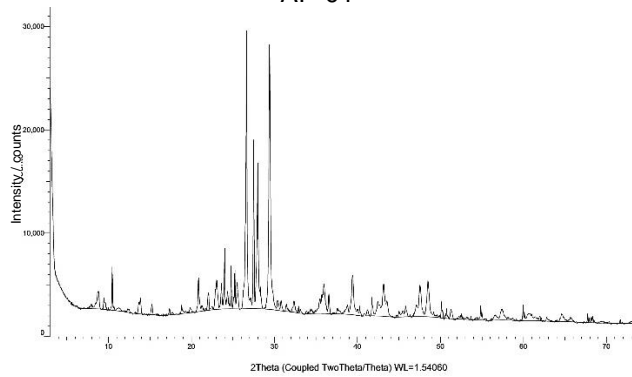
EVR-08



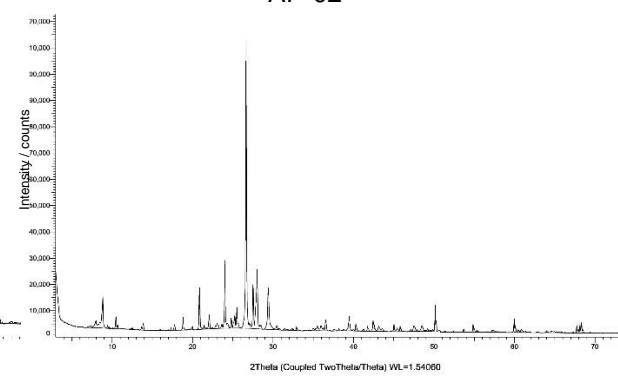
AP-01



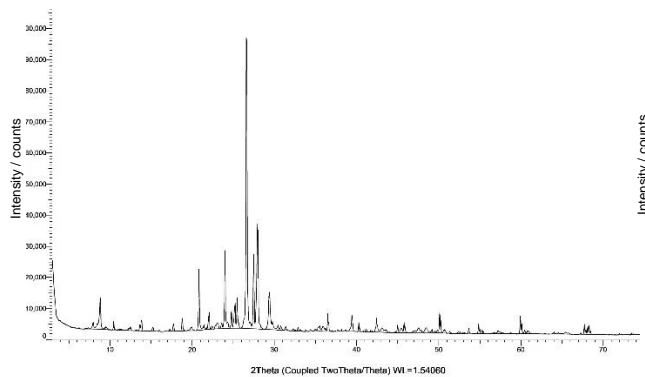
AP-02



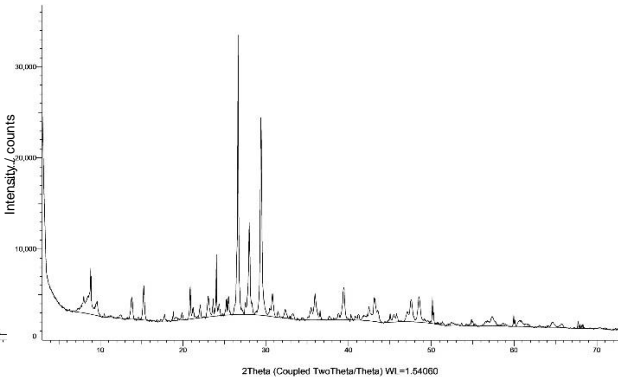
AP-03



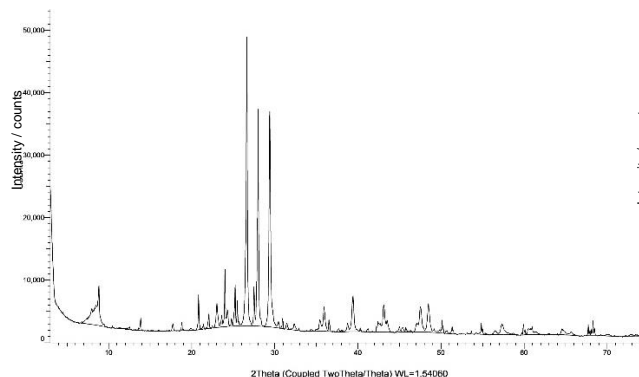
AP-04



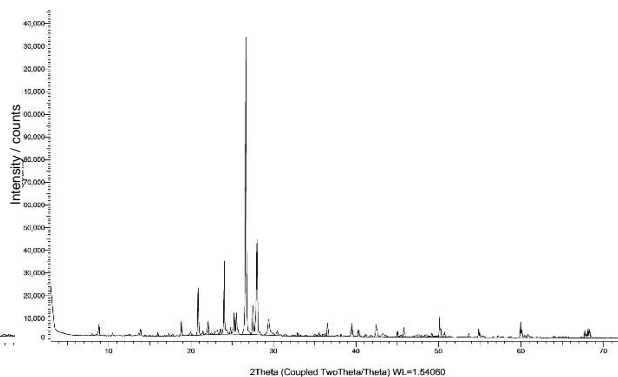
AP-05



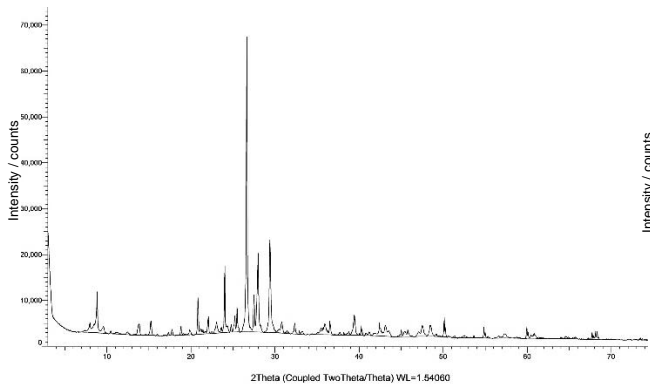
AP-06



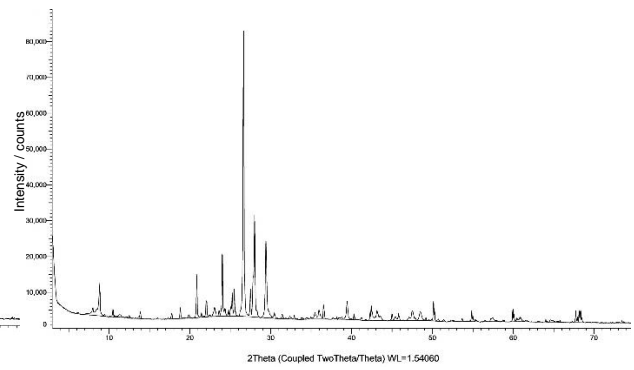
AP-08



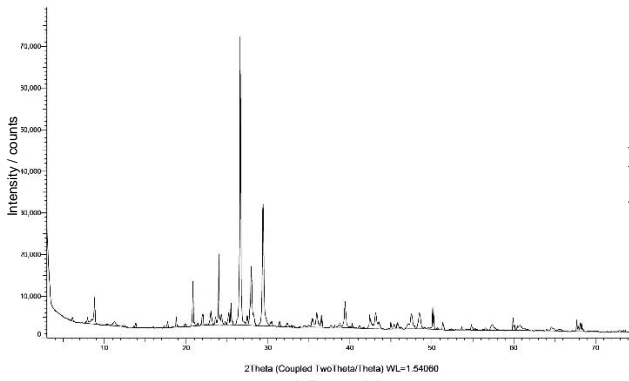
AP-09D



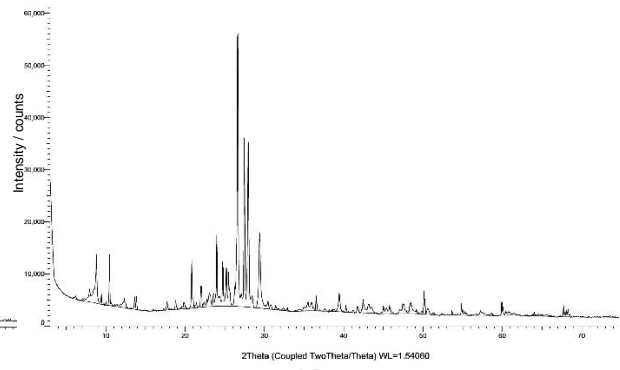
AP-09U



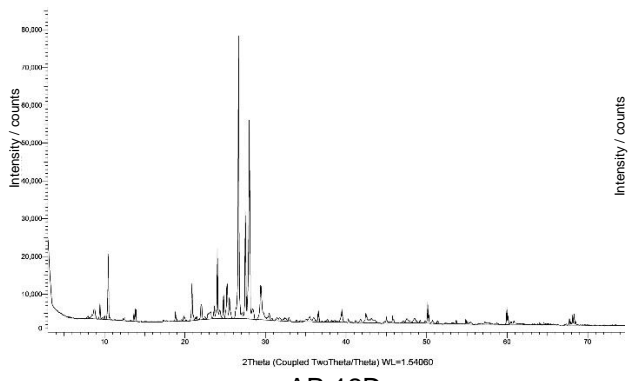
AP-10D



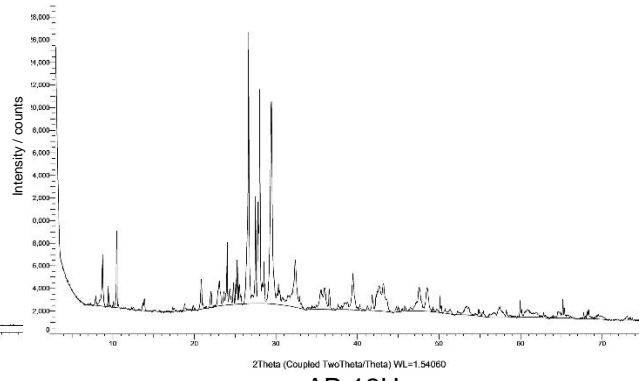
AP-10U



AP-11

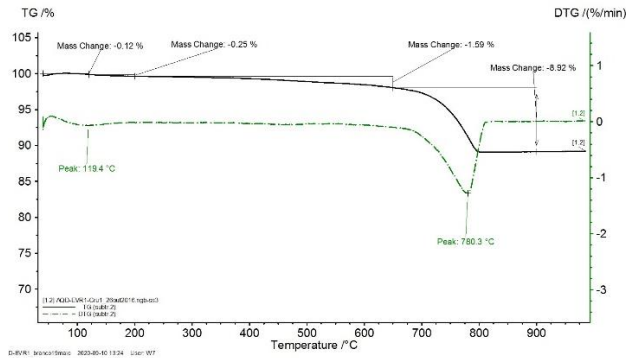


AP-12D

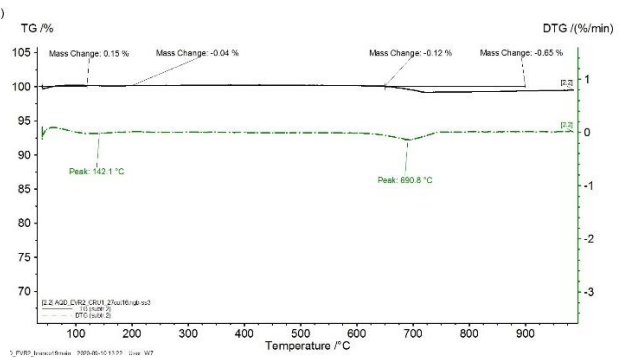


AP-12U

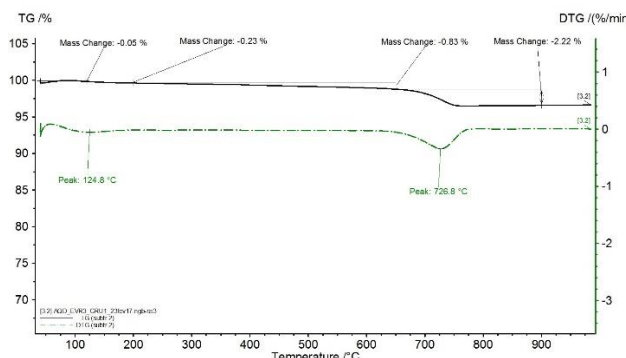
Appendix 9. Thermograms of the global fraction powders of the samples from the aqueduct of Água da Prata.



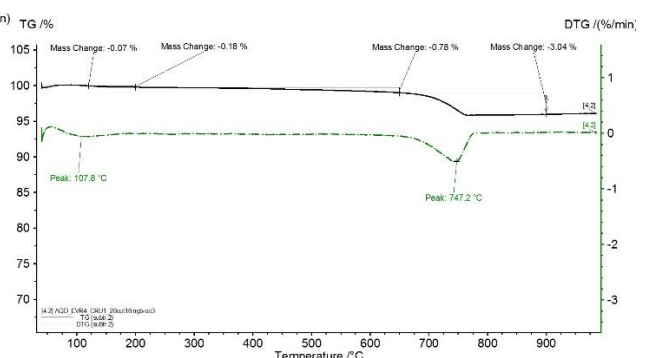
EVR-01



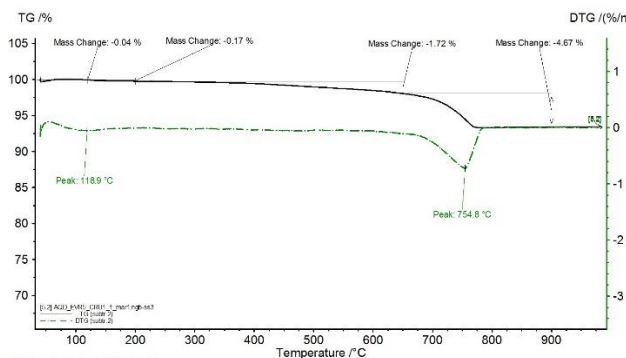
EVR-02



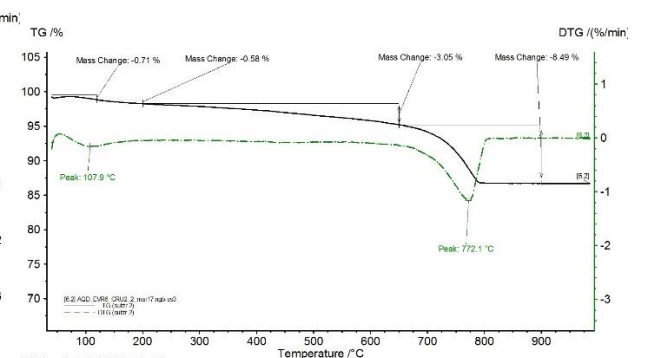
EVR-03



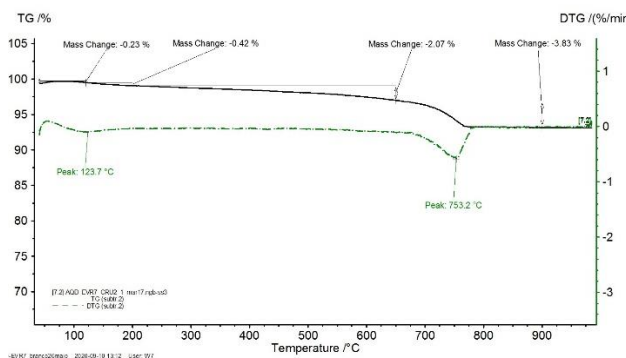
EVR-04



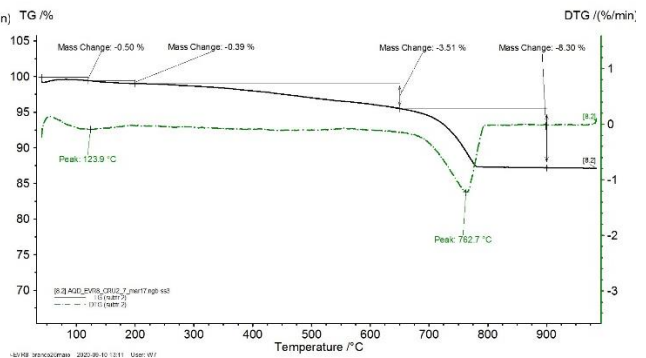
EVR-05



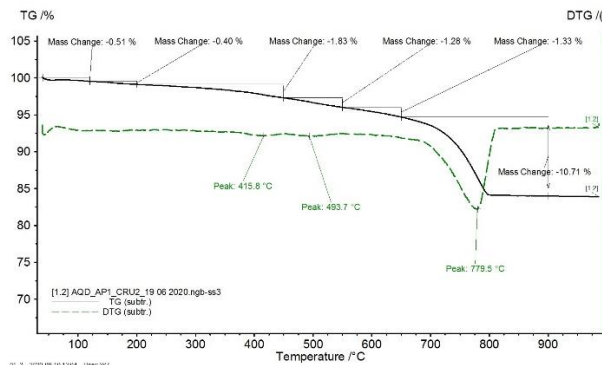
EVR-06



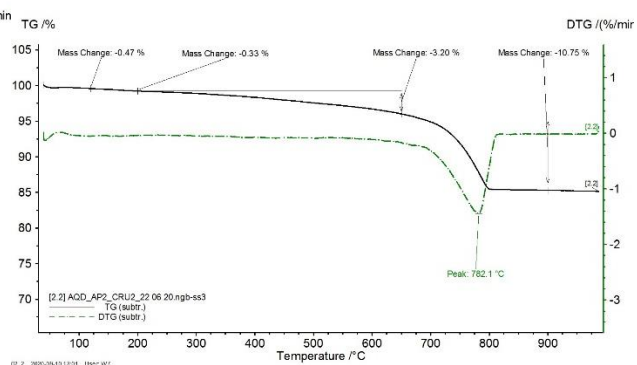
EVR-07



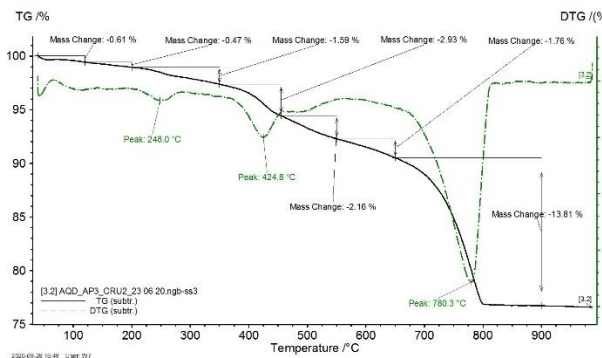
EVR-08



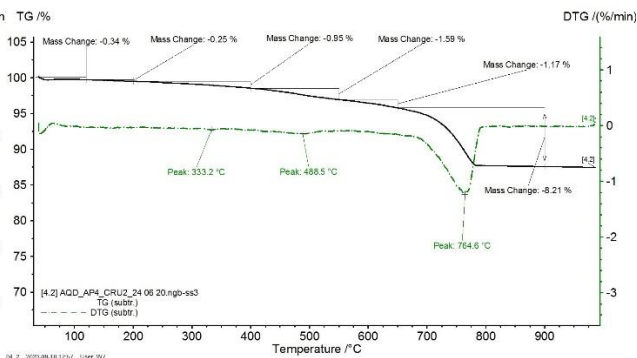
AP-01



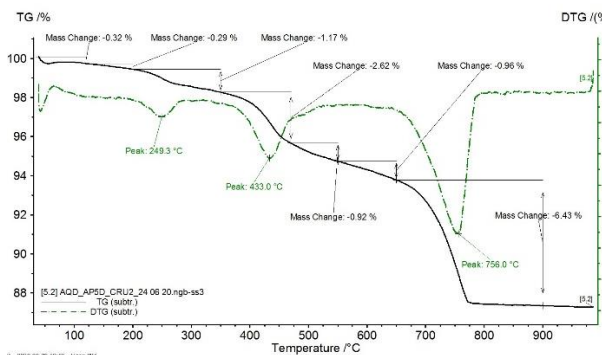
AP-02



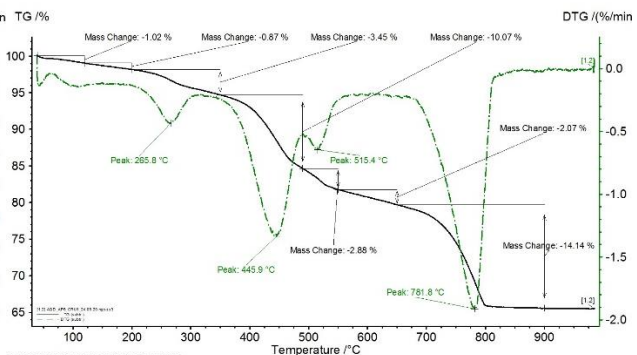
AP-03



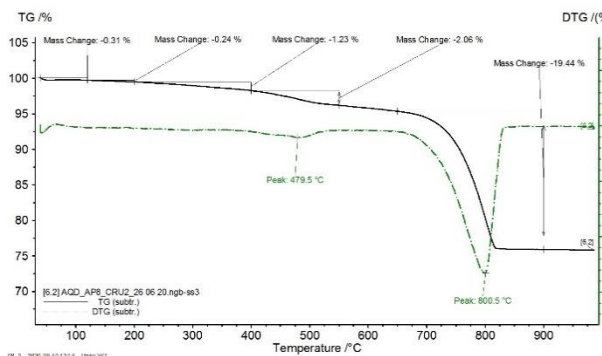
AP-04



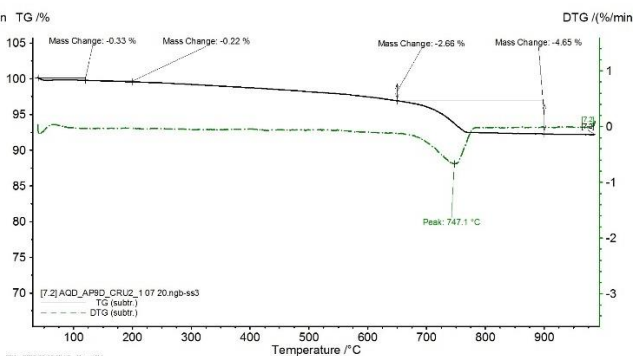
AP-05



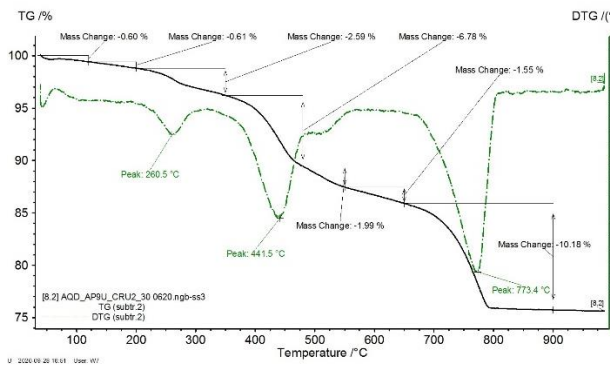
AP-06



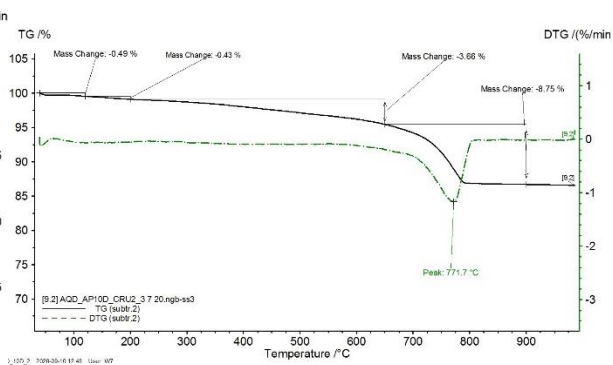
AP-08



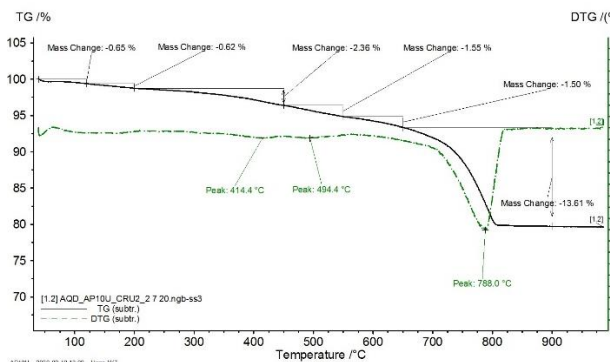
AP-09D



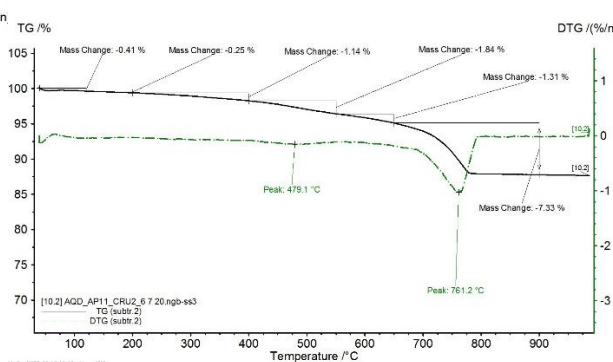
AP-09U



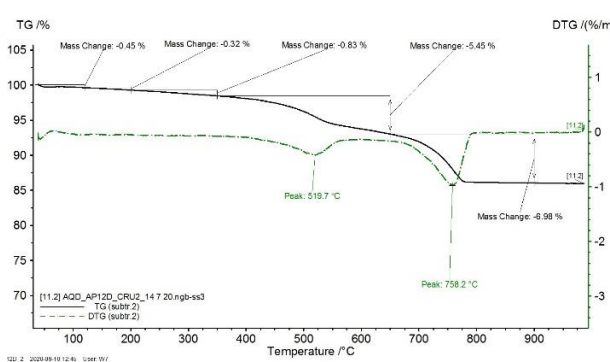
AP-10D



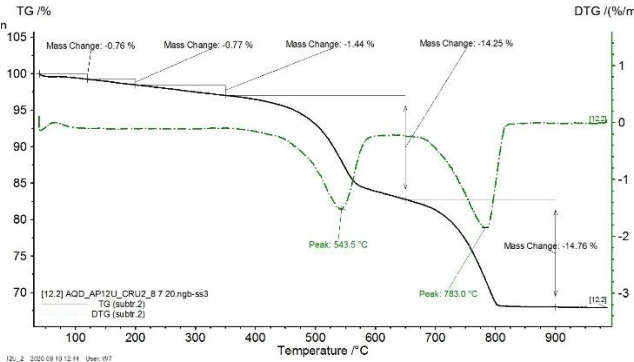
AP-10U



AP-11



AP-12D



AP-12U

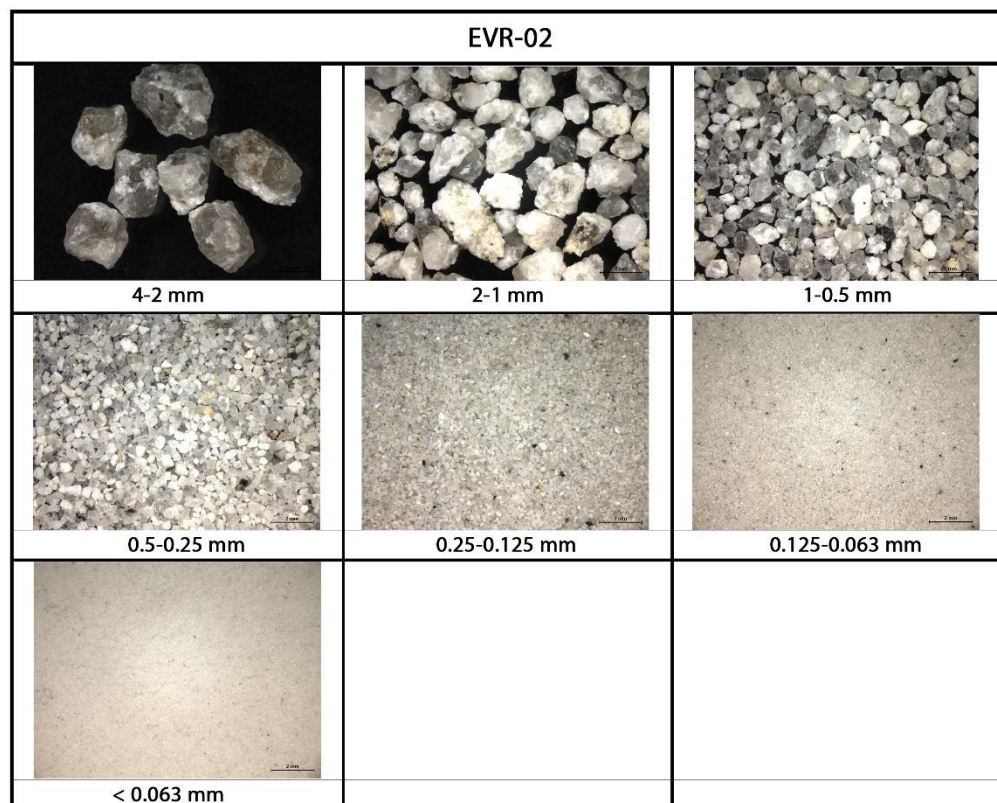
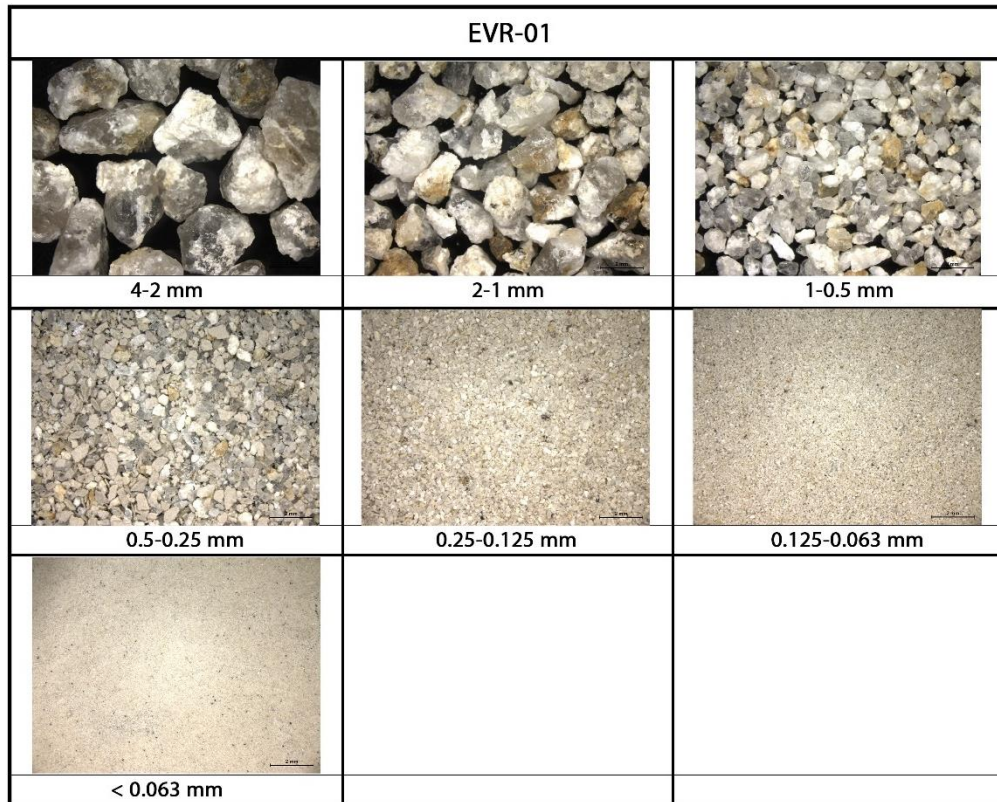
Appendix 10. Results of the acid attack analysis of the samples from the aqueduct of Água da Prata.

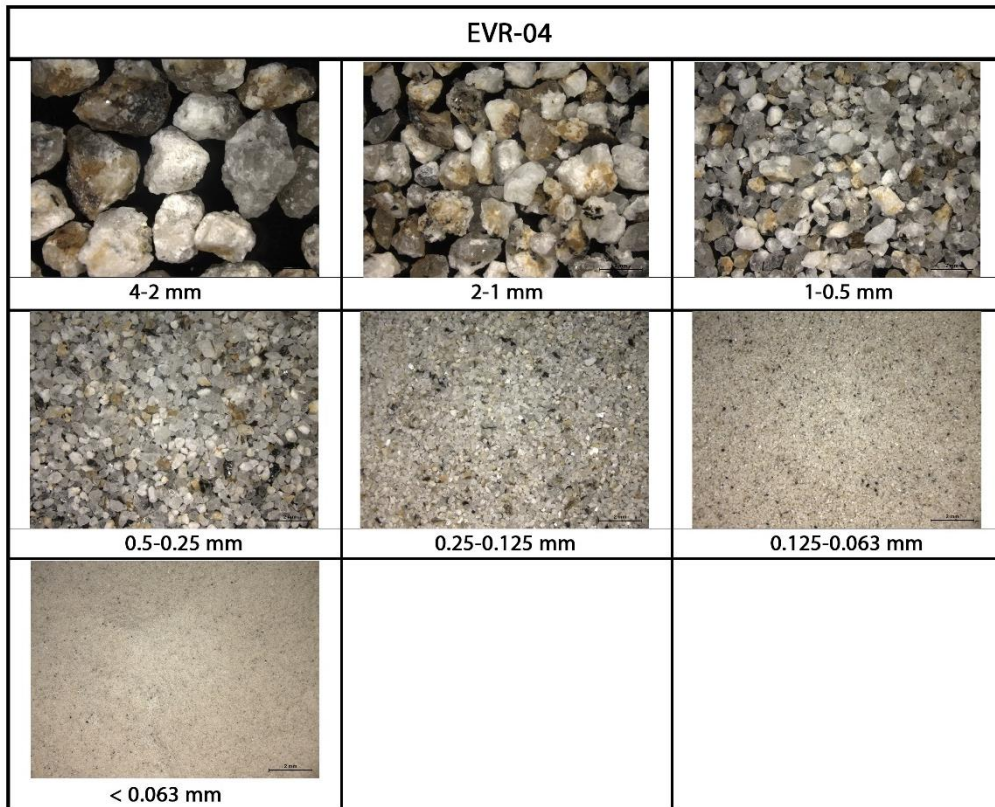
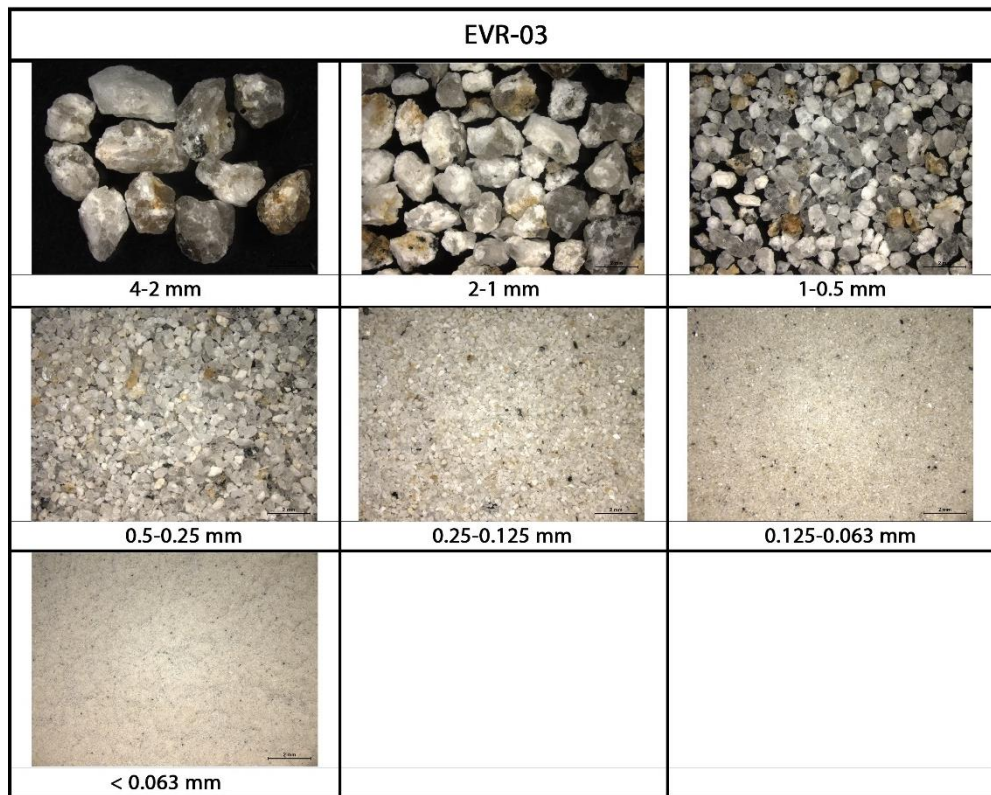
Sample Name		Weight (g)		Fraction (%)	
Sample	Test	Initial	Final	Soluble	Insoluble
EVR-01	A	10,459	6,671	63,78	36,22
	B	10,376	7,270	70,07	29,93
EVR-02	A	10,365	9,058	87,39	12,61
	B	10,136	9,035	89,14	10,86
EVR-03	A	10,456	9,098	87,01	12,99
	B	10,089	8,910	88,31	11,69
EVR-04	A	11,656	9,952	85,38	14,62
	B	11,203	9,581	85,52	14,48
EVR-05	A	10,240	8,260	80,66	19,34
	B	10,020	7,890	78,74	21,26
EVR-06	A	11,440	7,774	67,95	32,05
	B	11,896	8,192	68,86	31,14
EVR-07	A	10,186	8,092	79,44	20,56
	B	10,020	8,098	80,82	19,18
EVR-08	A	10,312	7,441	72,16	27,84
	B	10,206	7,252	71,06	28,94
AP-01	A	11,030	6,956	63,06	36,94
	B	11,126	7,532	67,70	32,30
AP-03		10,178	4,251	41,77	58,23
AP-04	A	10,806	7,215	66,77	33,23
	B	10,896	7,266	66,69	33,31
AP-05D	A	10,666	7,746	72,62	27,38
	B	10,878	7,702	70,80	29,20
AP-06	A	9,912	3,265	32,94	67,06
	B	10,012	3,213	32,09	67,91
AP-08	A	10,585	4,882	46,12	53,88
	B	10,702	4,793	44,79	55,21
AP-10D	A	10,755	7,133	66,32	33,68
	B	10,509	6,834	65,03	34,97
AP-11	A	11,720	8,274	70,60	29,40
	B	11,295	8,254	73,08	26,92

Appendix 11. Results of the granulometric analysis, grain size distribution of the insoluble residue.

Sample Name		Grain Size (g)							
Sample	Test	> 4 mm	4 - 2	2 - 1	1-0,500	0,500-0,250	0,250-0,125	0,125-0,063	< 0,063
EVR-01	A	0,000	0,200	1,650	0,759	0,890	1,399	1,341	0,529
	B	0,000	0,650	2,381	0,907	0,960	1,088	0,859	0,405
EVR-02	A	0,000	0,193	2,554	1,356	1,302	1,540	1,443	0,664
	B	0,000	0,132	1,939	1,076	1,637	1,915	1,534	0,773
EVR-03	A	0,000	0,225	2,581	1,272	1,321	1,533	1,400	0,756
	B	0,000	0,456	2,750	1,312	1,222	1,253	1,190	0,627
EVR-04	A	0,000	0,806	1,925	1,160	1,505	1,726	1,632	1,181
	B	0,000	0,792	2,226	1,102	1,014	1,442	1,718	1,167
EVR-05	A	0,090	0,880	1,690	1,460	1,520	1,470	1,100	0,000
	B	0,190	1,300	1,460	1,500	1,380	1,070	0,770	0,140
EVR-06	A	0,000	0,013	0,511	0,722	1,185	1,832	2,520	0,980
	B	0,000	0,017	0,445	0,829	1,252	1,946	2,439	1,217
EVR-07	A	0,084	0,788	1,806	1,627	1,436	0,892	0,672	0,773
	B	0,000	0,363	1,468	1,906	1,667	1,106	0,778	0,792
EVR-08	A	0,169	0,462	0,696	0,705	0,793	1,145	1,665	1,798
	B	0,000	0,354	0,577	0,819	0,981	1,317	1,760	1,441
AP-01	A	0,000	0,368	0,706	1,125	1,514	1,722	1,145	0,375
	B	0,000	0,293	0,708	1,183	1,623	1,890	1,453	0,435
AP-03		0,000	0,065	0,185	0,420	0,852	1,206	1,057	0,401
AP-04	A	0,140	0,462	1,254	2,145	1,658	0,859	0,519	0,191
	B	0,000	0,360	1,180	1,937	1,484	1,058	0,811	0,408
AP-05D	A	0,254	0,699	1,651	2,426	1,577	0,633	0,363	0,129
	B	0,217	0,588	1,770	2,420	1,637	0,632	0,328	0,100
AP-06	A	0,000	0,000	0,000	0,196	0,867	0,995	0,557	0,647
	B	0,000	0,000	0,005	0,244	0,969	0,958	0,469	0,527
AP-08	A	0,000	0,000	0,000	0,844	1,992	1,438	0,467	0,117
	B	0,000	0,000	0,002	0,651	1,870	1,561	0,498	0,168
AP-10D	A	0,000	0,279	0,459	1,300	2,445	1,575	0,711	0,307
	B	0,000	0,178	0,488	1,394	2,300	1,452	0,729	0,290
AP-11	A	0,000	0,157	0,771	1,081	1,229	1,382	2,725	0,909
	B	0,000	0,160	1,063	1,478	1,364	1,457	1,995	0,766

Appendix 12. Insoluble residues obtained after acid attack, observations under Stereozoom microscope.





EVR-06		
		
4-2 mm	2-1 mm	1-0.5 mm
		
0.5-0.25 mm	0.25-0.125 mm	0.125-0.063 mm
		
< 0.063 mm		

EVR-07		
		
> 4 mm	4-2 mm	2-1 mm
		
1-0.5 mm	0.5-0.25 mm	0.25-0.125 mm
		
0.125-0.063 mm	< 0.063 mm	

EVR-08		
 > 4 mm	 4-2 mm	 2-1 mm
 1-0.5 mm	 0.5-0.25 mm	 0.25-0.125 mm
 0.125-0.063 mm	 < 0.063 mm	

AP-01		
 4-2 mm	 2-1 mm	 1-0.5 mm
 0.5-0.25 mm	 0.25-0.125 mm	 0.125-0.063 mm
 < 0.063 mm		

AP-03		
		
4-2 mm	2-1 mm	1-0.5 mm
		
0.5-0.25 mm	0.25-0.125 mm	0.125-0.063 mm
		
< 0.063 mm		

AP-04		
		
> 4 mm	4-2 mm	2-1 mm
		
1-0.5 mm	0.5-0.25 mm	0.25-0.125 mm
		
0.125-0.063 mm	< 0.063 mm	

AP-05D		
		
> 4 mm	4-2 mm	2-1 mm
		
1-0.5 mm	0.5-0.25 mm	0.25-0.125 mm
		
0.125-0.063 mm	< 0.063 mm	

AP-06		
		
2-1 mm	1-0.5 mm	0.5-0.25 mm
		
0.25-0.125 mm	0.125-0.063 mm	< 0.063 mm

AP-08		
		
2-1 mm	1-0.5 mm	0.5-0.25 mm
		
0.25-0.125 mm	0.125-0.063 mm	< 0.063 mm

AP-10D		
		
4-2 mm	2-1 mm	1-0.5 mm
		
0.5-0.25 mm	0.25-0.125 mm	0.125-0.063 mm
		
< 0.063 mm		

AP-11		
		
4-2 mm	2-1 mm	1-0.5 mm
		
0.5-0.25 mm	0.25-0.125 mm	0.125-0.063 mm
		
< 0.063 mm		